FINAL TECHNICAL REPORT

Project title: Multifunctional Metallic and Refractory Materials for Energy Efficient Handling of Molten Metals

Award No: DE-FC36-04GO14038

Project Period: March 1, 2004 to May 31, 2008

Primary author: Xingbo Liu
West Virginia University
(304) 293-3111 ext. 2324
Xingbo.Liu@mail.wvu.edu

Co-Authors: Bruce Kang, West Virginia University
B. Gopalakrishnan, West Virginia University
James Hemrick, Oak Ridge National Laboratory
Vinod Sikka, Oak Ridge National Laboratory
Carl Irwin, West Virginia University

Principal Investigator: Ever Barbero
West Virginia University
(304) 293-3111 ext. 2337
ebarbero@wvu.edu

Subcontracting organizations:

Oak Ridge National Laboratory
James Hemrick
(865) 574-7601
hemrickjg@ornl.gov

Missouri University of Science and Technology formerly University of Missouri-Rolla
Jeff Smith
jsmith@mst.edu
(573) 341-4447

Energy Industries of Ohio
Larry Boyd
boyd@energyinohio.com
(216) 662-7044

Secat
Shridas Ningileri
sningileri@secat.net
(859) 514-4989 x114

Date: January 21, 2009

List of Project Partners with Point Of Contact

Partner	Contact Information
West Virginia University	Xingbo Liu (304) 293-3111 ext. 2324 Xingbo.Liu@mail.wvu.edu
Oak Ridge National Laboratory	James Hemrick (865) 574-7601 hemrickjg@ornl.gov
Missouri University of Science and Technology formerly University of Missouri-Rolla and RE Moore*	Jeff Smith (573) 341-4447 jsmith@mst.edu
Secat, Inc.*	Shridas Ningileri (859) 514-4989 ext. 114 sningileri@secat.net
Energy Industries of Ohio*	Larry Boyd (216) 323-1898 boyd@energyinohio.com
AK Steel Corp.*	Paul Janavicius (513) 425-2670 Paul_Janavicius@aksteel.com
Praxair Surface Technologies*	Stephen Wichmanowski (317) 240-2699 Stephen_Wichmanowski@praxair.com
Duraloy Technologies Inc.*	Roman Pankiw (724) 887-5100 techmgr@duraloy.com
Vesuvius McDanel*	Edward Dean (724) 843-8300 ext. 269 Ed.dean@vesuvius.com
Deloro Stellite*	Jim Wu (314) 983-0266 jwu@stellite.com
ILZRO*	Frank Goodwin (919) 361-4647 ext. 3018 fgoodwin@ilzro.org
Metaullics*	Mark Bright (440) 349-8810 marbri@pyrotek-inc.com
Alcan Rolled Products*	Scott Goodrich (304) 273-6707 Scott.goodrich@pechiney.com

Partner	Contact Information
Special Metals Corp.*	Chris Rock (304) 526-5452 crock@specialmetals.com
Sturm Rapid Response Center*	Jim Hamilton (304) 733-3229 Jim.Hamilton@sulzerpumps.com
Wheeling-Nisshin*	Frank Mollica (304) 527-4893 FrankM@Wheeling-Nisshin.com
Nucor Steel – South Carolina*	Allen Rogers (843) 336-6448 rogersa@nucorsteel.com
Nucor Steel – Crawfordsville*	Scott Sexton (765) 361-3259 ssexton@ns-ind.com
Nucor Arkansas*	Chris Calvin (870) 762-2100 ext. 1340 ccalvin@nucorar.com
MORCO*	Bill Headrick (636) 479-7770 bill@refractories.net
Blasch Precision Ceramics*	David Larsen (518) 436-1263 ext. 30 dlarsen@blaschceramics.com
Emhart Glass Inc.*	Steve Herrington (573) 437 2132 Steve.herrington@emhartglass.com
Harbison-Walker Refractories	Marc Palmisiano (412) 469-6102 MPalmisiano@anhrefractories.com
Vesuvius Monofrax*	Amul Gupta (716) 483-7170 Amul_Gupta@cp.vesuvius.com
Thermal Ceramics*	Jason Street (706) 786-1200 jstreet@thermalceramics.com
Magneco/Metrel*	Michael Anderson (630) 543-8560 mike@magneco-metrel.com
Allied Mineral Products Inc.*	Dana Goski (614) 876-0244 dgg@alliedmin.com

Partner	Contact Information
Kyanite Mining Corp.*	Jesse Brown (804) 983-2085 jessebrown@kyanite.com
The Techs*	James Anderson (412) 464-5000 ext. 2209 janderson@thetechs.com
Wheatland Tube Co.*	Robert Ferguson (724) 342-6851 ext. 286 Bob.ferguson@wheatland.com
Almatis*	Raymond P. Racher (412) 630-2819 Raymond.Racher@almatis.com
California Steel Industries Inc.*	John Wray (909) 350-6165 jwray@californiasteel.com
Fireline TCON Inc.*	Klaus-Markus (Mark) Peters (330) 743-1164 m.peters@firelineinc.biz

*Denotes cost share partner

Acknowledgments, Disclaimer, and Proprietary Data Notice

Acknowledgments

This report is based upon work supported by the U.S. Department of Energy, Office of Energy Efficiency and Renewable Energy, Industrial Technologies Program, Industrial Materials for the Future, under Award Number DE-FC36-04GO14038. The authors are also indebted to the following companies for supplying the refractory and scraper materials and coatings: Fireline TCON Inc., Deloro Stellite, MORCO, Metaullics, and Specialty Welding. We also want to acknowledge the guidance provided by the International Lead Zinc Research Organization.

Disclaimer

This report was prepared as an account of work sponsored by an agency of the United States Government. Neither the United States Government nor any agency thereof, nor any of their employees, makes any warranty, express or implied, or assumes any legal liability or responsibility for the accuracy, completeness, or usefulness of any information, apparatus, product, or process disclosed, or represents that its use would not infringe privately owned rights. Reference herein to any specific commercial product, process, or service by trade name, trademark, manufacturer, or otherwise, does not necessarily constitute or imply its endorsement, recommendation, or favoring by the United States Government or any agency thereof. The views and opinions of authors expressed herein do not necessarily state or reflect those of the United States Government or any agency thereof.

Table of Contents

List of Figures

List of Tables

Abbreviations and Acronyms

Abbreviation/Acronym	Definition
Al	Aluminum
Ar-4%H2	Argon – 4% of Hydrogen
ASTM	American Society of Testing Materials
BN	Boron-nitride
BSI	Back-scattered Electron Image
CA6	CaO•6Al2O3
CCD	Charge-coupled device
CGL	Continuous Galvanizing Lines
CGL	Continuous Galvalume Line
CLM	Cathodoluminescence Microscopy
Cr	Chromium
CSI	California Steel Industry
DSC-TGA	Thermal Gravity Analyzer
DT	Downtime
EDS	Energy Dispersive Spectroscopy
EDS	Energy Dispersive X-Ray Analyzer
EIO	Energy Industries of Ohio
EPMA	Electron probe micro analyzer
Fe	Iron
Fireline	Fireline TCON, Inc.
GA/GI	Galvanneal/Galvanizing
GEPDSS	Galvanizing Energy Profiler Decision Support System
GI	Galvanizing
ILZRO	International Lead Zinc Research Organization
IOF-WV	Industries of the Future – West Virginia
IR	High-intensity Infrared
lbf	Pounds force
MIRR	Modified Internal Rate of Return
Mo	Molebdum
MOR	Modulus of Rupture Testing
MORCO	Missouri Refractories Company, Inc.
NG	Natural gas
ORNL	Oak Ridge National Laboratory
Pa	Pascal
PHAST	Process Heating Assessment and Survey Tool
RGB	Red Green Blue
RT	Room temperature
SEM	Scanning Electron Microscopy
SEM/EDAX	Scanning Electron Microscopy/En
Si	Silicon
TC	Thermal cycle
UMR	University of Missouri Rolla now Missouri University of Science and Technology
VB DOT NET	Visual Basic Microsoft Application
VBA	Visual Basic Application

Abbreviation/Acronym	Definition
W	Tungsten
WC-Co	Tungsten Carbide-Cobalt
WVU	West Virginia University
XRD	X-ray Diffraction
Zn	Zinc
Zn/Al	Zinc/Aluminum

1.0 Executive Summary

1.1 Project rationale

The containment, handling, and processing of liquid metal are key parts of several metallurgical processes that are essential to an industrial economy. These include the application of corrosion-resistant coatings to steel sheet, and the melting and casting of liquid aluminum alloys. These processes are very energy intensive. In hot-dip Galvanize, Galvanneal, and Galvalume processes, rollers, bearings, guides and other submerged hardware undergo corrosion, wear, and buildup of dross (intermetallic particles) that degrade quality of sheet steel, cause frequent downtime of production lines, and severely reduce energy efficiency. Similarly, refractory linings used for containment of molten metals in aluminum production and metal casting undergo corrosion and wear that results in contamination of the melt, energy loss, and eventual corrosion and failure of container walls.

This project proposed to develop new understandings of the failure mechanisms causing these outages and from that knowledge develop new materials with increased service lifetimes. The topic of this project was ranked as high priority by industry partners and, as well, is a high priority research area in the ITP's *Steel Industry Technology Roadmap* [18], *Aluminum Industry Roadmap* [27], and DOE/ORO-2076 Report: "Opportunities for Advanced Ceramics to Meet the Needs of the Industries of the Future" [19].

1.2 Project goals and objectives

The goal of the project was to extend the lifetime of hardware submerged in molten metal by an order of magnitude and to improve energy efficiency of molten metal handling process. Assuming broad implementation of project results, energy savings in 2020 were projected to be 10 trillion BTU/year, with cost savings of approximately $100 million/year. The approach to achieving this goal was to:

1. Develop an understanding of the nature of galvanizing bath attack on existing and newly developed galvanizing pot hardware materials, focusing on the nature of dross buildup that is the most common cause of galvanizing line outages.
2. Develop an understanding of the nature of aluminum alloy attack on existing and newly developed refractory containment materials.
3. Develop an analysis software to show the benefits of using new materials developed in this program that give industrial partners the incentive to adopt the new materials and realize potential energy savings; technology transfer included energy audits of partner plants that demonstrated use and benefits of the analysis software developed in this project.
4. Subject the newly developed materials and processes to extensive testing and validation with inline trials at industrial partners' facilities.

1.3 Project team

The project team was comprised of materials research groups from West Virginia University (WVU) and the Missouri University of Science and Technology formerly University of Missouri – Rolla (UMR), materials experts from the Oak Ridge National Laboratory (ORNL), the Technical Director for the International Lead and Zinc Research Organization (ILZRO), industry experts from Secat and from Energy Industries of Ohio (EIO). Industry partners included six suppliers to

the hot dip galvanizing industry, four end-user steel companies with hot-dip Galvanize and/or Galvalume lines, eight refractory suppliers, and seven refractory end-user companies. Throughout the project, WVU, ORNL, ILZRO, EIA, UMR, and Secat met quarterly to assess project results and set goals and objectives for the next quarter. Every other quarter, industry partners met with the core research team to advise and help set research priorities.

1.4 Project results

New families of materials more resistant to degradation in hot-dip galvanizing bath conditions were developed. In particular, knowledge of the relationship between dynamic corrosion and formation of dross on roll surfaces, identified for the first time on this project, enabled the development of new corrosion and wear resistant materials with greater than 5X lifetime improvements. These results were validated through exposure of weld-overlay material samples for more than 33 days in an industrial setting.

Alloy 2020 weld overlay material and process were developed and applied to GI rolls. Alloy 2020 is a Fe-base superalloy that was found to be corrosion and wear resistance in molten Zn-Al environments and was considered to be a good material for development of new dross build-up resistant rolls. A new weld overlay procedure for Alloy 2020 was developed, including making the wire and developing a welding process, to coat the 316L stainless steel roll. Metaullics provided the alloy, Stoody made the wire, Specialty Weldings did the coating, and Duraloy did the machining. A processing patent has been filed with Metaullics, Stoody, ORNL, WVU and Specialty Welding as co-inventors. Industrial trials were conducted at the Nucor-Crawfordsville and Nucor-Arkansas facilities.

New Alloys and dross-cleaning procedures were developed for Galvalume processes. Sink roll scrappers made with Stellite 6B and Tribaloy T-401 were tested. Stellite 21 showed a 4.5X better wearing resistance. Based on a better understanding of dross build-up mechanisms as identified during the project, a new and improved scraping procedure was developed that is 1.5X more effective in dross removal than current procedures. Wheeling Nisshin has adopted Tribaloy T-401 as scraper overlay and is considering implementing the new scrapping procedures.

Two new refractory compositions, including new anti-wetting agents, were identified for use with liquid aluminum alloys. Bonite and TCON® were identified as new materials for improved corrosion and wear resistance, and which also offer better thermal management in molten aluminum contact applications. One material is a castable refractory based on calcium aluminate (Bonite) developed with industrial partner Missouri Refractories Company, Inc. (MORCO). The other material is an alumina/silicon carbide composite material (TCON®) identified in partnership with industrial partner Fireline TCON, Inc. (Fireline). These materials have been validated through the exposure of material samples for over 2,000 hours in an industrial setting at Energy Industries of Ohio (EIO). The materials were installed in an industrial trial at a commercial aluminum rod and cable mill in Hawesville, KY. Sections 5.4, 6.4, and 7.4 discuss extensive development, testing and commercialization activities of TCON® and Bonite by Fireline and MORCO.

A new thermal conductivity measurement technique was developed and validated at ORNL. The IR Thermal Diffusivity Method developed through this project was validated using current and previous measurements made on a high purity alumina (99.6% pure Coors Alumina) material that had been previously evaluated using Calorimetry (ASTM C202), Hot Wire (ASTM C1113), and Laser Flash (ASTM E1461) methods. Good agreement was found to exist between previous laser flash measurements and current IR giving validation to the new IR

technique and confidence in the differences previously seen between measurements made using the new IR technique and those reported in data sheets for commercially available refractory materials.

The Galvanizing Energy Profiler Decision Support System (GEPDSS) was developed at WVU. GEPDSS is a software model that uses inputs such as energy costs, equipment energy consumption, materials life, and production and rejection information. It then yields information on energy consumption and production, and potential energy and cost savings, product losses, and productivity rates as a result of implementation of new materials. Software produces accurate energy profile for the 5 industry partners, 3 used for development and 2 for validation. ILZRO is providing support for further development to enable evaluation of producing particular grades of steel utilizing varying heat treatment cycles.

Newly Developed CCW Laser Cladding Shows Better Resistance to Dross Buildup than 316L Stainless Steel: This newly developed laser cladding has strong resistance to the dross adhesion and shows less dross buildup on the surface than 316L stainless steel after 30 days lab-scale dynamic tests.

A novel method of measuring the corrosion behavior of bath hardware materials during exposure to liquid galvanizing metal alloys was developed and is the subject of a patent application. This technology enables continuous in-situ monitoring of high-temperature liquid metal corrosion. It is expected to enable an understanding never before achieved of the evolution over time of corrosion phenomena between liquid metal (e.g. zinc-aluminum solution) and submerged solid metal materials (e.g. coated 316L rollers and bearings). This is a significant advance over current state-of-the-art for measuring high-temperature liquid metal corrosion rates that are usually just average rates over days or weeks determined by weight loss measurements. This new approach provides insights into instantaneous corrosion mechanisms never before obtained in high-temperature liquid metal environments, thereby opening prospects of further improvements in materials performance and production cost savings.

1.5 Project in-line trials

Project in-line trials were conducted at Southwire Kentucky Rod and Cable Mill, Nucor-Crawfordsville, Nucor-Arkansas, Nucor-South Carolina, Wheeling Nisshin, California Steel, Energy Industries of Ohio, and Pennex Aluminum.

1.6 Cost, energy, and environmental benefits

Cost, energy, and environmental benefits resulting from the project are due to: i) a reduced number of process shutdowns to change hardware or lining material, ii) reduced need to produce new hardware or lining material, iii) improved product quality leads to reduced need to remake product or manufacturing of new product, iv) reduction in contamination of melt from degradation of refractory and metallic components, v) elimination of worn hardware will increase efficiency of process, vi) reduced refractory lining deterioration or formation of a less insulating phase, would result in decreased heat loss through the walls.

Expected energy, cost, and environmental benefits resulting from the project are given at five year intervals from 2005 through 2030 in Section 7.5. For example, projected 2015 benefits for the U.S. hot-dip galvanizing line industry, assuming 21% market penetration of the improved materials for hot-dip hardware, are energy savings of approximately 0.17 trillion BTU/year, cost savings of $1.2 billion/year, and carbon reductions of approximately 0.8 billion tons/year. Projected 2015 benefits for the U.S. aluminum industry, assuming 21% market penetration of

improved refractory materials, are energy savings of approximately 0.2 trillion BTU/year, cost savings of $2.3 billion/year and carbon reductions of approximately 1.4 billion tons/year. The carbon reduction benefit of the project for the hot-dip galvanize and aluminum industries combined is projected to be approximately 2.2 billion tons/year in 2015.

1.7 Pathways from research to commercialization

Pathways from research to commercialization were based on structure of the project's industrial partnerships. These partnerships included suppliers, industrial associations, and end users. All parties were involved in conducting the project including planning and critiquing the trials. Supplier companies such as Pyrotech Metaullics, Stoody, and Duraloy have commercialized products and processes developed on the project.

1.8 Degrees and patents for work on this project

Degrees and patents for work on this project include PhDs earned by Mark Bright, Jing Xu, Ashok Varadarajan and several masters degrees have been awarded. Patents have been awarded or are pending on i) bearing design for continuous galvanizing rollers, ii) Alloy 2020 weld overlay process, and iii) high-temperature electrochemical test procedures.

2.0 Introduction

Concern about liquid metal corrosion on the containment and submerged hardware is a very important issue in metal processing industries such as steel companies with hot-dipping lines, aluminum companies, metal casting companies, etc. Additionally, heat losses due to degradation of refractories by corrosion and poor thermal management are problematic for these same industries. For example, steel, metal casting, and aluminum industries suffer large energy losses due to the failure of refractory linings and poorly insulating refractory materials, requiring downtime for maintenance and/or resulting in contamination of the molten metal. Hot dipping lines such as Galvalume® require frequent down time for maintenance with consequent energy and productivity losses. Industries that would benefit from the outcome of this project include those that involve the containment or handling of liquid metal. The key sectors include steel companies with hot-dipping lines; aluminum companies and metal casting companies. Other industries which would also benefit from the approaches proposed in this project are: glass producers, pulp and paper producers, chemical producers, refractory producers, petroleum refiners, permanent-mold continuous die casting companies, and renewable energy systems manufacturers.

Therefore this project was under taken to reduce the liquid-metal corrosion of refractories and submerged hardware. Improvements in thermal management of liquid metal containers would allow (1) energy savings, (2) reduction of downtime and yield loss (3) improvement in overall product quality, (4) reduced repair and replacement cost of corroded components, (5) reduced environmental impact, and (6) improved economics. In addition, the technologies developed by this project increase the overall efficiencies of the steel, aluminum, metal casting, and die casting industries by decreasing the amount of wasted or rework materials, reducing downtime, and increasing the reliability of the operation systems. The project has resultant environmental and economic benefits as well. New materials research for specialized applications is a high-risk investment, which is less likely to be initiated by industry because of their current financial status and a significant cutback of their research facilities and staff. This type of research and development work demands not only long-term financial commitment but also integrated efforts of diverse materials expertise.

The research objectives of this project were to develop multifunctional metallic and refractory materials and surface treatment, coatings and claddings for life improvement of molten metal containment and submerged hardware and improved thermal management in aluminum, steel, and metal casting industries. **The project goal was to extend the molten metal containment and submerged hardware life by an order of magnitude and improvement of thermal efficiency** with energy savings of **333 trillion BTU/year** and cost savings of approximately **$1 billion/year by 2020**.

The focus for developing GEPDSS was to develop a generic tool for the facility staff to make informed decisions, pin point problem areas and understand energy flow more closely in their facility. This led to the identification all the energy points in the entire continuous galvanizing line and a careful study of the process. The research objectives were to create a model that ties all energy points on a continuous galvanizing line with respect to production and rejection rate, enabling sensitivity analysis and providing decision making information for managers and researchers. The challenge was to identify a basis for comparison and quantification of energy consumption in continuous galvanizing lines. The common unit of measurement for the galvanizing industry is tons of galvanized sheet steel produced. The facilities were also interested in obtaining information about increases in production along with the savings in

energy. The vision was not just to develop a tool that would help validate the project results but also something that would trace the production, rejection, downtime, idle and production durations, energy costs associated with production and rejection durations, generate detailed estimates for energy intensity and consumption for electricity and natural gas, and document the causes for line shutdowns.

3.0 Background

3.1 Background on Partner Organizations

The research team for this project includes West Virginia University (WVU), University of Missouri-Rolla (UMR), Oak Ridge National Laboratory (ORNL), International Lead & Zinc Research Organization (ILZRO), Secat Inc., Energy Industries of Ohio (EIO), Industries of the Future – West Virginia (IOF-WV), steel, aluminum, metal casting, alloy, refractory, ceramics, and coating companies, and hardware and equipment suppliers.

The overall project coordination was through West Virginia University. Project research and testing was conducted at WVU, ORNL, and UMR. Frank Goodwin of ILZRO was a key advisor on all aspects of the project. Extensive in-plant material coupon tests were conducted at steel industry partner companies, EIO, steel industry suppliers, and refractory companies. The industry trade associations and industry suppliers were the main source of marketing and commercialization efforts.

Critical plant in-line tests were conducted at Nucor-Crawfordsville and Nucor-Arkansas. The commercialization partners and pathways that are specific for the alloy case are illustrated in Figure 1. The case for refractories will follow the general pathway to commercialization.

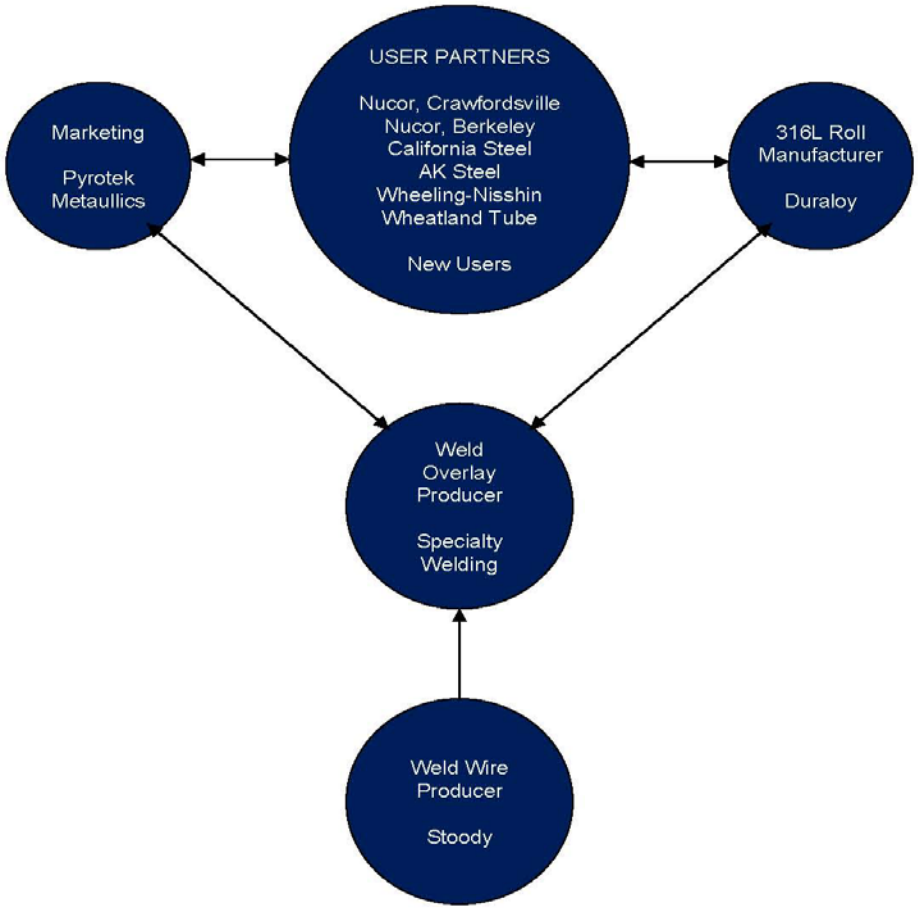

Figure 1 : IMF Commercialization Partners/Pathway

The partners on the project provided the expertise and benefits to the project shown in Table 1:

Table 1: Partner Oranizations

Type of Organization	Organizations	Description of Contribution
R&D organization	WVU:	Understanding of basic mechanisms of molten metal corrosion and mass transfer, materials and process modeling, molten metal testing, and metallurgical characterization. These faculty researchers have over 30 years experience in corrosion, modeling, and metallurgy.
R&D organization	ORNL:	Specialized experience in thermodynamic modeling of molten metal interactions, sessile drop surface tension measurements, bulk alloy development, refractory characterization and analysis, materials processing and production, material property characterization and analysis including thermal conductivity, molten metal testing, and microstructural analysis.
R&D organization	UMR	Expertise in the areas of microstructural analysis, modeling and corrosion testing of refractory materials. Ran a small oxy-fuel simulator furnace for analysis of exposure of refractory materials to oxy-fuel conditions. Expertise in the production, modification, and engineering of refractory materials.
R&D organization	IOF-WV	Maintains an active network of industry in the state of West Virginia and the U.S. Has broad capabilities to manage complex interdisciplinary projects, conduct surveys, plant assessments, facilitate communications, and interface with the U.S. DOE and other agencies.
Industry trade association	SECAT	Represents unified problem identification for a large number of aluminum-producing companies in Kentucky and elsewhere and assists in timely transfer of technology and implementation of new solutions. It also brings in the unique expertise from the University of Kentucky in carrying out certain specific tasks.
Industry trade association	EIO	Represents the aluminum, steel, and metal casting industries in Ohio. EIO assisted in conducting certain pilot scale tests in their aluminum foundry and transferred the technology to the relevant industries to this project in Ohio. EIO identified TCON® as a test material and brought Fireline in as a project partner.
Industry trade association	ILZRO	Specialized experience over several years with industry-sponsored research in hardware improvement for molten metal baths, excellent relationships with steel companies and zinc producers.

Type of Organization	Organizations	Description of Contribution
Metals Production Companies	Alcan Rolled Products, AK Steel, Wheeling Nisshin, Nucor-South Carolina, Nucor-Crawfordsville, Nucor-Arkansas, California Steel, The Techs, Special Metals	Specialized experience in identification of problems, implementation of proposed solutions, fabrication of prototype components, and availability of pilot-scale testing.
Metals industry suppliers and processors	Praxair Surface Technologies, Duraloy Technologies, Vesuvius McDaniel, Deloro Stellite, Metaullics-Pyrotek, Sturm Rapid Response	Expertise in problem identification and test materials and coating solutions, supply liquid-metal for testing, production testing of material coupons and prototype components.
Refractory Production and Processing Companies	MORCO, Blasch Precision Ceramics, Emhart Glass, Vesuvius Monofrax, Thermal Ceramics, Magneco/Metrel, Allied Mineral Products, Kyanite Mining, Fireline, Almatis	Specialized expertise in refractory application, supply refractory materials for testing.
Fabrication	Stoody and Specialty Welding	Did subcontract fabrication work for ORNL

3.2 Hot-dip galvanizing hardware issues

The process of continuous galvanizing of rolled sheet steel includes immersion into a bath of molten zinc/aluminum alloy. The steel strip is dipped in the molten bath through a series of driving motors and rollers which control the speed and tension of the strip, with the ability to modify both the amount of coating applied to the steel as well as the thickness and width of the sheet being galvanized. Three rolls are used to guide the steel strip through the molten metal bath. The rolls that operate in the molten Zn/Al are subject to a severely corrosive environment and require frequent changing. The performance of this equipment, the metallic hardware submerged in the molten Zn/Al bath, was the focus of this research. The primary objective of this research was to extend the performance life of the metallic hardware components of molten Zn/Al pot hardware by an order of magnitude.

Typical galvanizing operations experience downtimes on the order of every two weeks to change the metallic hardware submerged in the molten metal bath. This metallic hardware change is an expensive process for industry because it takes up to three days for a complete turn around to resume normal operations. Each roll bridle consists of a sink, stabilizer, and corrector roll with accompanying bearing components. The cost of the bridle rig with all components is as much as $25,000 dollars just for materials. These inefficiencies are of concern to the steel coating companies and serve as a potential market for many materials suppliers. This research effort served as a bridge between the market potential and industry need to provide an objective analytical and mechanistic approach to the problem of wear and corrosion of molten metal bath hardware in a continuous sheet galvanizing line. The approach of the investigators was to provide a means of testing and analysis that was both expeditious and cost effective.

3.3 Dross control issues

Steel sheet manufacturers across the globe; face a huge loss of production due to the molten metal corrosion of the pot hardware in continuous galvanizing lines (CGL). The development of steel sheet with corrosion resistant for more than 30 years using a high aluminum content zinc coating has made an impact in the construction industry. High aluminum content bath (55 wt %) causes severe corrosion of the pot hardware and causes huge repair and replacement cost with frequent stoppages. One of the main reason for stoppages is the severe dross formation over the submerged hardware (sink roll), which results in a poor coating layer over the steel sheet.

A good understanding of the mechanism of the dross formation over the submerged hardware has not yet been completely achieved. This research established (i) the dross formation mechanism by studying the effects of silicon presence and the hydrodynamic motion present in the CGL bath, and (ii) efficient removal of the dross formed over the sink roll using better scraper alloy with more than 3X life improvement and significant reduction of line stoppages.

3.4 Need for Energy Savings Software

Hot dip galvanizing lines have been in existence for a long period of time. Each line operates as a production system with coil steel being processed, heat treated, moved, coated, and packaged. There are energy consuming equipment all along the line in terms of motors, natural gas burners, molten metal pot, and compressed air driven air knives. The galvanizing line personnel have an excellent understanding about the production capacities and productivity losses due to production shutdown. However, the energy aspect is often not transparent to the line personnel and hence energy intensity of manufacturing in (MMBtu/ton) is not very well understood. Furthermore, it is difficult for the line personnel to evaluate the economic impact of investments to improve the line efficiency and also analyze the effect on energy intensity. There

is hence a need for research into building a tool to allow galvanizing lines to analyze the impact on efficiency and resources based on efforts for improving line efficiency in terms of reduced energy consumption.

3.5 Refractory issues

Heat loss due to the degradation of refractories used for molten metal containment and process thermal insulation has long been a problem for the aluminum industry. Deterioration of refractory materials leads to decreased thermal efficiency of aluminum processing units through production outages resulting in significant energy losses due to reduced product quality/yield prior to shut down and lost product during shut down. Also, large amounts of energy are lost during cooling of the furnace and are then required for reheating of the furnace.

This problem has been a concern as far back as the 1950's when Brondyke studied the penetration of silica refractories by molten Al at 700-1000^{o}C using both traditional cup testing and immersion testing [1]. At that time, commercial alumina-silica refractories used for aluminum melting applications were tested. It was found that wetting of the refractories led to subsequent penetration and exposure to molten Al. These results indicated that the problems associated with alumina-silica refractories resulted from the penetration of molten Al, side-wall build-up, and formation of corundum and metallic silicon due to metal reaction of Al with the Si and Si-bearing constituents. Subsequently there was an increase in volume of penetrated product, which would lead to generation of tensile stresses due to aluminum oxide build-up caused by oxidized aluminum and its alloy components around the metal line. The presence of tensile stresses would ultimately cause cracking in the refractories. Additionally, dissolution of Si occurred in the molten Al, with the penetration rate controlled by diffusion of Al and Si through the aluminum oxide.

To address this problem in current aluminum processing systems, physical, chemical, and mechanical property characterization and analysis were undertaken in this project. Both materials commonly used by industry and newly developed materials were analyzed in an effort to understand the corrosion and wear mechanisms associated with aluminum contact refractories and areas to target for improved materials.

4.0 Experimental Equipment, Methods, and Procedures

4.1 HDG coatings and materials issues

4.1.1 Survey

A survey on hot-dipping hardware was distributed to all the industrial partners and companies worldwide through ILZRO. The results of this survey are summarized below:

Twenty-two companies, including international companies, returned surveys: eleven from the molten bath hardware consumers (including Galvanize, Galvanneal, and Galvalume lines), five from the refractory consumers and six from the refractory producers.

1. **The molten metal temperature range in their baths** were from 860°F (GI) to 1,100 °F (GL); the steel Sheet tension ranged from 2,000 lbf to 11,500 lbf; sheet gauge ranged from 0.02 in to 0.135 in; and line speeds ranged from 200 to 650 ft/min.
2. **Reasons for Line Stoppage included:** (4 lines) dross build up, (all) bearing wear, (all) preventative maintenance, and (2) product change between bath composition. Average time for one campaign is 14 to 30 days for GI/GA, and 4 days for GL, respectively.
3. **Submerged Roll Specifics**:

   Sink Roll

   • (4) 316L SS, (3) coated

   • (2) CF-3M, (1) coated

   Stabilizer Rolls

   • (4) 316L SS, uncoated

   • (2) CF-3M, uncoated

   Coatings: WC, SDG 2003B (Praxair)

   Sleeve Material

   – (2) Stellite 6, (2) 316L SS coated, (1) CF-3M coated, (1) Ocmalloy #7

   – Depth of wear: up to 0.35 in/campaign

   Bushing

   – Geometry: (4) partial circle/half moon, (2) wear bars

   – Material: (2) Stellite 6, (1) ceramic, (1) 316L SS coated, (1) Ocmalloy #7

   – Depth of wear: 0.43 in – 0.75 in (11-20 mm) per campaign (alloy), .020 - .030 per campaign (ceramic)

   Sleeve Material

   – (3) Stellite 6, (2) 316L SS coated, (1) Ocmalloy #7

   – Depth of wear: .0625 in – 0.25 in (2-6 mm) per campaign

   Bushing

   – Geometry: (4) partial circle/half moon, (2) wear bars

   – Material: (2) Stellite 6, (1) ceramic, (1) 316L SS coated, (1) Ocmalloy #7

   – Depth of wear: .0635 in – 0.25 in per campaign

4. **Problems encountered include**: freezing or lock up of stabilizer rolls, cracking of bearings when worn thin, effects of dross, and rapid wear of dross scraping devices for higher aluminum baths wear.

The results of this survey provided the state-of-art status of pot hardware in hot-dip industries and the baseline for our research on this project.

The following experimental methods were employed in the research and development of pot hardware materials and coatings for continuous galvanizing process.

4.1.2 Lab-scale static corrosion tests

Lab-scale static corrosion tests were carried out at ORNL. The samples in one inch by one inch size were submerged into cups of molten GI alloy provided by Wheeling-Nisshin for various time intervals. After the tests, weight changes of the samples were measured. SEM/EDAX analyses were carried out to understand corrosion mechanisms.

4.1.3 Lab-scale dynamic corrosion/dross buildup tests.

Lab-scale dynamic corrosion/dross buildup tests were carried out at WVU. The samples with the dimensions of one inch diameter and 12 inches long were rotated in the molten GI alloy provided by Wheeling-Nisshin for up to 30 days. After the tests, SEM/EDAX analyses on cross section samples were carried out to evaluate the samples' resistance to dross buildup and to understand corrosion/dross buildup mechanisms.

4.1.4 Sessile-drop Tests

Static Sessile-drop Tests

A solid cube of Zn or Al alloy was placed on the solid substrate prior to heating. The apparatus used for the static sessile drop experiments is shown in Figure 2, and its corresponding schematic drawing is illustrated in Figure 3. It consisted of an induction furnace (Figure 2b), using an evacuating system with a rotary pump. In the inductive furnace chamber, the sample substrate was place on a ceramic support rod, which sat in a ceramic catch pan for protection, in case the molten metal dropped off the base and contaminated the furnace. The metal cube was located in the center of the induction heating coil for evenly distributed heating (Figure 3). The front window, made from quartz was installed in the inductive furnace, allowing a color CCD camera to continuously monitor the experiments. The resolution of the camera is 640 by 480. Three Type-S thermocouples (with ceramic sheath) were inserted into the furnace chamber (Figure 2b) by the feed-through for monitoring the refractory substrate temperature, molten metal drop temperature, and the reaction temperatures, respectively.

Before the experiment, the solid substrate and the Zn or Al alloy cube were ultrasonically cleaned in acetone. The substrate was then carefully placed into the center of the inductive heating coil in the vertical furnace chamber. A cube of Zn or Al alloy was placed on top of the tested substrate. The sealed chamber was evacuated to a vacuum of 10^{-6} Pa. Following evacuation, the inductive furnace chamber was heated to the required testing temperature. The cube of metal was allowed to melt and the wetting behavior between the molten metal and solid substrate was observed.

Dynamic Sessile Drop Experimental

A modified dynamic method was also employed in which molten Zn or Al alloy was dropped on the solid substrate by a heated delivery device. This modified method was developed to study

the dynamic wetting behavior as this approach has been suggested to be closer to the application conditions [2].

The apparatus used for the dynamic sessile drop experiments is schematically illustrated in Figures 4 and 5. It consisted of a 33 kW horizontal circular infrared furnace, using an evacuating system with a rotary pump and refilling gas system supplying purified Ar-4%H2. The quartz furnace chamber was enclosed on one end by a copper lid and slide device, which was used to move the experimental assembly inside the chamber. A small diameter quartz tube was also passed through the copper lid and extended to a location directly above the sample substrate where the tube was bent 90º and its diameter was reduced. This tube was used to contain the zinc or aluminum alloy wire segment during heating and melting, which produced the molten metal drop for the dynamic test. Both sealed end caps of the furnace assembly contained quartz windows allowing a color CCD camera to continuously monitor the experiments. The resolution of the camera is 640 by 480. Three Type-S thermocouples (with ceramic sheath) were inserted into the horizontal quartz test chamber through the copper end plate for monitoring the substrate temperature, molten metal drop temperature, and the reaction temperatures, respectively.

Before the experiment, the substrate and the zinc or aluminum wire segment were ultrasonically cleaned in acetone. The substrate was then carefully slid into the center of the horizontal chamber. A wire segment of Zn/Al alloy was placed into the quartz tube used for delivering molten zinc to the substrate. This tube was inserted through the copper end plate into the IR chamber. The chamber was evacuated and refilled. While the metal segment in the quartz tube was kept at the cold zone, the IR quartz chamber was heated up to the required temperature at a rate of 30ºC per minute. The furnace was allowed to stabilize for 20 minutes before the zinc segment was slowly moved from the cold zone to the hot zone of the furnace where it was allowed to melt and pass through the vertical portion of the delivery tube as a molten drop onto the test substrate. Similar to the static test method, the entire duration of the experiment was captured and recorded by the camera and VCR, from which the video still frames were extracted and analyzed.

(a) **(b)**

Figure 2 : Apparatus of the static sessile drop unit
(a) test unit; (b) induction heating coil and thermocouples

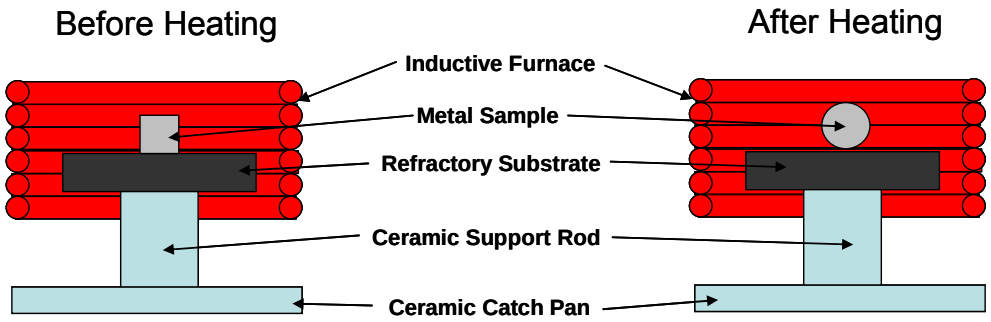

Figure 3: Schematic sketch of the static sessile drop unit

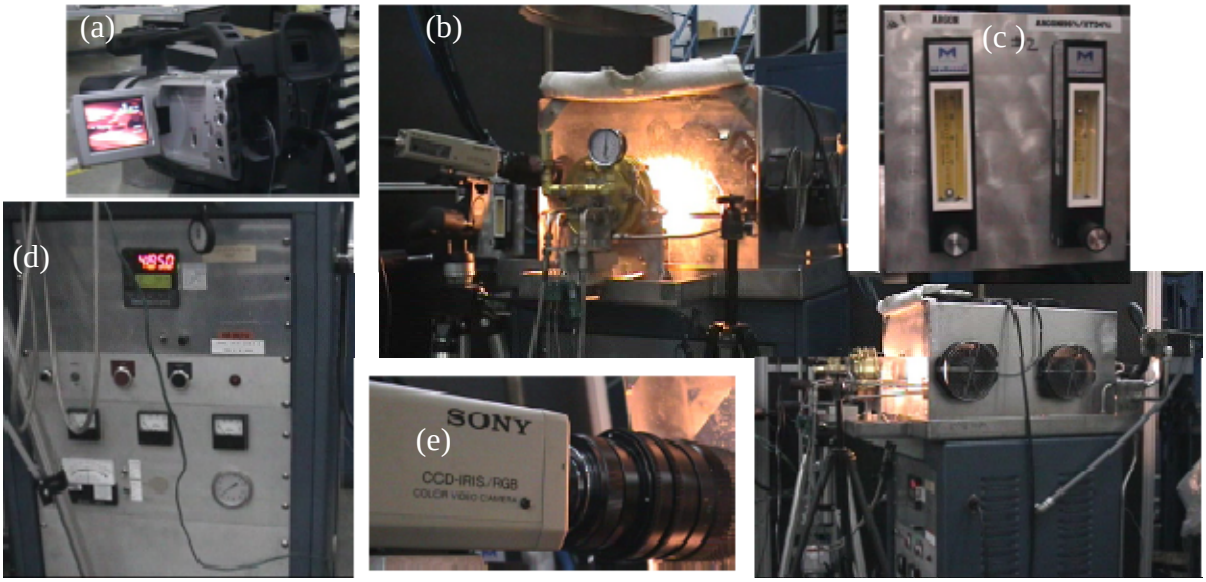

Figure 4: Apparatus of the dynamic sessile drop units (a) videocassette recorder (b) 33 kW horizontal circular infrared furnace front view (c) flow meter for Ar-4%H_2 (d) furnace controller (e) CCD camera (f) infrared furnace side view

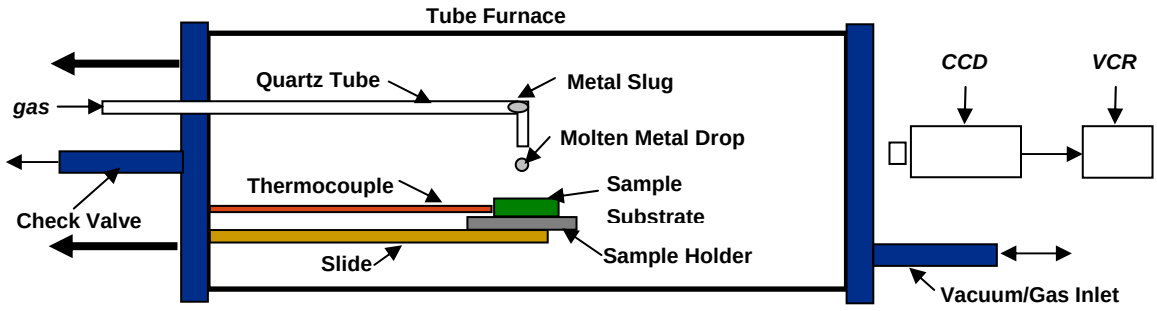

Figure 5: Schematic sketch of the dynamic sessile drop unit

4.1.5 Static Corrosion Tests – In-Plant

Static corrosion tests were carried out in the continuous galvanizing baths at our industrial partners for up to 150 days. Two different kinds of overlay samples were employed in the tests. One kind consisted of 4-in.-OD by 1-in.-wall tubes with 2020 weld overlay. The tube sections were 24-in. long with weld overlay section varying from 8- to 12-in. long. These tubes are shown in Figure 6 (a). Another type of samples, 2-in.-wide sections, are shown in Figure 6 (b).

Figure 6: CF3M (316L) tubes weld overlaid with 2020 for in-plant testing. (a) tubes; (b) 2-in-wide samples

The samples were submerged into the industrial baths. After the tests, SEM/EDAX analyses on cross section samples were carried out to evaluate the samples' resistance to dross buildup and to understand corrosion/dross buildup mechanisms.

4.2 Dross control and scraper design in GL

The objectives of this part of the research were to: (1) study the dross formation mechanism on the submerged hardware in continuous galvalume bath under static and dynamic conditions by means of lab scale tests, morphological analysis and chemical composition analysis, (2) study the effect of dynamic factors such as rotation speed and temperature on the dross nucleation and growth, (3) compare and evaluate the performances of various new materials which have high wear and corrosion resistance and (4) develop and test a new scraping method based on the dross formation mechanism.

Dynamic Scraper Wear Test Set-up

The objective of this research was to identify a material with improved wear resistance for use as a scraper to maintain the sink roll surface smooth and to develop a more efficient scraping method to maintain the roll surface. In order to carry out the tests under simulated industrial conditions, the test set-up shown in Figure 7 was assembled.

The test rig consists of a portable furnace, a furnace controller, a 15 HP motor, a speed reducer, a motor controller and a three phase power panel controlling each single device separately in case of any emergency.

Furnace: The furnace was designed in such a way that the entire furnace when fully laden with molten metal was easy to move over the guard rails. The furnace was a rectangular metal box, which was comprised of heating panels and the crucible. Sixteen heating panels were placed in

a circular array and the entire panels take about 36kW of power in order to maintain the metal in liquid condition. The furnace flooring was well insulated with ceramics and sealed with refractory cement in order to reduce heat loss through the bottom. A crucible was placed In the middle of the furnace which could hold up to 550 lbs of molten aluminum.

Furnace Controller: The furnace controller was fully equipped with an automatic or mechanical controlling device, allowing the operator to program it for a long period of time. Two K-type thermocouple were provided. One placed near the heating elements monitors the temperature of the heating elements to avoid fusing of the same in case of any short circuit due to liquid metal leak. The other is to control the heating rate depending upon the amount of metal inside the crucible.

15 Hp Motor: A three phase 15Hp motor is used to rotate the shaft which was submerged in the molten bath and rotated at a constant speed. The rotating of shaft needed a high torque motor to overcome the initial friction due to the density of the molten bath. But high torque motors have high RPM, in order to reduce the speed a DODGE speed reducer was attached in between the shaft and the motor as shown in the Figure 7.

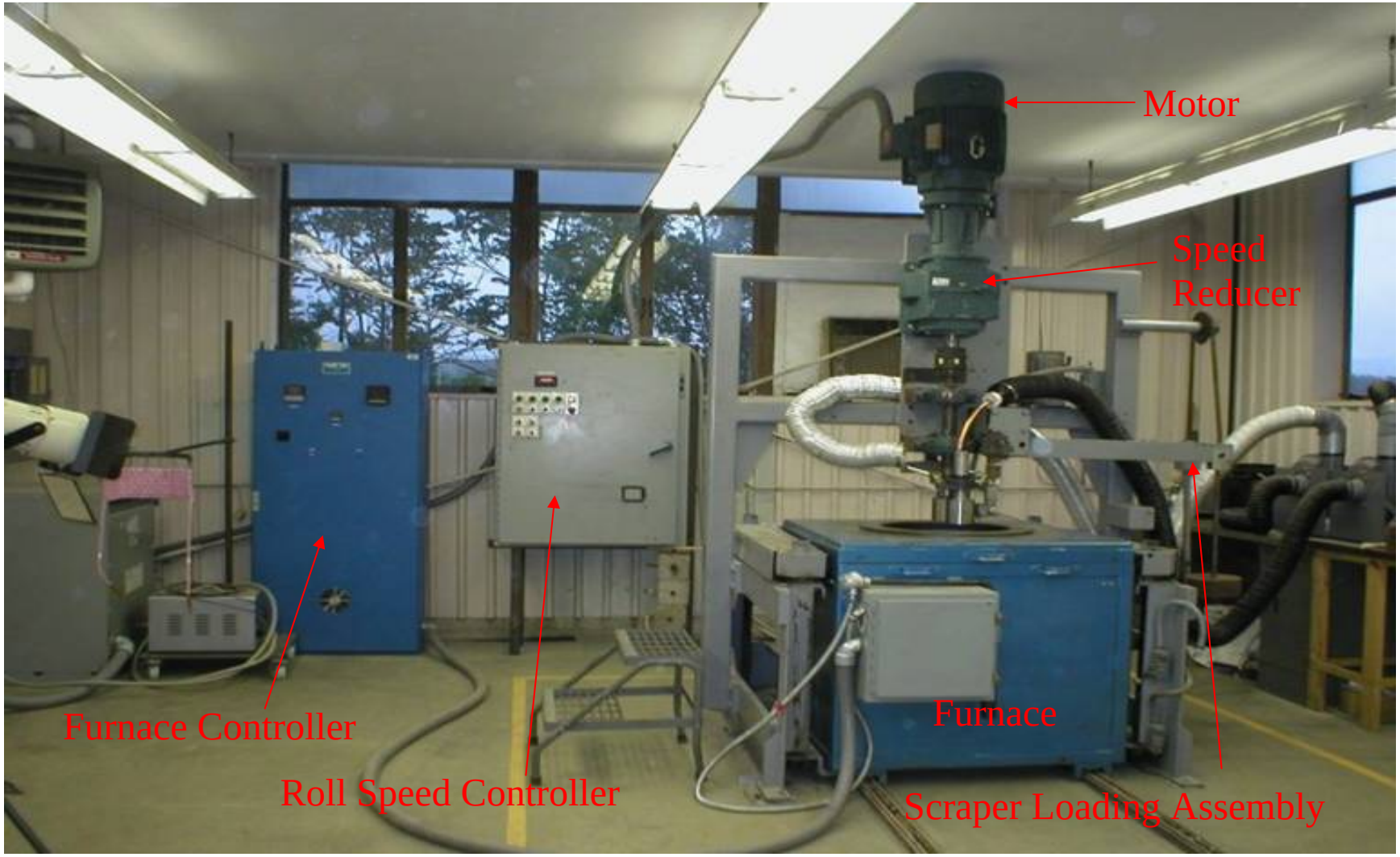

Figure 7: Dynamic Scrapper Wear Test Set-Up

Scraper Set-up: In CGL, the scrapers used are 320mm X 135mm X 40mm (12.6”x5.3”x1.6”) which are spot welded to the scraper arm. First the scraper was scaled down corresponding to the roll diameter and the space available in the bath, so that the scraper would come back to the rest position when the scraping action was completed, without damaging the crucible walls. Based on this consideration, the scraper was scaled down to 4”x 2.5”X 1” with an Ø0.5” hole on the top face as shown in Figure 8, so that they can be fastened and removed from the loading arm. The scraper is supported by two rectangular arms on either side with a spacer in the middle, so that the load applied is always on the tip of the scraper.

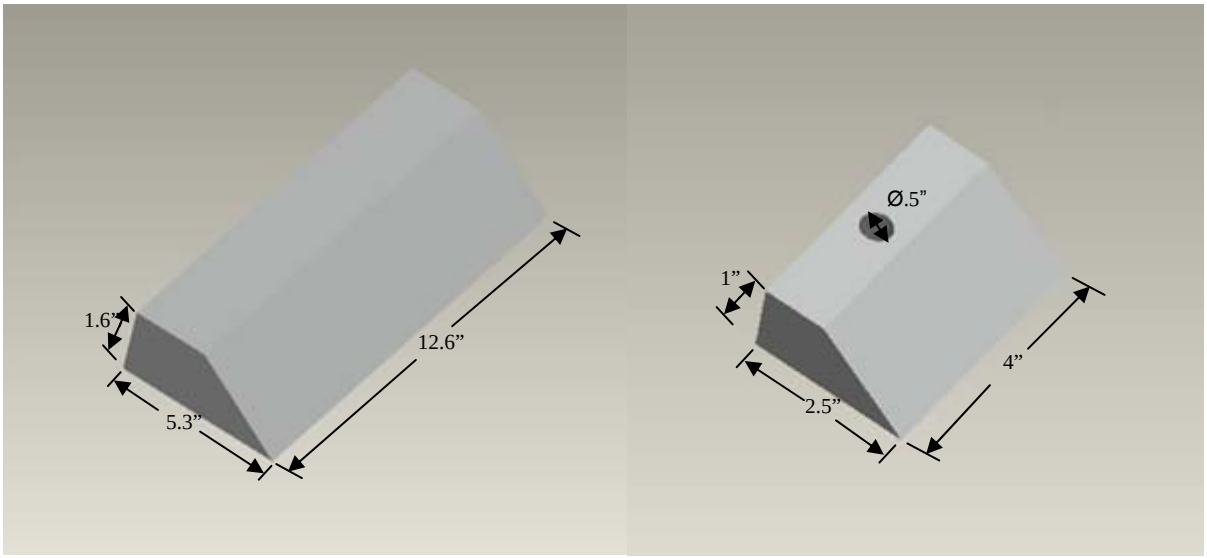

Figure 8: Actual and Scaled down Scraper Dimensions

Scraper Tip Overlay: Many hard or wear resistant materials can be considered for scraper tip overlay, but the important factor to be considered was that it must have high corrosion resistance in the Zn-Al environment at high temperatures and the corrosion products if formed must not alter the bath composition. Three such alloys are commonly used for pot hardware. Their composition is shown in Table 2:

Table 2: Scraper overlay Composition (%)

	Stellite 21	Stellite 6B	T-401
Cobalt	59.25	53.90	60.50
Nickel	2.50 max	3.00 max	1.50
Iron	3.00 max	3.00 max	1.50
Carbon	0.25	1.10	0.3
Chromium	27.00	30.00	16.00
Manganese	1.00	1.00	
Molybdenum	5.50	1.50	16.00
Silicon	1.50	2.00	1.20
Tungsten		4.5	

Preliminary Test Start-up

A trial run was conducted to detect or correct any short comings. The roll shaft motor was started and allowed to rotate and adjusted for the set 108 RPM. The entire scraper assembly made up of 316L steel and a stellite 21 tip was coated with boron-nitride (BN) to avoid the corrosion attack on the scraper arms. The roll shaft and the scraper assembly which was submerged in the bath, was preheated to 1000^{o}F in order to avoid the thermal shock due to immersion. The test parameters and the conditions are given in the Table 3 below and Figure 9 shows the steps carried out before each test (assembly, dip-in, homogenizing).

Table 3: Test Conditions and Parameters

Bath Chemistry	Galvalume (GL) (55% Al, 1.6% Si, 43.4%Zn)
Bath Temperature	1200^{o}F
Roll RPM	108
Time for Initial Dross Build-up	~1 Hr
Scraping Duration	2 minutes every 30 minutes
Total Testing period	10 hours
Roll Material	309 Stainless steel
Scraper	Stellite 21 Overlay tip on 309 SS

(a) assembly **(b) Dip-in** **(c) Homogenizing**

Figure 9: Various Steps followed Prior Testing

4.3 GEPDSS

GEPDSS Version 1.0 allows the user to investigate the effect of improved pot hardware and/or improved process equipment in continuous galvanizing lines on detailed process oriented energy consumption [12,13]. It also allows the user to perform an economic analysis on energy efficiency measures resulting from improved pot hardware. The user is able to choose up to a maximum of three product types such as structural steel, anneal steel, and automotive steel and input the data regarding the energy consuming equipment specific to those individual process lines. Once data entry is completed on the energy costs and the capacities and utilization profile of energy consuming equipment on individual product lines (referred to as “processes” in GEPDSS), the user is able to input the production system parameters such as the details of each campaign identified by the date of the campaign, number of turns the campaign lasted, the amount of production achieved during the campaign, the amount of rejection during the campaign, and the reasons for the rejection or line stoppage in terms of pot hardware failure.

GEPDSS maintains a chronological record of each campaign on each product line and determine the energy consumption details during production and during downtime. GEPDSS allows the user to modify the production system parameters and energy parameters and investigate the effect on specific energy consumption (MMBtu/ton), economic desirability of investment in pot hardware, and do a comparison between different product lines.

The performance criteria for the model is how accurately it is able to compute the annual electricity and natural gas costs of a manufacturing facility that is engaged in the production of coated sheet steel products utilizing galvanizing lines. The annual energy costs for five galvanizing line facilities were compared with the results produced by GEPDSS. The model computation was within 5% of the actual results. In addition, the model's performance was analyzed by varying key parameters within reasonable ranges and the output parameters were checked for accuracy and reasonableness. This validation phase was extensive and involved a detailed set of virtual experiments that presented data for analysis.

The model has several inputs and produces a variety of outputs for analysis. The worksheet allows the user to enter the monthly energy consumption and costs that are obtained from utility. The two different tables for electric and natural gas uses this information to calculate the marginal $/MMBtu cost for each energy stream. The user enters the different coating processes, up to a maximum of three product (process) types. Also the user has to provide data pertaining to the production and shutdowns due to pot hardware failure in this worksheet. The user enters the information about all the energy consuming equipment that is used during a particular process and this information can be identified uniquely with three separate product types (processes). The user is provided with an option to select the process or make changes to existing energy consumption data. The options showing Process 1, 2 and 3 corresponds to the three product types (processes) or coating materials the user has earlier specified in Process/Product Details.

The user is provided with a sketch of the galvanizing line (for each process or product type) with energy consuming equipment listed on the diagram and their usage in MMBtu/hr or kW. This usage can be analyzed during production periods as well as during process downtime. The energy and power consumption by various equipment groups for a particular process can be analyzed in MMBtu/hr. This information is available for production as well as during downtime. Also the cost of energy, hydrogen and nitrogen consumption during production and downtime can be determined. Details of production and rejection for each process along with its natural gas consumption, electricity consumption, hydrogen and nitrogen consumption, their associated costs on a monthly basis is available for analysis.

A graphical representation of overall energy consumption, consumption by each equipment category, production data, and percentage of time each process is operating is generated. These graphical representations are available for each of the processes. Quantities of production and rejection, percentages of productive time, downtime, and other relevant parameters are reported. In addition, a data log of various shutdowns is stored for the user. This data log gets updated as the user fills in the process/product table. A modified internal rate of return (MIRR) is obtained, on investment for the new pot hardware. The user enters the capital and operating costs for the hardware as investment. Also the desired rate of return is specified by the user. Based on the increased annual production and energy savings obtained the modified internal rate of return is calculated on the investment.

This worksheet compares the existing scenario with the proposed scenario where the campaign period has increased due to better pot hardware material. The annual energy consumption, MMBtu/ton and annual production are obtained for both the cases and the energy and cost savings are also calculated. The user is able to investigate changes to the campaign time period

as to its effect on MMBtu/ton and total energy and cost savings to be achieved in incorporating long lasting pot hardware material.

The model is capable of accurately depicting the specific energy consumption and detailed natural gas and electricity consumption in galvanizing line equipment. It is capable of accurately determining the energy impact of any equipment level changes on the line, including improvement of the life of the pot hardware. The main weakness of the model is that it does not allow for varying process parameters on the line such as line speed, gage thickness, heat treat cycles, soaking time-temperature distributions, and continuous natural gas usage control systems in burners.

Initial visits were conducted to leading galvanizing facilities. The entire process and the basics of the continuous galvanizing process were studied thoroughly. A list of all the common equipment was documented. The energy intensive equipment and energy consumption points were noted. The systems development was completed and the details of the systems diagram are shown in Figure 10.

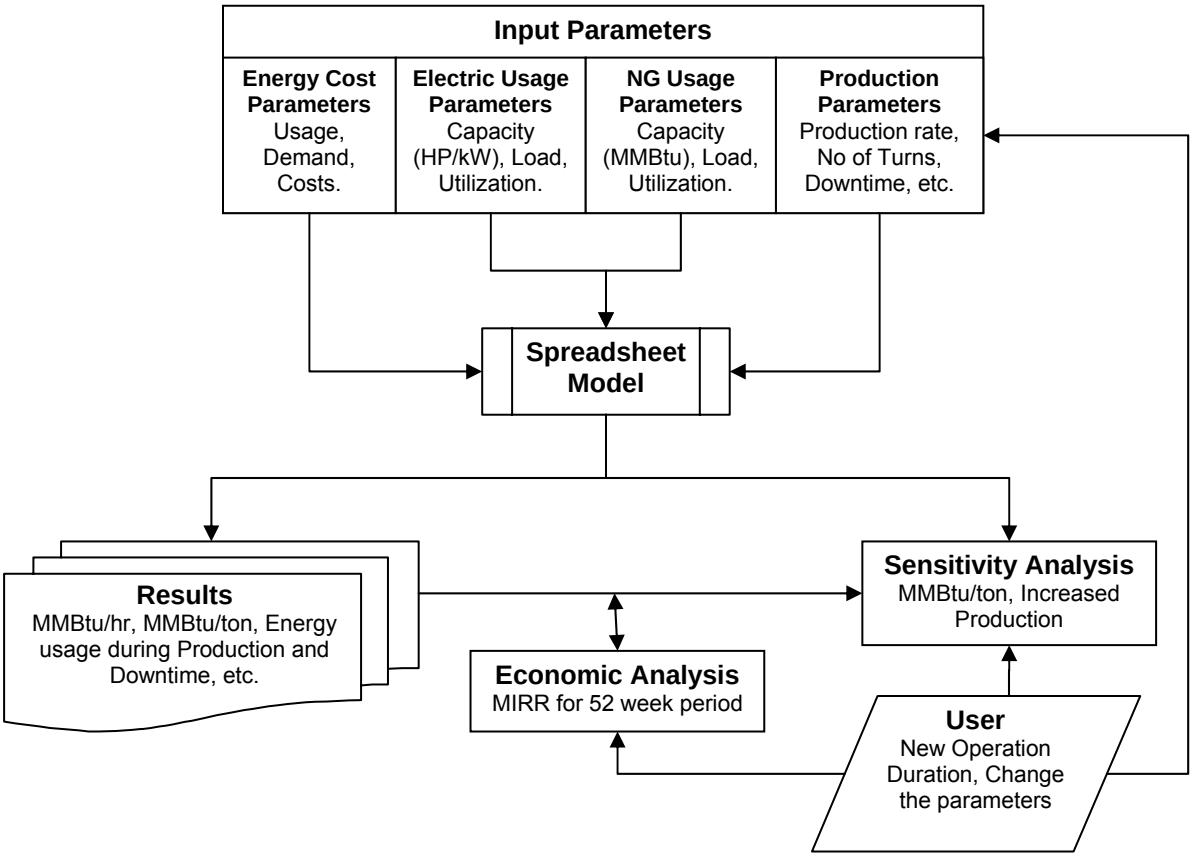

Figure 10: System Diagram

Table 4 shows an example of the list of equipment and energy specific equipment aspect points generated from the initial site visits. The plant personnel were interviewed to get details of general shop floor practices, production schedules and maintenance plans. Information regarding bath hardware, bath chemistry and issues relating to the service life of the hardware was discussed with plant personnel. Using all the data collected from visits, and referring to the literature describing continuous galvanizing practices, a list was prepared, which consisted of all

of the different equipment that is used in continuous galvanizing in the order of the process flow. Figure 11 summarizes the research approach.

Table 4: Sample list identifying energy intensive equipment, type of fuel, point of usage

Sr. No	Equipment	Fuel Type	Point of Usage
1	Payoff reel mandrel	Electric	Motor
2	Welding m/c	Electric	Welder
3	Accumulator	Electric	Several DC Motors
4	Annealing Furnace	Natural Gas (Supporting gases: N2, H2)	N.G. Burners
5	Cooling Tower	Electric	Fan Motor
6	Zn pot	Electric	Induction pot
7	Line motors to pull strip	Electric	DC Motors
8	Air knifes	Electric	150 HP Blower
9	Temper Mill	Electric	Motors
10	Miscellaneous pull motors / equipment	Electric	Motors
⋮	⋮	⋮	⋮

The generated equipment list was utilized in the process of analyzing the operational characteristics of each piece of equipment. For example, for the Payoff Reel, its application, and the operational aspects of the governing motor drive was studied in terms of energy consumption. Similarly, the second equipment-annealing furnace was selected, its application analyzed and the energy consumption details examined in terms of the natural gas burner. The process was repeated for all the equipment present in the list. Table 5 shows an example of data collection form for natural gas equipment. Table 6 shows an example of the data collection form for various electric motors.

Table 5: Example of Survey Form for Different Natural Gas Equipment

Equipment Name	MMBtu/Hr or SCFH for each Burner	Number of Burners with same capacity	Load Factor (%)	Utilization Factor (%)	Recuperator (Yes/No)	Status during downtime (On/Pilot/ Low Fire)	Load Factor During Shutdown (%)
Pre-Heat Section	0.24	24	80	100	Yes	ON	20

Table 6: Example of Data Collection Sheet for Electric Motors

Equipment Name Containing the Motor							
HP	**No. of Motors of Same HP**	**Load Factor (%)**	**Utilization Factor (%)**	**# of Standby Motors**	**Are the motors running during Shutdowns (YES/NO)**	**Load Factor During Shutdown (%)**	**Eff.**
60	2	60	80	1	NO	60	91

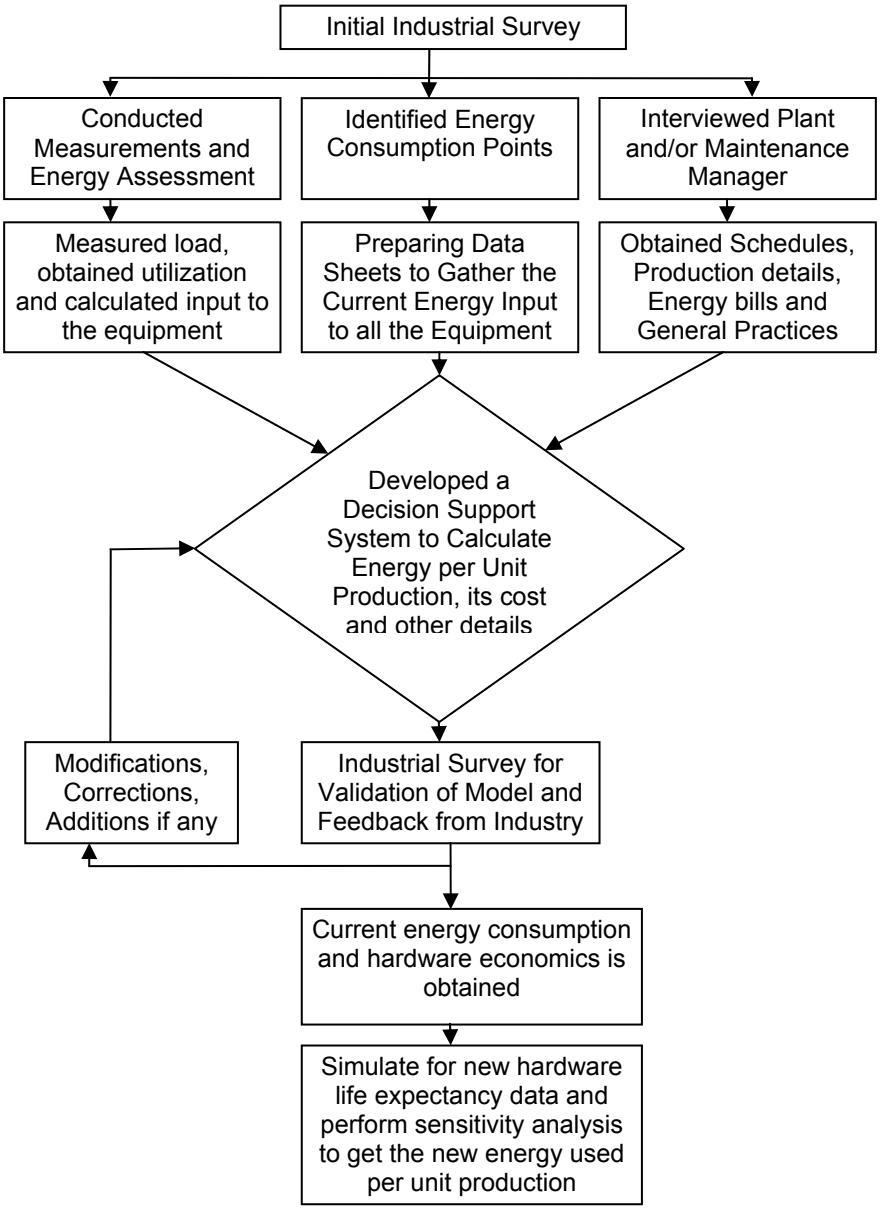

Figure 11: Research Approach

The model (GEPDSS) was developed to handle up to three different processes performed on the galvanizing lines. This resulted in development of four independent Excel™ files, each consisting of a number of Excel™ sheets. One file represents one particular process and each file consists of multiple spreadsheets called modules. These modules are interconnected with formulas and share data within the four Excel™ files. The handling of these four files was out of the scope of Visual Basic Application (VBA) in Excel™. Thus, an independent VB DOT NET program was developed that was capable of handling and accessing these Excel™ sheets while working out of Excel™ environment. Figure 12 shows the welcome screen of GEPDSS.

Figure 12: Welcome screen of GEPDSS

This screen has three sections, namely the input section, the analysis section and the results section. The input section is further divided into three major parts. The input screen for natural gas consuming equipment is shown in Figure 13. Similarly there are input screens for electricity consuming equipment, production rejection details, nitrogen hydrogen data and other equipment in the line. The software along with the detailed installation process is available for download at http://www.iofwv.nrcce.wvu.edu/industry_sectors/crosscut_areas/imf.cfm or by contacting Dr. Gopalakrishnan. The user may need to install supporting software called Microsoft Dot Net framework 2.0.

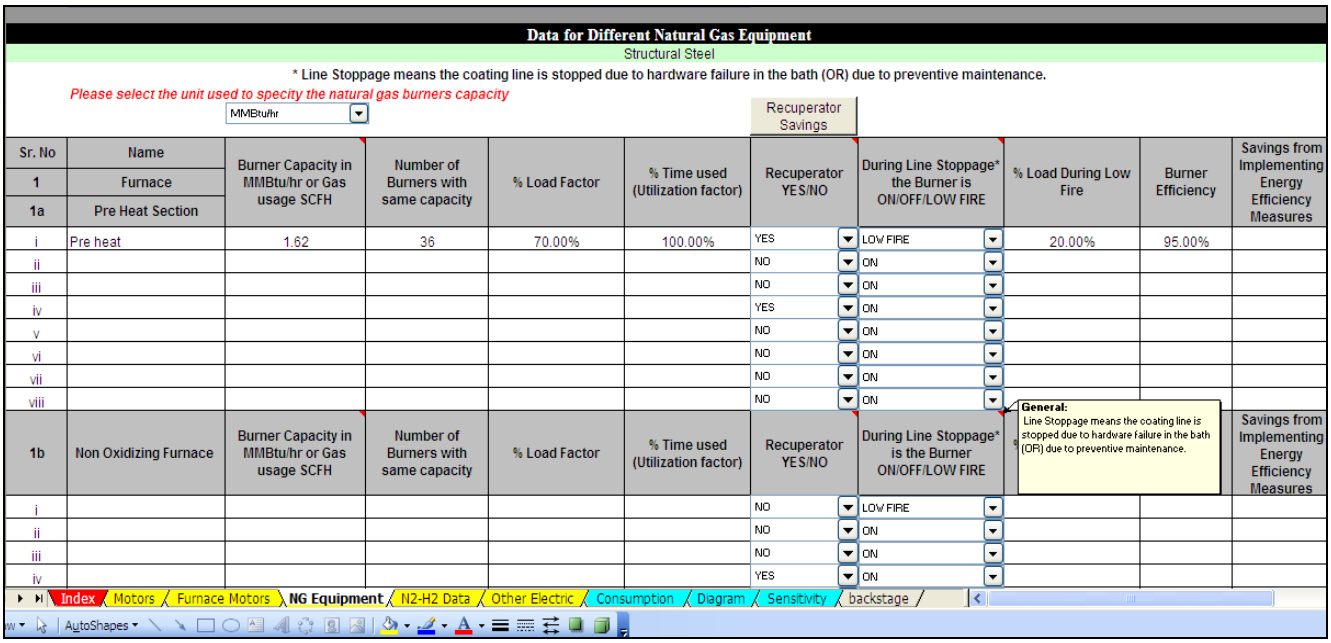

Data for Different Natural Gas Equipment

Structural Steel

* Line Stoppage means the coating line is stopped due to hardware failure in the bath (OR) due to preventive maintenance.

Please select the unit used to specity the natural gas burners capacity

MMBtu/hr

Recuperator Savings

Sr. No	Name	Burner Capacity in MMBtu/hr or Gas usage SCFH	Number of Burners with same capacity	% Load Factor	% Time used (Utilization factor)	Recuperator YES/NO	During Line Stoppage* the Burner is ON/OFF/LOW FIRE	% Load During Low Fire	Burner Efficiency	Savings from Implementing Energy Efficiency Measures
1	Furnace									
1a	Pre Heat Section									
i	Pre heat	1.62	36	70.00%	100.00%	YES	LOW FIRE	20.00%	95.00%	
ii						NO	ON			
iii						NO	ON			
iv						YES	ON			
v						NO	ON			
vi						NO	ON			
vii						NO	ON			
viii						NO	ON			

General: Line Stoppage means the coating line is stopped due to hardware failure in the bath (OR) due to preventive maintenance.

1b	Non Oxidizing Furnace	Burner Capacity in MMBtu/hr or Gas usage SCFH	Number of Burners with same capacity	% Load Factor	% Time used (Utilization factor)	Recuperator YES/NO	During Line Stoppage* is the Burner ON/OFF/LOW FIRE	Savings from Implementing Energy Efficiency Measures
i						NO	LOW FIRE	
ii						NO	ON	
iii						NO	ON	
iv						YES	ON	

Index | Motors | Furnace Motors | NG Equipment | N2-H2 Data | Other Electric | Consumption | Diagram | Sensitivity | backstage

AutoShapes

Figure 13: Input for natural gas consuming equipment

4.4 Refractories

4.4.1 Survey

The intent of this survey was to determine (1) typical life of refractory linings and tundishes for molten metal and glass containment applications, (2) the presence and type of any surface treatments applied to refractory linings, (3) the typical modes of failure for refractory linings and tundishes, (4) typical criteria for the “end-of-life” determination regarding failed refractory linings and tundishes, and (5) availability of materials from in-plant production hardware for microstructural characterization of failure mechanism(s). The survey was prepared by WVU, with input from ORNL and UMR, and distributed to companies representing the aluminum, glass, metal casting, and steel industries. Twenty-two companies, including international companies, returned surveys: eleven from the molten bath hardware consumers (including Galvanize, Galvanneal, and Galvalume lines), five from the refractory consumers and six from the refractory producers.

4.4.2 Post-mortem Analysis

Early in the project, while multiple metal handling processes were still being considered, several refractory materials provided by the industrial in-kind partners were analyzed. These metal processes were later removed from consideration when the project focused its efforts on the aluminum and galvanizing industries.

Test specimens were evaluated by a combination of methods including reflected light microscopy, transmitted light microscopy, cathode luminescence, and Scanning Electron Microscopy (SEM) for morphological and phase analysis. X-ray diffraction was also used to identify the phases present before and after service or before and after testing. Energy dispersive spectroscopy (EDS) was used to determine the elemental composition of individual phases/corrodents and inductive coupled spectroscopy was used to determine the chemical composition of the bulk samples.

The key salvaged materials analyzed during this project were high alumina (>80 % Al_2O_3) and Al_2O_3-SiO_2 (50-60 % Al_2O_3) spent castable refractories obtained from a natural gas fired reverberatory aluminum alloy melting furnace of a small engine manufacturer after three years of service processing a 3000 series aluminum alloy. Degradation mechanisms present in the salvaged material were ascertained by the analysis methods identified above. All samples were taken below the metal line from large blocks or masses of spent refractory lining that were in direct contact with the molten aluminum alloy. Samples were first cut in half to visually identify any variation in color and macro-structures, then photographed for a record of sampling location. Samples analyzed are shown in Table 7.

Table 7: Salvaged Refractory Samples from Small Engine Manufacturer Furnace
(Full description of this analysis will be published in an article accepted by *The International Journal of Applied Ceramic Technology* [5].)

Sample ID	Description	Location
Sample-1A	Light reddish-tan in color, mullite castable, not in contact with alloy	Cold side behind metal penetration
Sample-1B	Light tan to yellow in color, mullite castable, not in contact with alloy	Hot side behind metal penetration
Sample-2A	Intense reddish-tan in color, mullite castable, not in contact with alloy	Cold side behind metal penetration
Sample-2B	Light tan in color, mullite castable, not in contact with alloy	Hot side behind metal penetration
Sample-3	Light tan in color, high alumina castable, in contact with alloy with 1-cm thick metal-penetrated black zone	Hot face in metal penetration region
Concretion	Deposit of frozen aluminum alloy with corundum accretion from furnace sidewall	Refractory surface deposit
Mushroom	Sidewall refractory with thin black coating	Metal penetration region

Samples were analyzed from areas behind the metal penetration zone, in the metal penetration zone, and from surface deposits. Areas in worn or reacted zones were studied along with areas in zones thought to be near virgin. Compositions of the refractories were identified, along with binder phases and additives present.

Missouri S&T performed post mortem analysis, in collaboration with ORNL, of refractory specimens from testing in other tasks of the project. Analysis was performed by optical microscopy, scanning electron microscopy, Cathodoluminescence microscopy and Energy Dispersive Spectroscopy. The goal of this analysis was to identify the corrosion and failure mechanism(s) limiting the life of the parts and to determine any effects of exposure to elevated temperature during the thermal conductivity testing. The outcome of this analysis was used to set the direction for development of materials throughout the project.

Upon completion of static cup testing, the cups were cut along the cross section to study penetration. Based on visual observation of the penetration and its effects, tested materials were then ranked in order of resistance to penetration. See Figure 14 below.

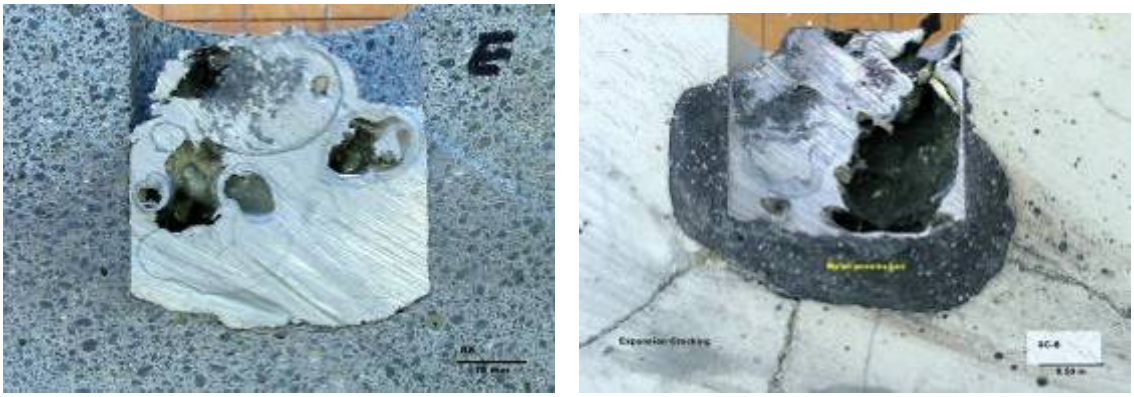

Figure 14: Cross Section after cup testing. Left – Good Material; Right – Weak Material

A piece of the refractory was then selected for microscopy and cored out of this cross-section. It was then mounted in epoxy and prepared for microscopy after multiple stages of grinding and polishing. A typical microscopy sample is seen in Figure 15. It includes all the phenomena occurring in the sample during cup testing such that the material can be completely analyzed during one microscopy event.

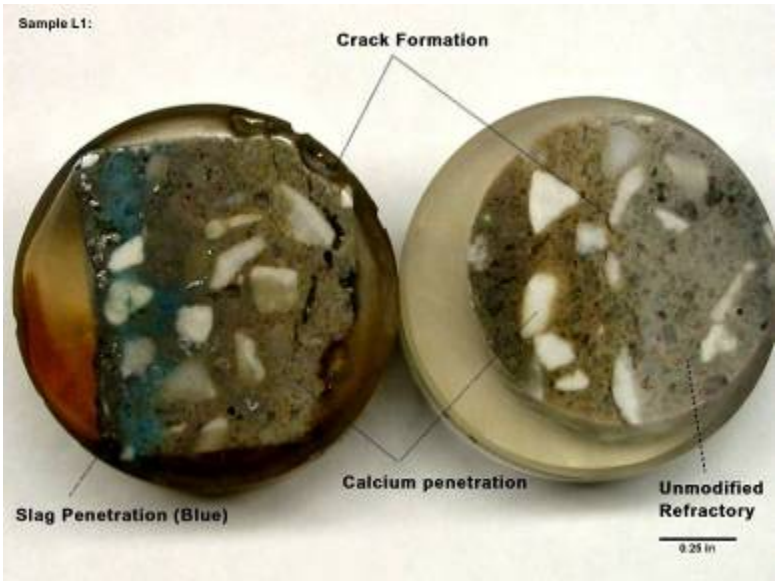

Figure 15: Typical Microscopy sample ready for analysis

Scanning Electron Microscopy, Energy Dispersive Spectroscopy and Cathodoluminescence Microscopy were performed on all tested materials.

4.4.3 Materials Testing

Static and dynamic corrosion testing of currently used materials in molten aluminum, a molten metal selected by metal casting industry, and in Zn-45% Al were performed. The same containment and hardware materials were also subjected to sessile drop wetting studies in the same metal/alloy systems. Through this testing, an understanding of the corrosion and wear mechanisms associated with molten metal contact was sought and areas for improved materials development were defined. Since refractory materials also provide thermal insulation, thermal conductivity measurements were also performed utilizing a newly developed experimental technique that allows measurement on bulk refractory materials.

Static laboratory corrosion testing was performed at ORNL on refractory samples obtained from Fireline (dipped in pure aluminum at 700°C). Tests were conducted for 500 and 1000 hours. Testing was also performed in a more corrosive aluminum alloy (7075) provided by industrial partners. Results of testing were shared with industrial partners. XRD analysis techniques were used to analyze samples of castable refractory. The composition of virgin materials provided a basis for comparison with *postmortem* analysis data from materials analysis and analysis of corrosion samples.

Missouri S&T (formerly UMR) conducted simulative static corrosion testing of existing refractories used for molten aluminum alloy (AL 5083) handling. Static corrosion testing was performed by the cup testing method. Test materials were provided by in-kind partners (Kyanite Mining and MORCO) and were received either in the form of 55 lb bags or 9-in straight bricks. Castable materials were cast into 9-in straight brick shapes using the prescribed water content and firing schedule. The designation for samples has been made using an internal system of identification to protect the identity of the provided materials.

Sample preparation is shown schematically in Figure 16. All materials received from in-kind partners were made into standard 9-in straight bricks (9” x 4.5” x 2.5”). These bricks were then machined into cup test specimens as shown in Figure 16. Each brick was cut into half and each section was machined to accommodate an aluminum alloy plug for the static cup tests. For this purpose, a 1.5” diameter hole was cored into the sectioned brick piece to a depth of 1.5”.

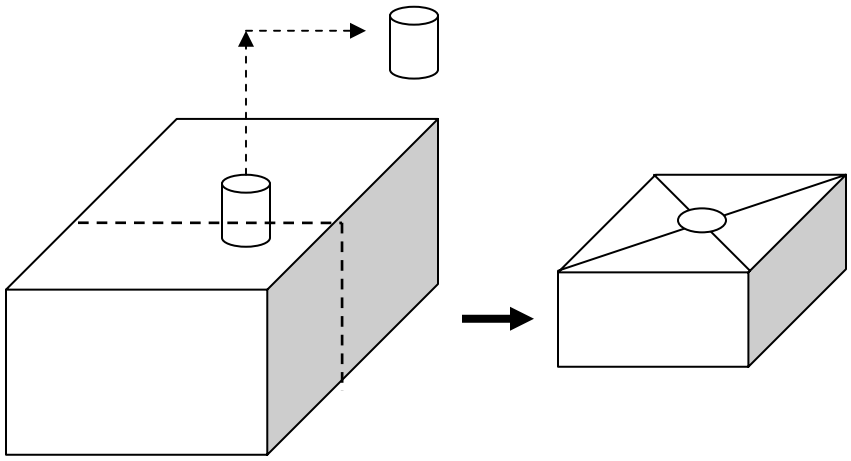

Figure 16: Machining Process to Prepare Refractory Sample for Static Cup Testing

The cored out piece was used to measure the materials apparent porosity and bulk density using appropriate ASTM standard test. The following tests were performed on all received materials

- Bulk Density and Apparent Porosity as per ASTM C 830
- Static Cup Testing (Task 2.1.1)
- Post Mortem Analysis (Task 2.1.4)
    - Scanning Electron Microscopy
    - Cathode Luminescence Microscopy
    - Energy Dispersive Spectroscopy

The parameters for static cup testing were determined with the intention of simulating an aggressive furnace environment. Existing test parameters based on the "ALCOA 72 hour test" were found to be insufficient to aggressively test modern refractory materials, therefore a new test was developed with the highlights of the new static cup testing parameters shown in Figure 17.

- Heat and to 1200°C and pre-oxidize sample for 5 hours
- Cool to 1000°C
- Cold Al 5083 plug introduced at 1000°C
- Hold at 1000°C for 10 days (240 hours)
- Steam atmosphere maintained during entire test.
- Cool to room temperature

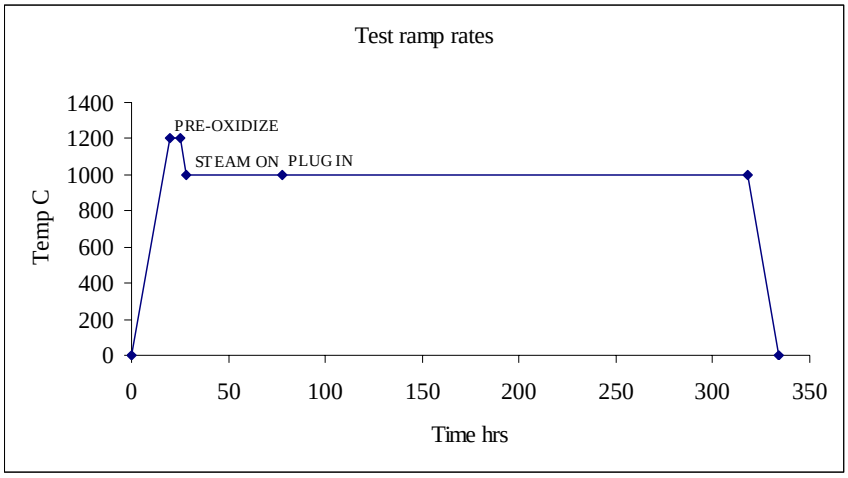

Figure 17: Test Ramp Rates for 10 Day Static Cup Test

Static corrosion data was used as a screening test to select materials meeting or exceeding the project goals and to down-selected materials for dynamic testing in the laboratory. Dynamic corrosion testing was used to measure the corrosion rates under conditions similar to those found in molten metal baths along with wear resistance when coupled with applied force.

Materials that were found to meet or exceed the dynamic corrosion and wear data goal for the project were then down-selected for in-plant testing. These tests involved fabrication of larger samples than coupons and the required fixturing for immersing them in production bath environments. Such tests were conducted at various plants, with exposed samples analyzed for corrosion data and phase formation information.

4.4.4 Thermal Conductivity Testing

For refractory lined vessels, it is generally desired to minimize transmission of heat from the inside to the outside. Therefore, a material with low thermal conductivity is necessary [3]. In other areas of the process, materials with high conductivities may be required to pull heat away from a part or piece of hardware. Therefore, an accurate characterization of thermal conductivity over the entire process temperature range is needed for candidate molten metal handling materials. Since mechanisms of heat transfer also vary with temperature, it is of further importance to characterize materials over a range of temperatures [4]. At the time this project was started, measurement of thermal conductivity of refractory materials at elevated temperatures was limited to small sample sizes (laser flash) or antiquated methods (hot wire, guarded hot plate) which have their own inherent problems. To address this problem, a new method was developed at ORNL to utilize the High Intensity Infrared lamp located there for the measurement of thermal conductivity of bulk refractory samples over a range of elevated temperatures.

The new method for measurement of thermal conductivity of refractory materials at elevated temperatures developed at ORNL is based on the theory of the laser flash method, but is capable of measuring samples on the order of 200 x 250 x 50 mm at temperatures up to 1000^{o}C. To this end, a method was developed utilizing the high-intensity Infrared (IR) source housed at ORNL. This unique instrument is capable of generating extremely high power densities, on the order of 3.5 kW/cm^2, using a single lamp. This makes the lamp ideal for heating a material to high temperatures along with providing concentrated heating to a sample in very short periods of time. Therefore using a single instrument, a refractory sample could be heated to a specified test temperature and then tested at that temperature.

Testing is performed by “flashing” the brick surface in a fashion similar to the laser flash technique. Yet, as opposed to the small spot area (≈10 mm^2) sampled by the laser flash technique, a large surface area (200 x 250 mm) is heated using the IR source. Additionally, due to the high power density of the IR lamp, thickness of the refractory brick is not a limitation and samples up to 50 mm in thickness (compared to 2 mm for the laser flash method) can be measured (dependent on conductivity of the sample). An infrared camera focused on the back surface of the refractory is used to measure the temperature increase due to the thermal flashing and the subsequent heat flow through the refractory brick can be calculated using software developed by ORNL.

The test sample is heated within a refractory furnace box shown schematically below in Figure 18. This box consists of SALI® board insulation on the top and bottom and Watlow® furnace elements comprising the sides of the box. The base of the box is constructed of steel plate to provide rigidity. A quartz window is incorporated into the top of the box to allow penetration of energy from the IR lamp and a slide port exists in the bottom insulation and metal plate to allow access for an IR camera during testing. An additional SALI board panel can be used over the slide port to provide insulation during heating and when measurements are not being made.

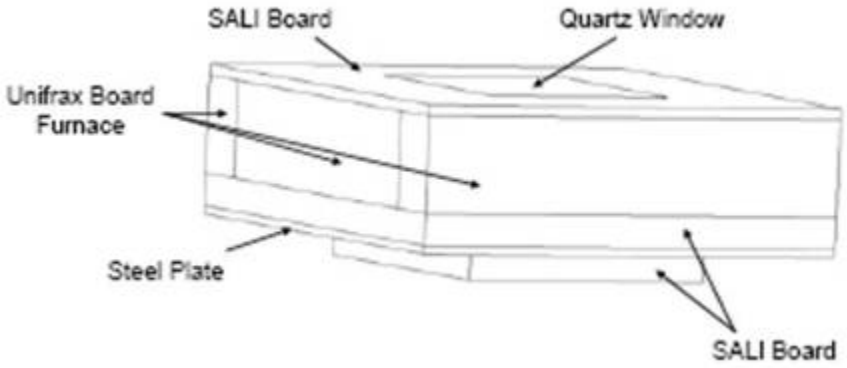

Figure 18: Refractory Furnace Box

A schematic of the entire test system is shown below in Figure 19. The conductance of the thermal wave generated by the IR lamp is captured by a high-speed IR camera focused on the rear surface of the brick. Temperature changes across the entire sample can then be monitored in this fashion. At the heating surface, the IR camera can be set-up to take four images per heating cycle. (See Figure 19 below) A lock-in thermal wave technique developed at ORNL is then used to generate phase and amplitude images of the sample. These images are further processed to generate thermal diffusivity or thermal conductivity maps of the brick. These processes can also be automated to simulate thermal aging of the refractories. Although the current system is limited to ≈1000°C, with proper design of the IR window and filtering system, it is expected that measurements of thermal conductivity could be collected up to temperatures on the order of 1400-1600°C.

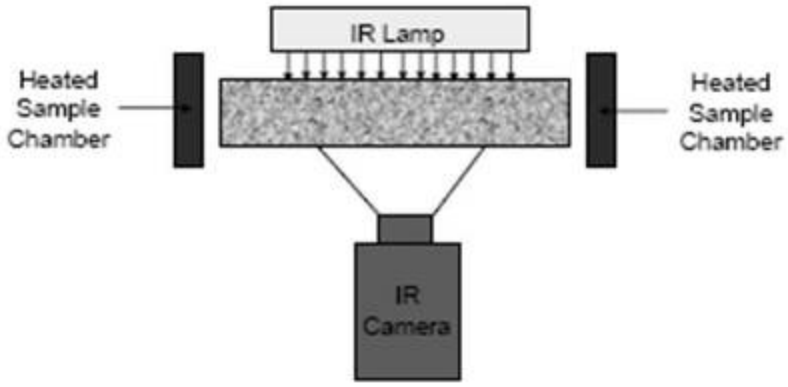

Figure 19: Schematic of IR Camera Set-Up

Thermal diffusivity values are calculated using the "half-rise-time" method which evaluates the time required to reach half the maximum signal intensity ($t_{1/2}$). The heat loss parameter, k is then calculated using:

$$k = A + B*(t_{0.75}/t_{0.25}) + C*(t_{0.75}/t_{0.25})^2 \qquad \textbf{Equation 1}$$

where: A = -0.3461467
B = 0.361578
C = -0.06520543
$t_{0.25}$ = time required to reach 25% of maximum value
$t_{0.75}$ = time required to reach 75% of maximum value

Using equation 2, the thermal diffusivity (α) can be calculated using:

$$\alpha = \frac{k * L^2}{t_{1/2}} \qquad \textbf{Equation 2}$$

where: k = heat loss parameter from Equation (1)
L = sample thickness
$t_{1/2}$ = half-rise-time

This can be found in reference 6.

4.4.5 Development of Refractory Corrosion Model

The purpose of this research was to develop a dynamic corrosion model for refractory materials of interest in this project. Up to now, there has not been a generalized dynamic corrosion model available, although corrosion models for individual situations have been proposed during the past decades. This is largely due to the lack of common corrosion mechanisms present across the different industries. In this task, attempts were made to formulate a comprehensive dynamic corrosion model and to develop a materials corrosion database based on the experimental data obtained by ORNL and UMR during this project. Data from the supporting refractory organizations and found in literature was also used to supplement the experimental data. Materials modeling and corrosion database predictions, along with experimental data from the project, was then used as the basis of subsequent refractory and coating/surface treatment design.

4.4.6 Thermodynamic Refractory Calculations

Three analyses were performed at ORNL to evaluate the energy savings possible due to improvements made in refractory materials as developed by this project.

The first analysis was performed using the DOE software tool PHAST. This analysis assumed a hypothetical reverberatory furnace in an Aluminum plant with energy coming from electricity, natural gas, and steam. The furnace was water cooled with dimensions of 20 x 12 x 16 feet and an internal temperature of 1038^{o}C (1900^{o}F). Dual layer refractory was used on the top and sides of the furnace consisting of low/ultralow cement castable and insulating fire brick on the top and fireclay brick and insulating fire brick on the sides. The bottom was insulated with castable. Improvements in wall losses through better insulation, improvements in net and gross heat required by the furnace, energy used and thermal efficiency were all calculated.

The second analysis was performed using basic heat transfer theory as shown in Figure 20 below. Calculations were performed assuming a three layer refractory wall. Thermal conductivity and thickness of each layer were changed to evaluate different wall constructions. Heat flux through the wall was also calculated.

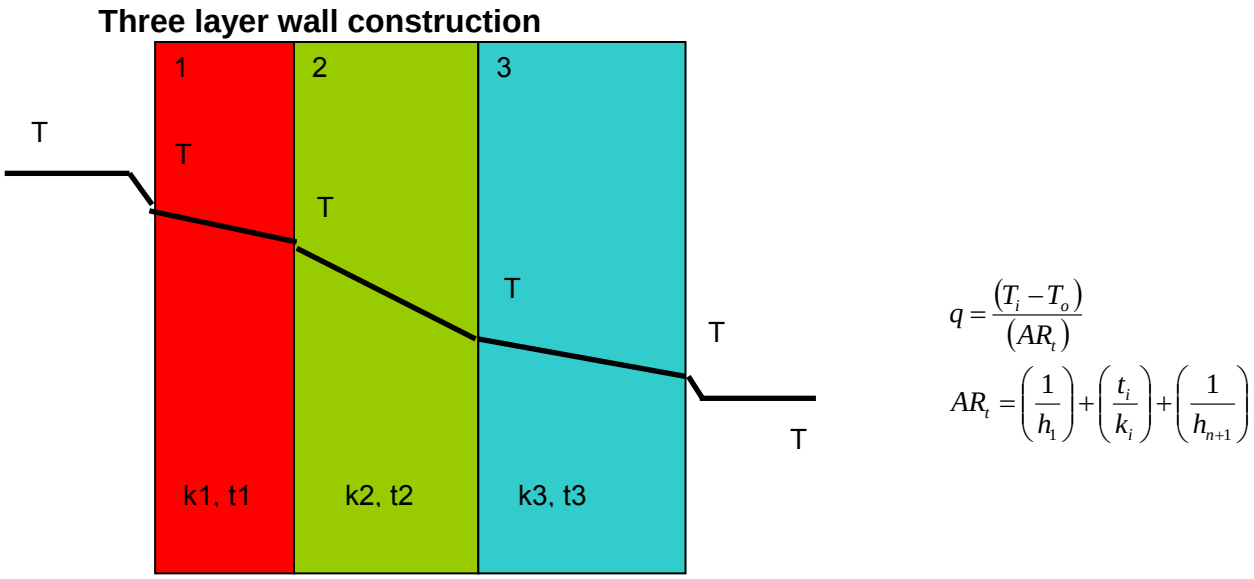

Figure 20: Heat Transfer Theory

Heat flux (q) was calculated based on the internal furnace temperature (T_i), the external ambient temperature (T_o), the area of refractory (A), and the thermal resistance of the refractory layers (R_t). The product of the refractory area and thermal resistance (AR_t) can be further reduced to a summation of the heat transfer coefficients at the inside ($1/h_1$) and outside surfaces ($1/h_{n+1}$) and the thickness and conductivity of each refractory layer (t_i/k_i).

The final analysis was conducted using the DOE software tool, 3E Plus to produce estimates of energy savings possible through the use of improved refractory materials. Estimates obtained using the 3E Plus software were validated against previous predictions obtained using the PHAST tool and predictions made using heat transfer theory. Initial estimates were made using values generated for the TCON® TC1 and TC2 materials along with estimates of the bonite castable conductivity to estimate the furnace surface temperature, heat losses, and thermal efficiency of a candidate refractory wall composed of these materials. An additional analysis was later carried out using the DOE software tool, 3E Plus to produce estimates of energy savings possible through the use of improved refractory materials using experimental values generated for both the TCON® materials and the bonite castable conductivity to estimate the furnace surface temperature, heat losses, and thermal efficiency of a candidate refractory wall composed of these materials.

A separate task was undertaken to use thermodynamic modeling as a tool to predict the phase formation when liquid metal comes in contact with the refractory lining. Calculations were performed based on the experimental data provided ORNL and UMR and on data found in the literature. This model was then used to predict the phase formation for currently used materials. The model output, once verified, was used to explore new materials and to select suitable refractory material to meet at least one of the following criteria:

1. react with the environment to form protective surfaces in-situ
2. are functionally graded to give the best combination of thermal, mechanical and physical properties and chemical stability
3. are relatively inexpensive, reliable materials

Thermodynamic considerations:

Thermodynamics can be used to effectively describe the deterioration process of a refractory lining in contact with molten metal by considering the chemical resistance of an oxide to molten metal attack as expressed by the general equation for a refractory metal oxide MO_x in contact with aluminum.

$$3MO_{x(s)} + 2xAl_{(l)} \rightarrow 3M + xAl_2O_{3(s)} \qquad \textbf{Equation 3}$$

As a general guideline, all materials in the electrochemical series of metals will be reduced by metals below themselves in the series. Therefore, it can be safely estimated that all of the common refractory oxides will be reduced by molten aluminum; i.e. they are thermodynamically unstable. From the electrochemical series, the presence of alloying elements like Mg and Ca will contribute towards a more aggressive chemical environment and make the refractory oxides further unstable.

The Gibbs free energy of a reaction gives a thermodynamic measure of the driving force for a reaction to occur spontaneously. When this free energy is below zero, the reaction is said to be spontaneous. Thus, if a metal-refractory interaction is expressed in the form of a reaction, and has a negative free energy, then the products of that reaction can be considered to contribute towards deterioration of the refractory lining. These reactions can be put in to a thermodynamic analytical software package such as FactSAGE to simulate the equilibrium reaction products so that the associated free energy values can also be calculated.

Aluminum + Refractory = Corundum + Reduced metal compound Equation 4

As a basis for modeling, it was attempted to simulate within FactSAGE, the interaction between one mole of alloy and one mole of a refractory ingredient. The alloy in this case was a mixture of 95% Al and 5% Mg by weight. Hence the alloy basis for modeling is 0.94479 Al + 0.05521 mol Mg. It was previously attempted to model the entire refractory mix; however, this was not feasible owing to the large number of components in a typical refractory mix.

4.4.7 Identification of New Materials

Based on the understanding of corrosion damage mechanisms and ThermoCalc™ modeling, new material systems were identified as a base. The base system was then further modified for its multi-functionality through the concept shown in Figure 21. The new refractory systems were then designed and prepared into coupons for corrosion, wetting testing, and thermal conductivity measurement.

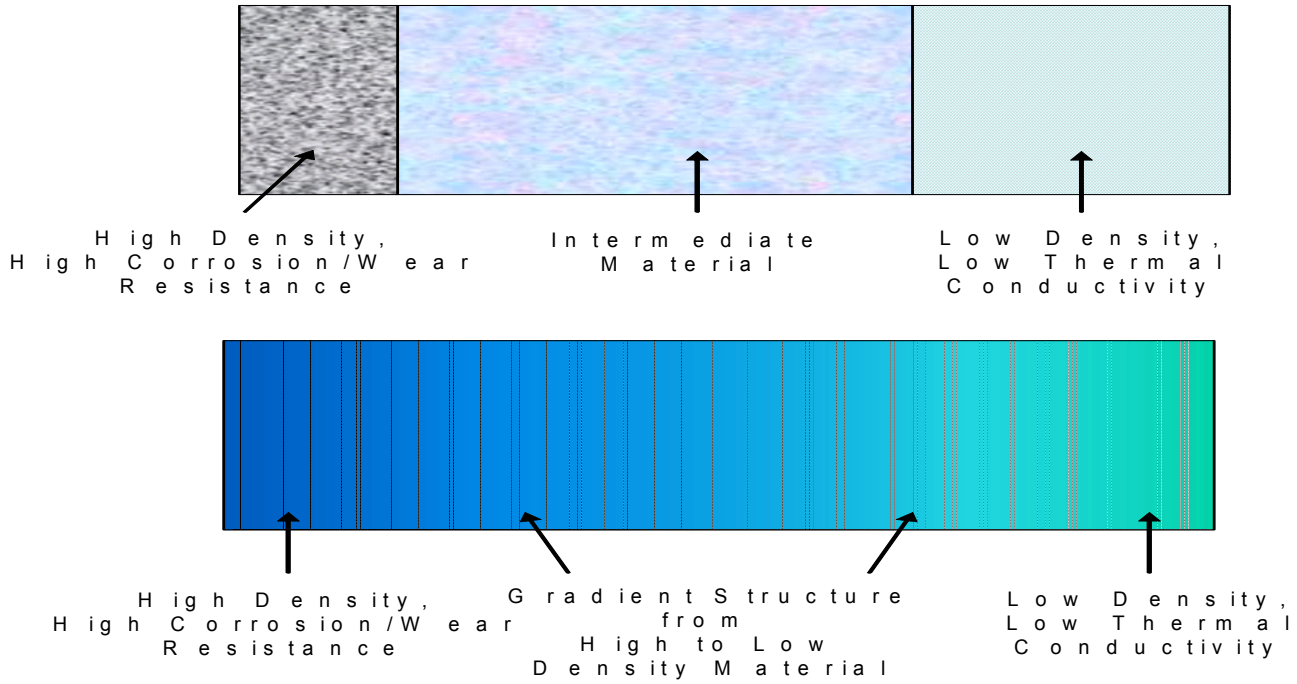

Figure 21: Various Composite Lining Systems Found

4.4.8 Refractory Component Testing

The best performing materials based on static and dynamic corrosion testing and wear testing were fabricated into prototype components. The prototype components were fabricated by the supplier companies and evaluated by steel or aluminum companies. After testing, the prototype components were removed from service and characterized for corrosion, wearing resistance and micro-structural changes.

Energy Industries of Ohio (EIO) was selected as the site of the first industrial test of the refractory materials (TCON® and bonite castable) developed through this project. Full industrial trials were planned for Pennex Aluminum near Philadelphia, PA and several other aluminum plants in Kentucky and Ohio. Additionally, independent trials were pursued by Fireline and MORCO on the TCON® and bonite materials, respectively. Also, ORNL was approached by several domestic and foreign aluminum manufacturers for further information on the materials developed under this project following the publication of the *ITP E-bulletin* highlight on the refractory side of the project (August 2007) and the associated articles published by ASM International (e-newsletter) and in the *American Ceramic Society Bulletin*.

EIO conducted the first industrial trial. For the EIO trial, a small melter (shown in Figure 22) was lined with six 0.63" TCON® plates (shown in Figure 23) backed by bonite castable. An alumina crucible (20" diameter, 23" height) was lined with the TCON® and bonite materials and used to melt and contain 5083 aluminum alloy (composition shown in Table 8). The plates were designed to fit together (the six forming a solid ring) and embedded in bonite castable to form a corrosion/wear resistant zone at the top of the crucible along the metal line. The remainder of the crucible (below the metal line) was lined with only bonite castable. This created a vessel with a volume of 4,021 $in.^3$ (16" dia., 20" height).

Figure 22: Small Melter

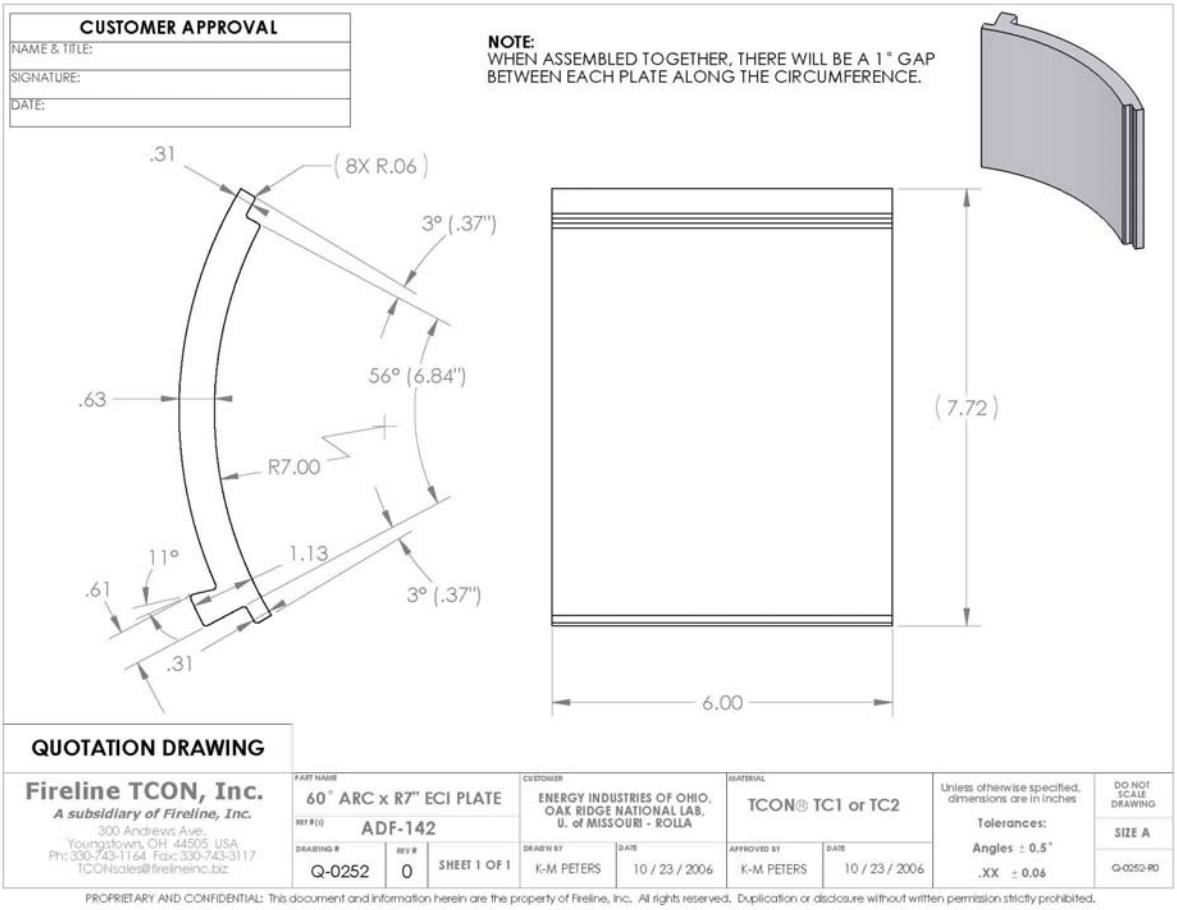

Figure 23: Conceptual Drawing of TCON® Plates

Table 8: Chemical Composition of Aluminum 5083 Alloy

Component	Al	Cr	Cu	Fe	Mg	Mn	Si	Ti	Zn
Wt. %	92.4 - 95.6	0.05 - 0.25	Max 0.1	Max 0.4	4 - 4.9	0.4 - 1	Max 0.4	Max 0.15	Max 0.25

Prior to installation, finite element modeling was performed to estimate stresses expected due to thermal expansion and volumetric constraints. An example of the estimated stress distribution at 900^{o}C (values in MPa) is shown in Figure 24. Based on this information, final design details were determined for tooling and plates were produced by Fireline. Bonite castable was supplied by MORCO and metal for the trial was supplied by ORNL from metal previously supplied by various industrial partners.

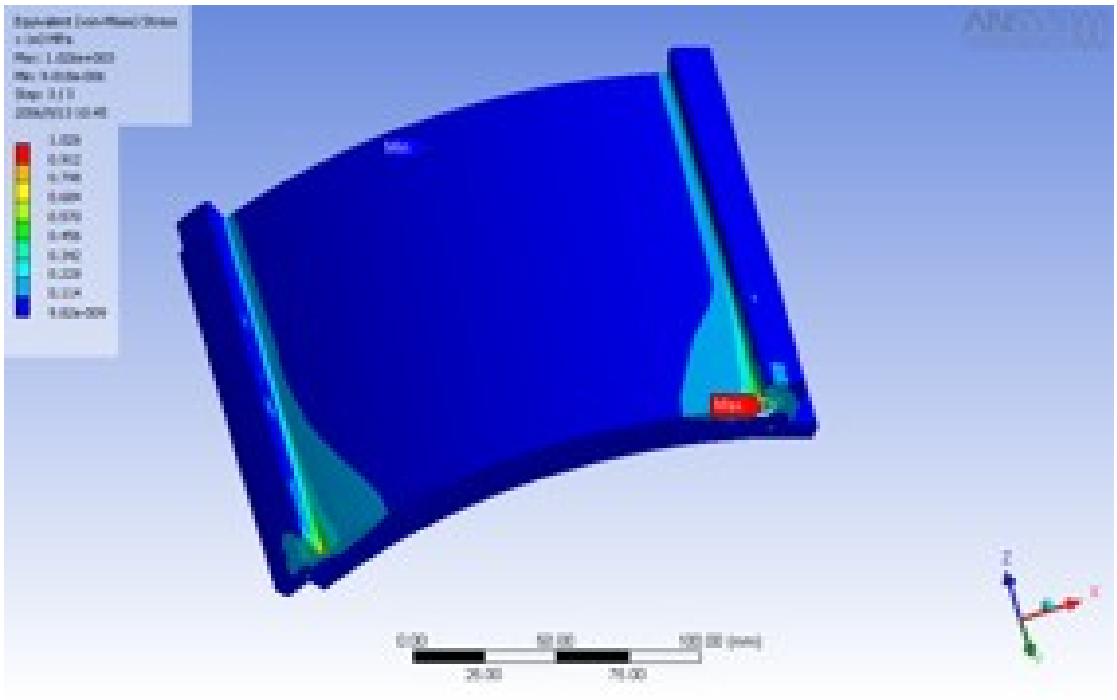

Figure 24: Example of the Estimated Stress Distribution at 900°C

A schematic of the test set-up is shown in Figure 25.

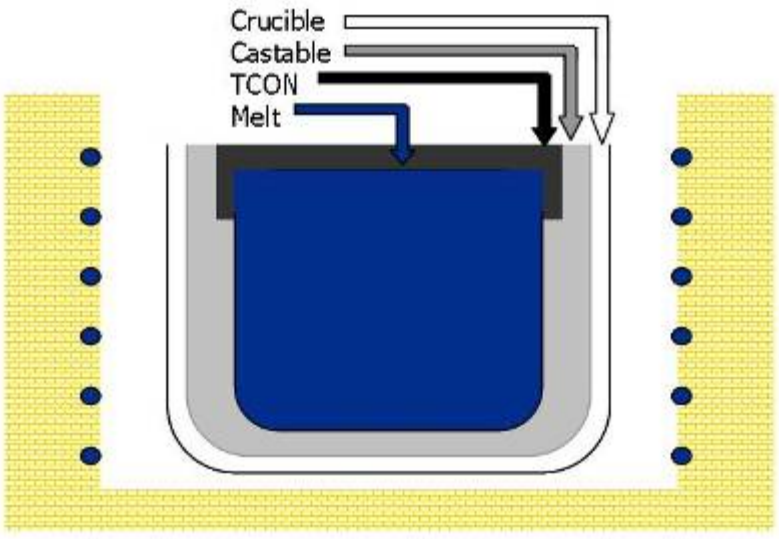

Figure 25: Schematic of the Test Set-up

After curing the refractory for one week at room temperature, the furnace was slowly heated to 843^{o}C (1550^{o}F) over a one week period to complete the curing of the bonite castable. The crucible was charged with 325 lbs. of solid aluminum that was melted over three days. This created a melt line 3" from the top of the vessel (in the middle of the 6" high TCON® plates) and a metal volume of 3,270 in.^{3}. The test was run for 83 days (2,000 hours) with periodic (every one to three days) sampling of the metal for Mg content and scraping of the dross from the top of the melt and TCON® plates. Mg content was replenished using solid magnesium metal and the metal line was kept constant by adding additional solid 5083 alloy. Dross removal was performed by scraping with a metal rod in a fashion to simulate the harsh standard practices used by industry. Following completion of the test, the entire test assembly was sent to ORNL for sectioning and analysis by ORNL, UMR, and Fireline.

5.0 Results

5.1 HDG coatings and materials issues

5.1.1 Static Lab-scale Corrosion Tests

Current Materials and Coatings

316L Stainless Steel: Test results showed that after a one-day dipping test, the reaction layer had a thickness of about 0.5 micron at the surface of the sample. There were several dross particles with the size range of three to five microns surrounding the steel sample but few of them attached to the surface [22, 23].

Figures 26 (a) and (b) show that after a four-day dipping, the thickness of the reaction layer increased to about 30 microns and there were several sub-layers formed. On the top of the reaction layer, there were two dross layers formed. The one next to the reaction layer is a semi-continuous dross layer with an average dross size of five microns, and on the top of this layer, there are several large dross particles with an average size of 30 microns. It is believed that these big dross particles are from the bath.

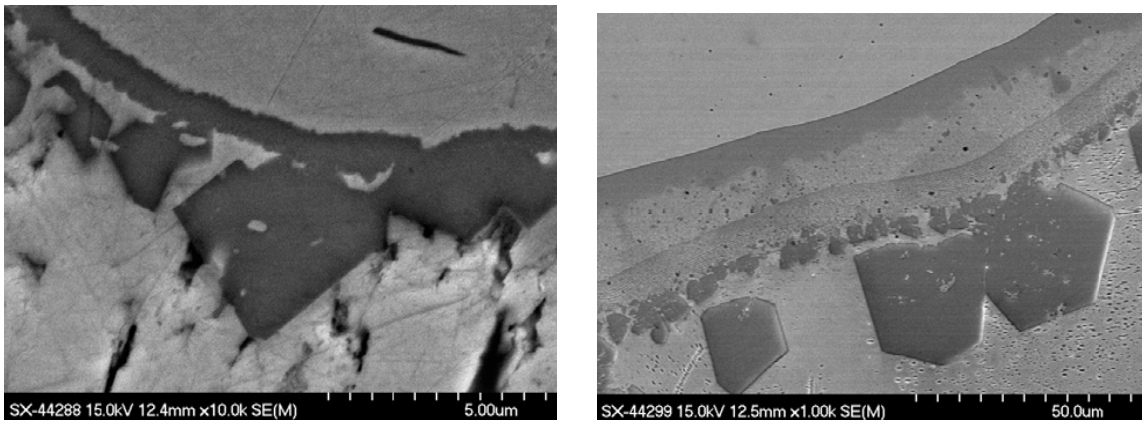

(a) 316L, static, 1 day **b) 316L, static, 4 days**

Figure 26: SEM micrographs of 316L stainless steel after lab-scale static dipping test in Zn-0.22% Al for various times

WC-Co coating: WC-Co coating is a thermal-spray coating that has become more and more popular in the GA/GI industries, because it has been proven that this coating is more corrosion and dross buildup resistant than the 316L-type stainless steel. During this project, static dipping tests of WC-Co coating in a GI (Zn-0.22%Al) bath were performed for up to 15 days.

Figure 27 shows the WC-Co coating after dipping in GI (Zn-0.22Al%Al) for 15 days. The coating was supplied by industrial partner, Praxair Surface Technologies, and the substrate was 316L stainless steel. The top layer in both pictures is the steel substrate, the middle layer is the coating, and the bottom layer is frozen Zn bath. It is indicated in the pictures that the coating shows almost no-wetting with the Zn bath, and there is a crack between the bath and the coating. However, there are more pores in the coating after the 15-day dipping than in the virgin coating, which shows the degradation of the coating. In addition, there are few dross particles attached to the coating surface after a 15-day dipping test.

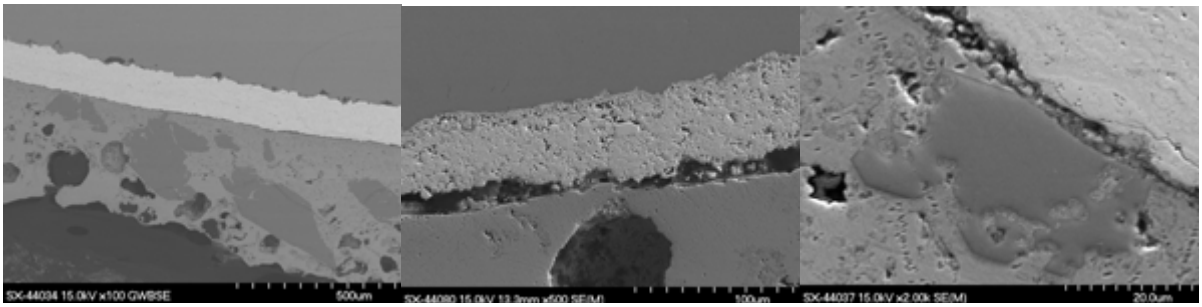

Figure 27: WC-Co coating after dipping in lab-scale Zn-0.22%Al bath for 15 days

Newly developed materials and coatings

Figure 28 (a) is the back-scattered electron image (BSI) of the interfacial dross layers formed by the immersion of the 316L specimen, partially coated by Alloy 2020 weld overlay, in the galvanizing bath (Zn-0.22%Al) at 465ºC for 30 days. As seen in Figure 28 (a), the bright area on the left of the micrograph is the Alloy 2020 weld overlay (also shown as Figure 28 (b)) while the dark area on the right side is 316L stainless (also shown as Figure 28 (c)). To the right of the substrate, a relatively thick dross layer was observed attaching on the 316L surface, but no continuous dross layer was built up on Alloy 2020 except where scattered small dross particles were detected. Both 316L and Alloy 2020 had a uniform, continuous interfacial reaction layer formed on the side of the base materials. More details are shown in close-up images in Figures 29 (a) and 29 (b) comparing the wettability of the base materials by dross. The conclusion was drawn that Alloy 2020 weld overlay had better non-wetting performance than 316L stainless [24].

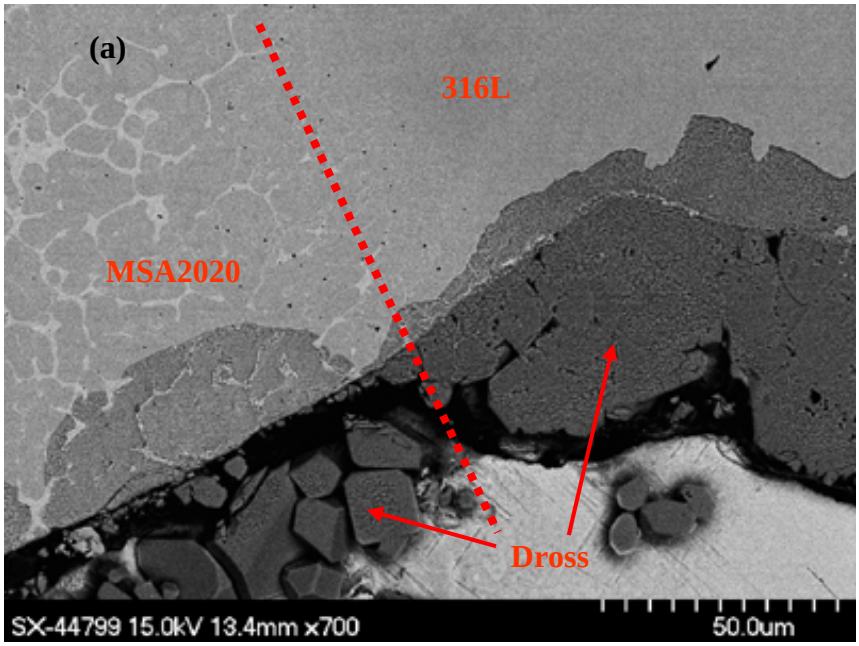

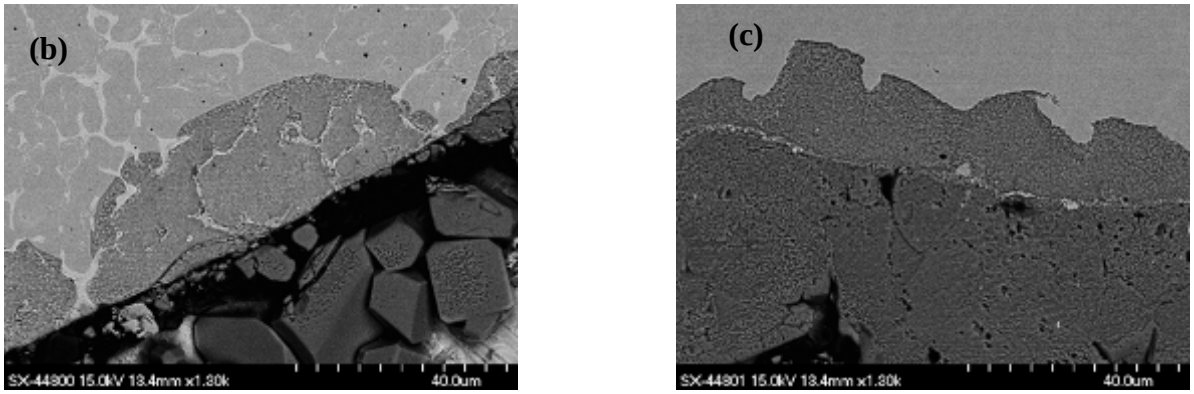

Figure 28: Static molten metal corrosion and dross buildup test in GI bath at 870ºF for 30 days on materials (a) Alloy 2020 weld overlay (b) 316L stainless

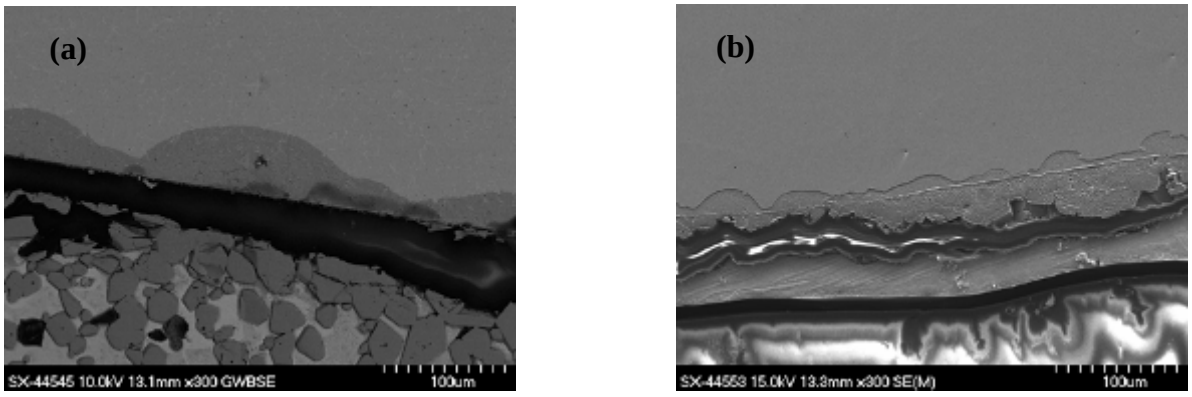

Figure 29: Static Molten Metal Corrosion and Dross Buildup Test at 870ºF for 81 days in GI bath at Nucor Steel's Crawfordsville, Indiana plant (a) Alloy 2020 Weld Overlay (b) 316L stainless

Dynamic Lab-scale corrosion tests

316L stainless steel: A series of dynamic corrosion/dross-buildup tests on current roll materials – 316L stainless steel in GI bath were carried out. The testing temperature was 460°C and the rotation speed was 60 rpm. The testing times were one day, two days, four days, and five days. The Zn, provided by Wheeling-Nisshin, was saturated with Fe, and had 0.22%wt aluminum content. After the tests were conducted, samples were analyzed by SEM/EDAX and microprobe.

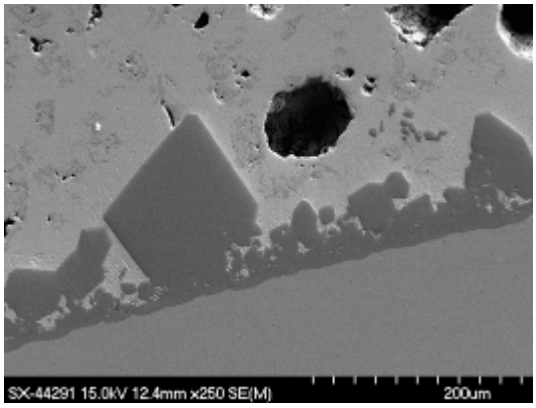

(a) 316L, Dynamic, 1 day

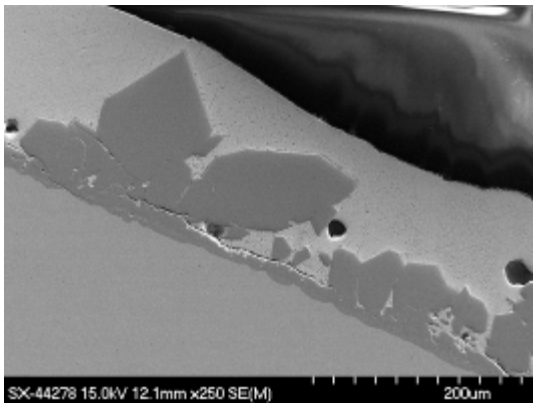

(b) 316L, Dynamic, 2 days

Figure 30: 316L stainless steel bars after lab-scale dynamic test in Zn-0.22%Al bath

Figure 30 shows the SEM micrographs of 316L stainless steel samples after lab-scale dynamic test inZn-0.22%Al bath at one day and two days. It is indicated in Figure 30(a) that after one day dynamic test: (1) there was a reaction layer with the thickness of about five to ten microns formed at the surface of the steel; (2) there was a semi-continuous dross layer with the average dross particle size of 15 to 20 microns next to the reaction layer; and (3) there were few big dross particles, with the size of 50 to 150 microns, attached to the dross layer. After the two-day test the results indicated: (1) the reaction layer thickness was slightly increased; (2) the particle size of the dross particles formed semi-continuous layer was increased; and (3) the size of big particles remained the same.

By comparing dynamic tests results with static results, the conclusion was: (1) the reaction layer after the dynamic test was much thicker than after the static test; (2) the size of the dross particles was bigger than after the static test; and (3) the agglomeration of dross particles was faster than after the static test.

2020 Overlay Coating: As shown in Figure 31, Alloy 2020 weld overlaid 316L specimen did not have significant change after the dynamic test which ran for up to 30 days. SEM/EDAX micrographs (Figure 28a) of the overlay indicated that it had better resistance to the dross buildup than bare 316L, although the overlay was also attached by few dross particles. Under the SEM microanalysis and the EDS elemental line scan across the sample-molten line interface, a reaction layer was found between the Alloy 2020 and dross, by the side of the overlay, as is shown in Figures 32 and 33. EPMA elemental mapping, shown in Figure 34, indicates that part of the overlay layer was corroded and replaced with the reaction layer. As shown in Figure 34, this layer was enriched with Mo & W & Cr, as well as Fe, Zn, and Al. The microstructure of Alloy 2020 is carbides embedded in Fe-matrix. Apparently, these carbides (WC, MoC, & $Cr_{23}C_6$) remain stable in Zn/Al baths, while Fe-matrix reacts with the bath and forms Fe-Zn-Al intermetallic compounds. In addition, it is interesting that another five micron

thick under-scale was found between the reaction layer and Alloy 2020 overlay, and it was enriched with both Al & Fe, shown as Figure 35. The RGB microprobe mappings, showing the elemental distribution, indicate that the under-scale was continuous and bonded with the Alloy 2020 and reaction layer at both sides.

By comparing Alloy 2020 overlay dynamic tests for 15 days and 30 days, no obvious difference was found on the thickness of either dross buildup or reactive layer formation after extending dynamic testing duration from 15 days to 30 days, as shown in Figure 32.

Figure 31: Alloy 2020 weld overlay attacked by GI bath after 30 days at 870ºF

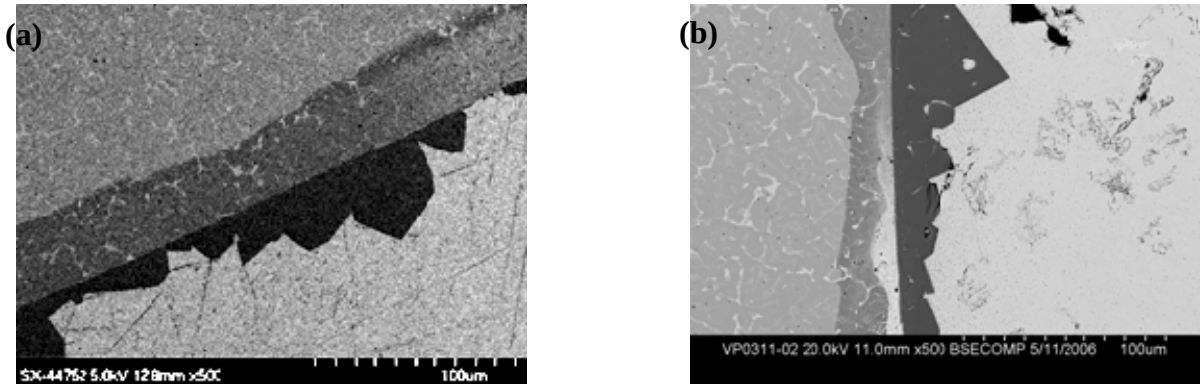

Figure 32: Dynamic molten metal corrosion and dross buildup test on Alloy 2020 weld overlay in GI bath at 870ºF (a) 15 days (b) 30 days

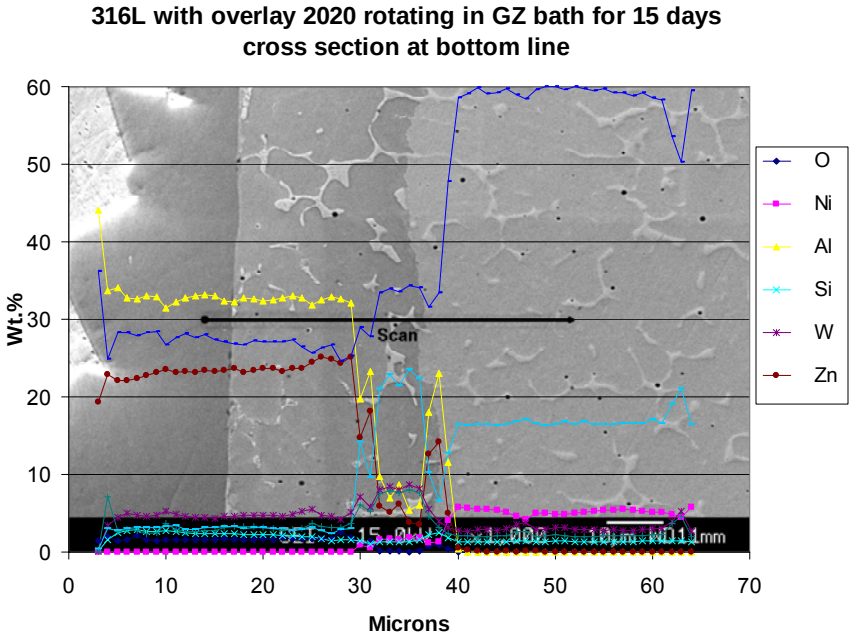

Figure 33: Cross section line scan of dynamic molten metal corrosion and dross buildup tests Alloy 2020 overlay in GI bath at 870ºF after 15 days rotation (rotating rate 60 rpm)

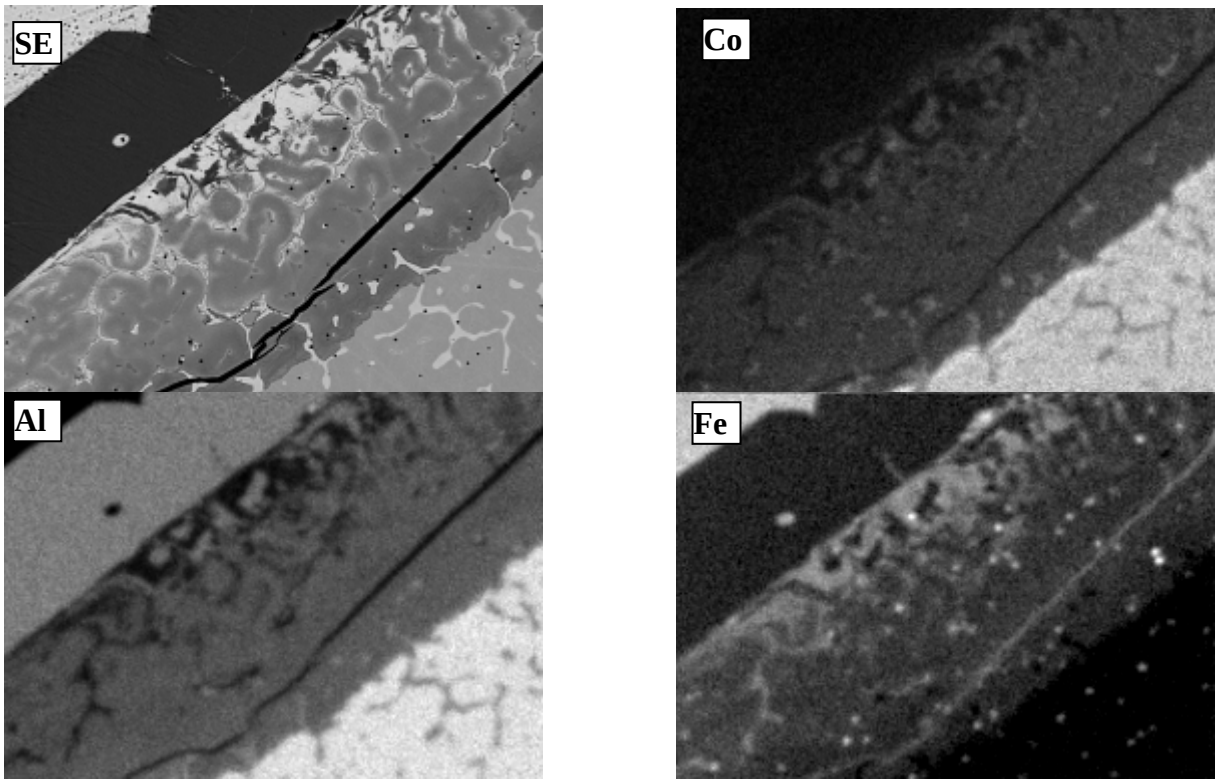

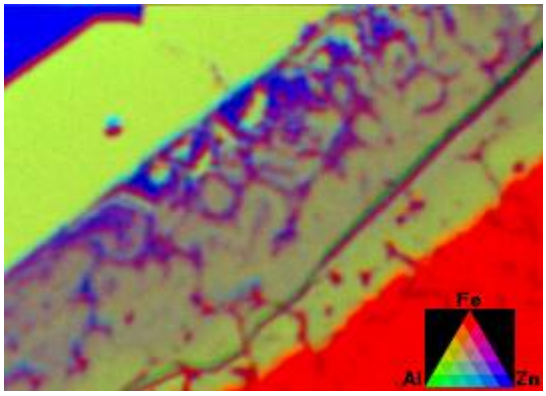

R : G : B = Fe : Al : Zn

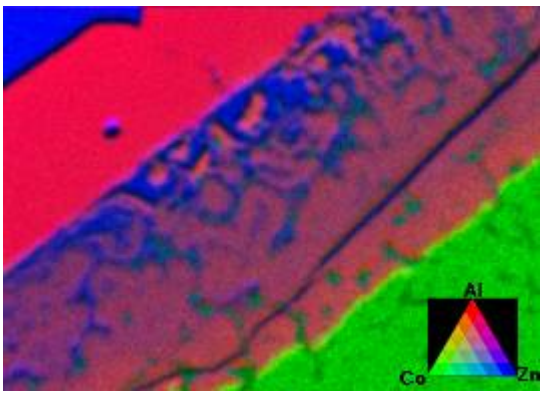

R : G : B = Al : Co : Zn

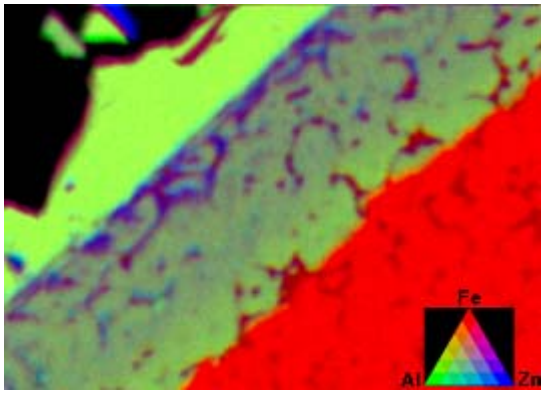

R : G : B = Fe : Al : Zn

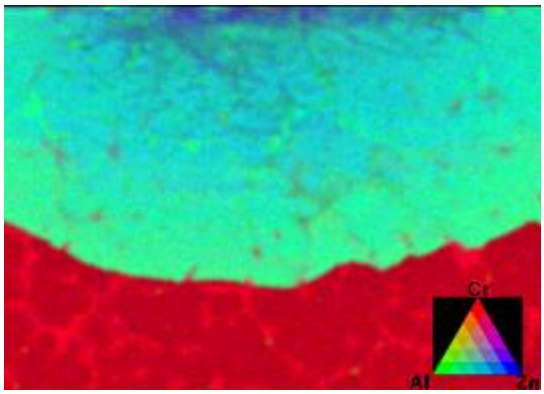

R : G : B = Cr : Al : Zn

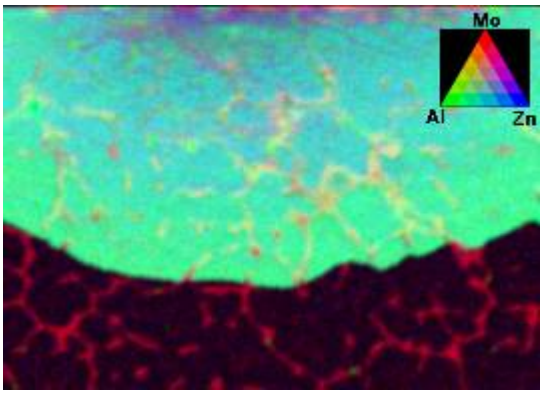

R : G : B = Mo : Al : Zn

Figure 34: Dynamic molten metal corrosion and dross buildup tests Alloy 2020 overlay in GI bath at 870ºF after 15 days rotation (rotating rate 60 rpm)

(a)

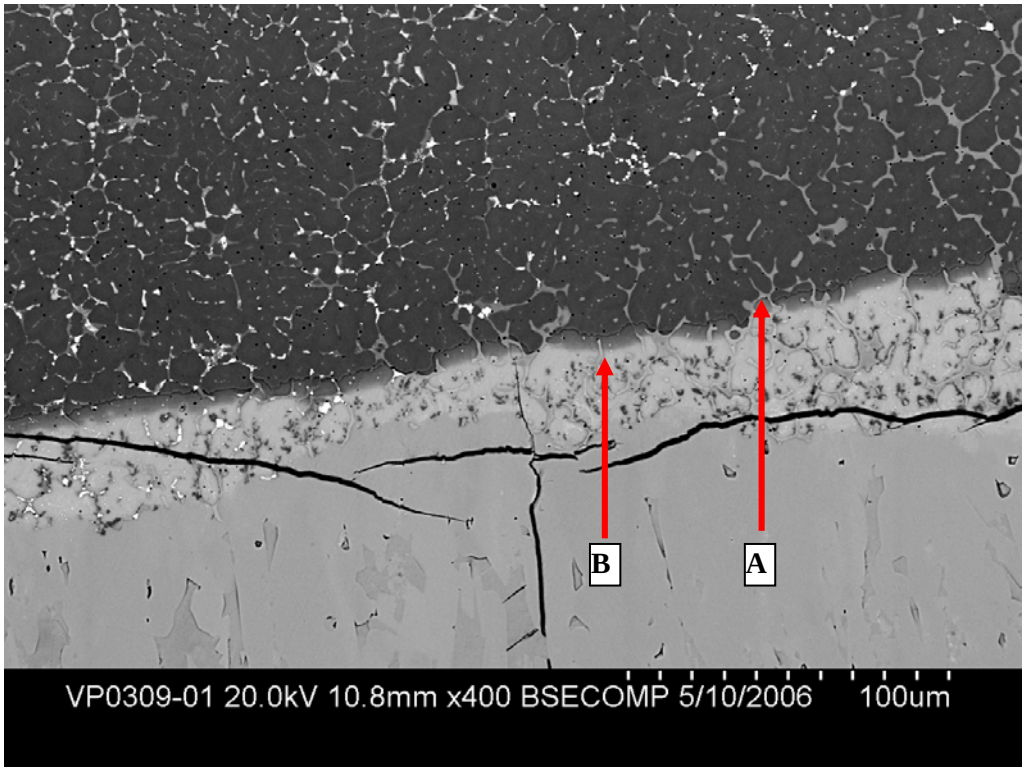
B
A
VP0309-01 20.0kV 10.8mm x400 BSECOMP 5/10/2006 100um

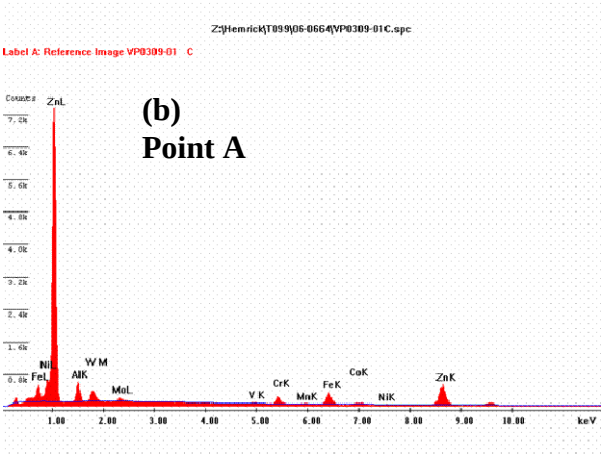
Z:\Hemrick\T099\06-0664\VP0309-01C.spc
Label A: Reference Image VP0309-01 C
(b)
Point A
ZnL
NiL
FeL
WM
AlK
MoL
VK
CrK
MnK
FeK
CoK
NiK
ZnK
keV

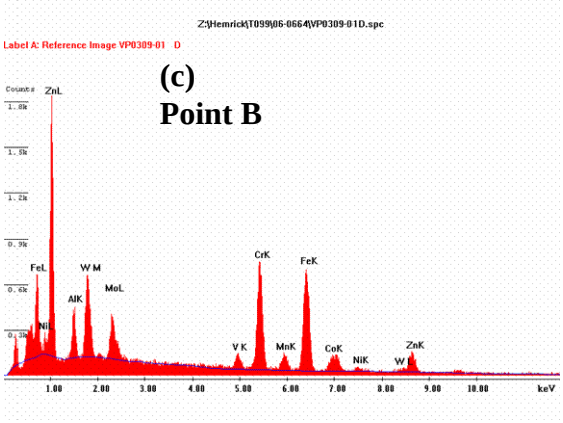
Z:\Hemrick\T099\06-0664\VP0309-01D.spc
Label A: Reference Image VP0309-01 D
(c)
Point B
ZnL
NiL
FeL
WM
AlK
MoL
CrK
FeK
VK
MnK
CoK
NiK
ZnK
keV

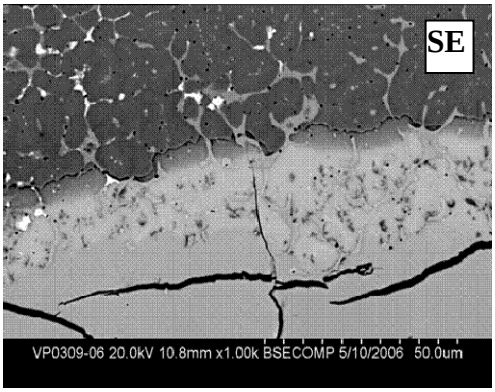
SE
VP0309-06 20.0kV 10.8mm x1.00k BSECOMP 5/10/2006 50.0um

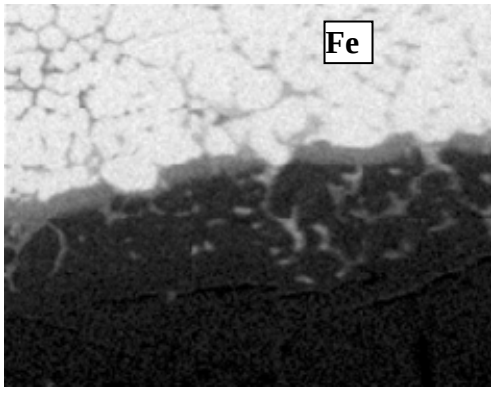
Fe

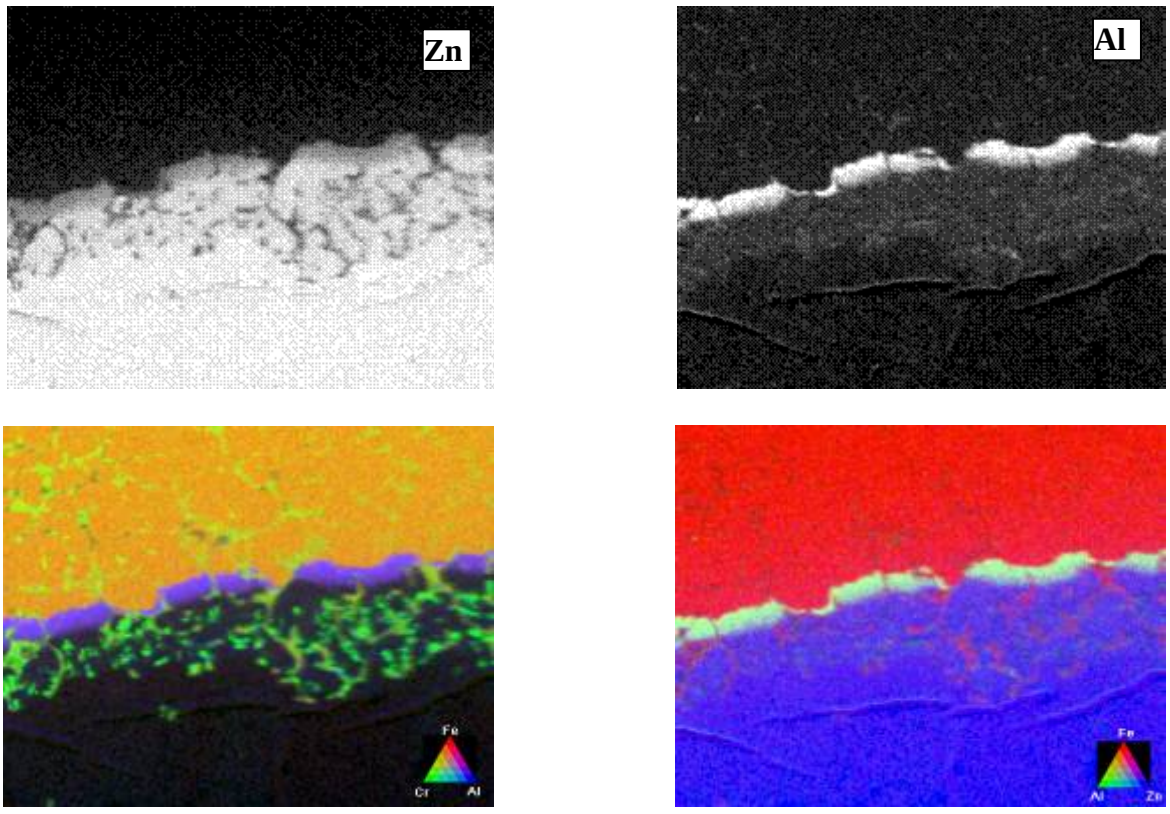

R : G : B = Fe : Cr : Al

R : G : B = Fe : Al : Zn

R : G : B = Cr : Mo : W

R : G : B = Cr : W : Al

Figure 35: Dynamic molten metal corrosion and dross buildup tests Alloy 2020 overlay in GI bath at 870ºF after 30 days rotation (rotating rate 60 rpm)

5.1.3 Sessile-drop Wetting Tests

In this task, performed by WVU personnel at ORNL, sessile drop tests for newly developed Alloy 2020 coating were performed and compared to 316L stainless steel and cast-Alloy 2020. Primary results are presented in Figure 36 [25].

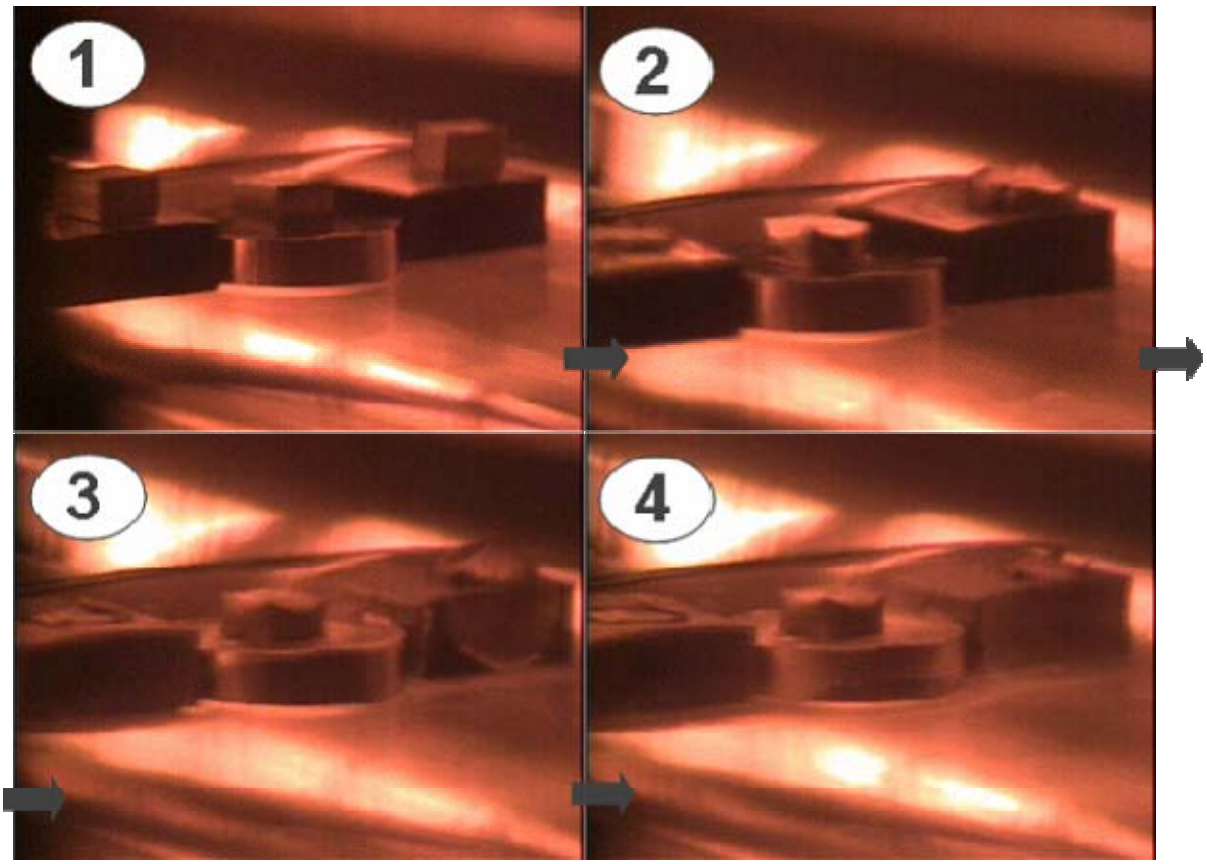

Figure 36: Static sessile drop wetting test results

Experimental results, provided the general ranking of the wetting - reacting speed among the three substrate materials tested against the liquid zinc-0.22 wt% Al as follows.

MSA 2020 - cast
↓ increasing
MSA 2020 overlay on SS316L
↓ attack
SS316L

Because of processing, the Alloy 2020 overlay has a different microstructure than cast Alloy 2020, resulting in different wettability against the molten zinc. However, once they are penetrated by the molten zinc, the reaction mechanism with molten zinc is the same. Both of them form a thin under scale after attacked by the molten zinc, which has the same thickness under the same testing condition. This layer is mostly alumina with some zinc in it [26].

As compared to Alloy 2020 cast and Alloy 2020 overlay, 316L has poor corrosion resistance against molten zinc attack, compared with cast Alloy 2020 and Alloy 2020 overlay. An aluminum enriched under scale was found between 316L and Zn-0.23wt%Al under every experimental condition tested. The thickness of this scale is affected by both temperature and time. At the same temperature (such as 465 °C), extending time makes it grow thicker from 0.2 micron (two hrs) to 1 micron (four hrs). Meanwhile, for a given time (such as two hrs), increasing temperature makes it thicker from 0.2 micron (465 °C) to 5 micron (485 °C).

5.1.4 In-plant Tests Results

5.1.4.1 Current Materials

A number of 316L stainless steel coated samples were tested in California Steel Industries'(CSI) GI bath for various times, and the samples were analyzed by means of optical microscopy, SEM/EDAX and microprobe.

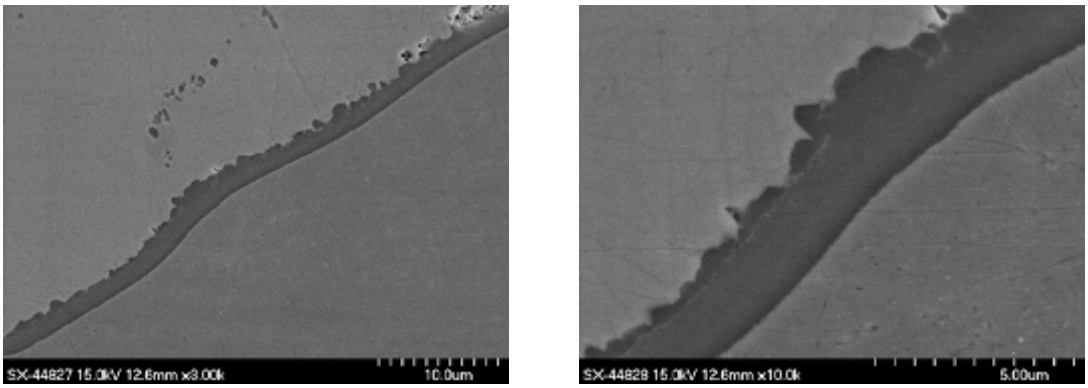

(a) 316L, 1-day in CSI, low magnification; (b) 316L, 1-day in CSI, high magnification

Figure 37: 316L sample after 1-day dipping test in California Steel Industries' GI bath

Figure 37 shows the 316L sample after one-day dipping test in the CSI GI bath. It is indicated in the figure that the thickness of the reaction layer is about two microns and the average size of dross particles is about 0.5 micron. Comparing these results with WVU's lab-scale test, it was observed that the reaction layer was thicker and the dross particle was slightly smaller than that of lab-scale test.

Figure 38 shows the distribution of Fe, Zn, Al, and Cr in the vicinity of the reaction layer. It is indicated in the figure that there are at least three sub-layers in the reaction layer: the "internal corrosion" sub-layer next to the steel substrate, the continuous sub-layer formed by tiny-dross particles, and the frozen bath sub-layer between these two sub-layers. The figure shows that the Al content in the reaction area was lower than that of the big dross particles.

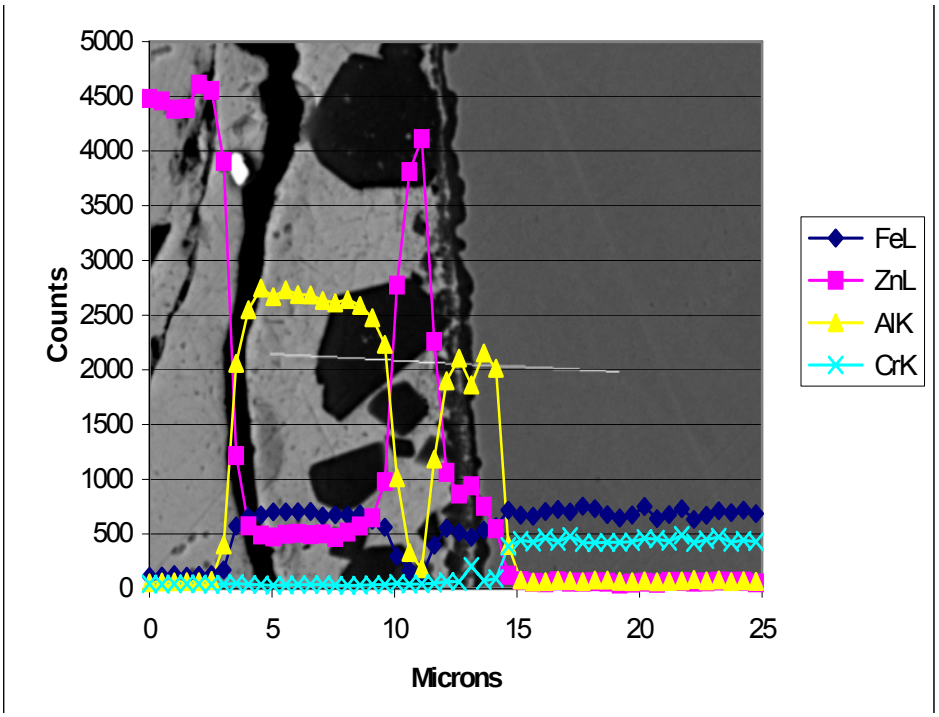

Figure 38: Line-scan of the 316L sample after 1-day test in CSI bath

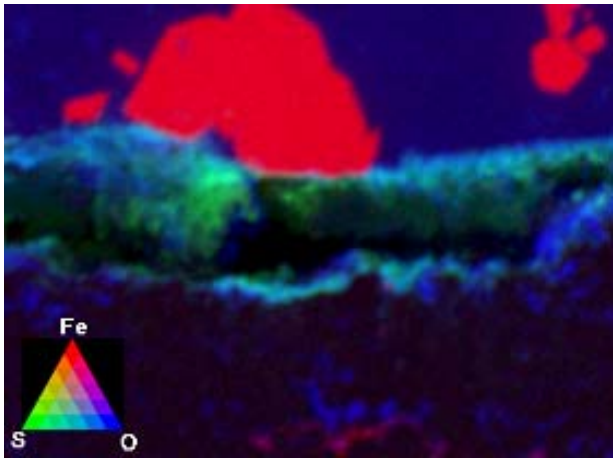

Figure 39: Microprobe Fe-S-O mapping of the WC-Co coating after 3-day dipping test in California Steel Industries

Figure 39 shows the microprobe Fe-S-O (RGB) mapping of the WC-Co coating after the three-day static dipping test in CSI's GI bath. It is indicated in Figure 39 that there were few dross particles attached to the coating surface although the majority of the surface was not wetted with the Zn-Al alloy. Figure 39 also shows that there has been some Fe-penetration into the coating and this is believed to be the source of the failure of the coating after long-term service. Figure 39 shows that there are oxygen and sulfur segregation in the cracked area between the frozen bath layer and the coating.

5.1.4.2 Newly Developed Coating

In this task, performed at ORNL, samples of newly developed coating for sink and stabilizer rolls in continuous galvanizing – weld overlay of alloy 2020 on 316L, were tested in the baths of several industrial plants for as long as 154 days as shown in Table 9.

Table 9: In-Plant Testing of Samples of 316L/2020

Company	Test Duration (Days)	
Nucor, Crawfordsville	30	150
Nucor, Berkeley	33	76
Nucor, Arkansas	30	174
California Steel	30	90

Microstructural analysis of both tubular and bar specimens was completed after in-plant testing trial times varying from 30 to 174 days. The dross and reaction data for all of the specimens analyzed are summarized in Table 10. The plot of reaction depth for all data for 316L and 316L with 2020 weld overlay is compared in Figure 40. The data shows that the reaction depth can be expressed by:

$$\textit{Reaction depth } (R) = Ae^{Bt} \text{ ,} \qquad \textbf{Equation 5}$$

where

A and B = constants,
t = bath exposure time in days.

Table 10: Dross and Reaction Data on All In-plant Trial Samples of 316L and 316L/2020

Company	Location	Sample Type	Comments	Exposure Days	2020		316L	
					Dross	Reaction	Dross	Reaction
Nucor	Crawfordsville, Indiana	Tube		33	35	58	85	26
Nucor	Crawfordsville, Indiana	Tube		48	230	110		
Nucor	Crawfordsville, Indiana	Tube		48	200	65		
Nucor	Crawfordsville, Indiana	Tube		81	140	44	889	32
Nucor	Crawfordsville, Indiana	Tube	2020 wire-1	30	56	44		
Nucor	Crawfordsville, Indiana	Tube	2020 wire-2	30	115	36		
Nucor	Crawfordsville, Indiana	Bar		30	40	62	56	20
Nucor	Crawfordsville, Indiana	Bar		150	20	280	200	100
Nucor	Crawfordsville, Indiana	Bar		150		300		125
Nucor	Berkeley, South Carolina	Bar	2 in. from bottom	33	800	50	1200	20
Nucor	Berkeley, South Carolina	Bar	4 in. from bottom	33	160	24	940	26
Nucor	Berkeley, South Carolina	Bar	6 in. from bottom	33	400	40	1060	24
Nucor	Berkeley, South Carolina	Bar		76	165	95	211	40
Nucor	Hickman, Arkansas	Bar		30	180	36	260	24
Nucor	Hickman, Arkansas	Bar		174	77.5	50	155	27.5
California Steel	Fontana, California	Bar		30	100	20	290	65
California Steel	Fontana, California	Bar		90	180	105	90	110

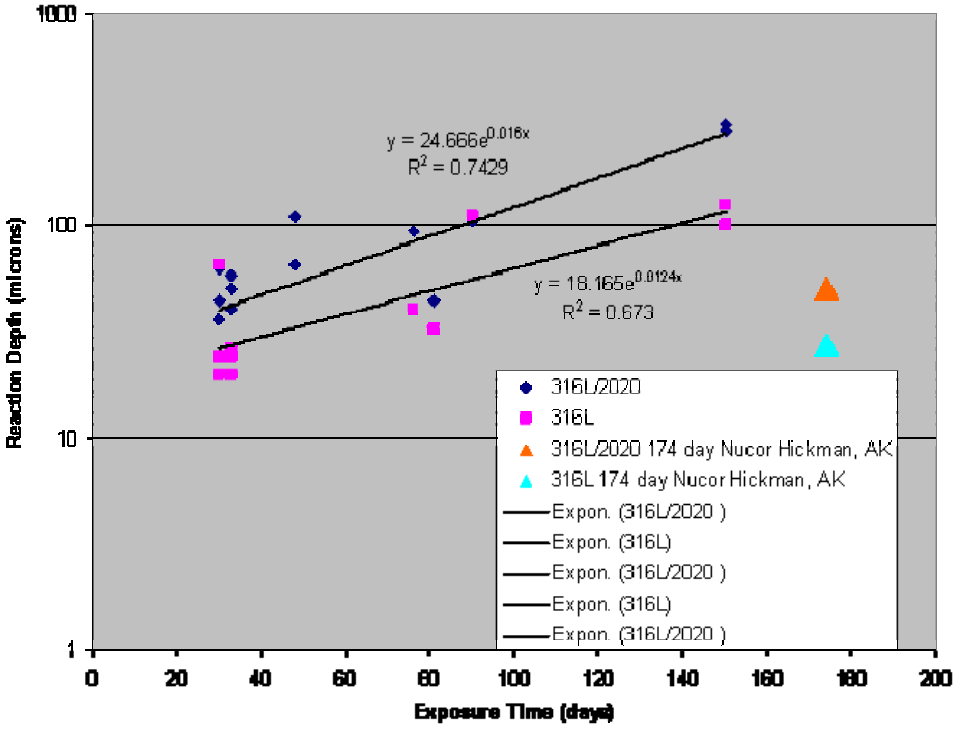

Figure 40: Plot of reaction depth for all in-plant exposed samples of 316L and 316L/2020

The values of constant *B* for 316L and 316L/2020 were 0.012 and 0.016, respectively. These values of *B* suggest that Eq. (27) can be rewritten as:

$$R = Ae^{0.015t} \qquad \textbf{Equation 6}$$

The values of constant *A* for 316L and 316L/2020 were 18.2 and 24.7, respectively. This suggests that at time zero or initial contact with molten zinc, the 2020 surface reacted quickly and then it grew at a rate very similar to that of 316L. The rapid formation of the initial reaction may be responsible for less dross formation on 316L/2020.

The dross thickness for 316L and 316L/2020 are compared in Figure 41. This plot shows similar trend for 316L and 316L/2020 with the exception of difference in constants. A general equation for dross thickness, *D*, can be presented as:

$$D = A'e^{-0.005t} \qquad \textbf{Equation 7}$$

where

A' = the constant and its values are 387 and 185, respectively, for 316L and 316L/2020.
t = time in days.

Equations (6) and (7) and the respective constants were used to calculate the dross thickness plus reaction build-up on 316L and 316L/2020. The calculated values are plotted in Figure 42. This graph shows that if 7 mil of the weld-overlay surface is removed every 60 days, the 316L/2020 will continue to outperform 316L. Furthermore, at a removal rate of 7 mil/60 days, a

3.5-mm (140-mil) –thick weld overlay will last over three years with significantly improved performance over 316L.

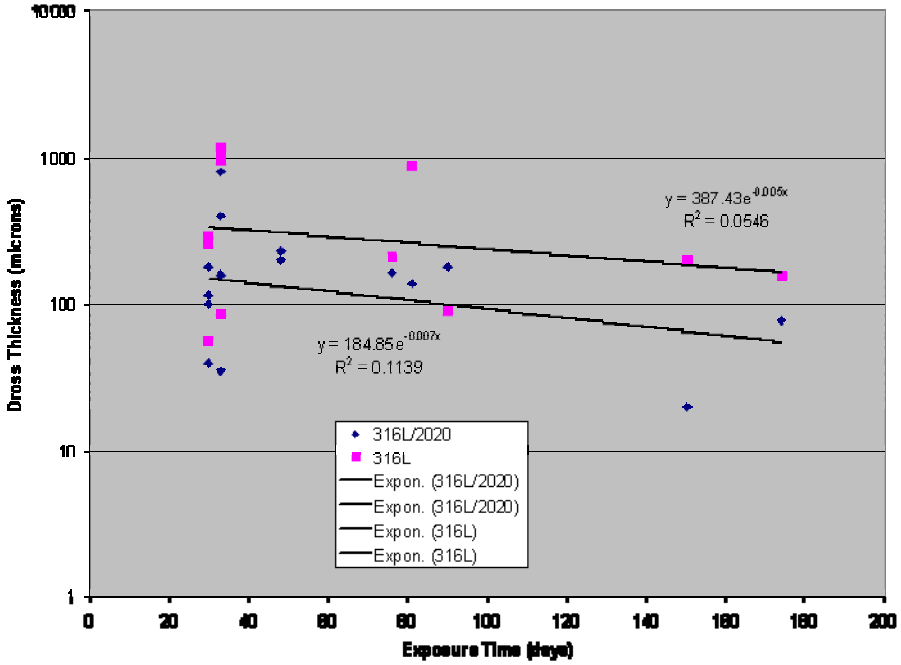

Figure 41: Plot of dross thickness as a function of exposure time for all in-plant exposed samples of 316L and 316L/2020

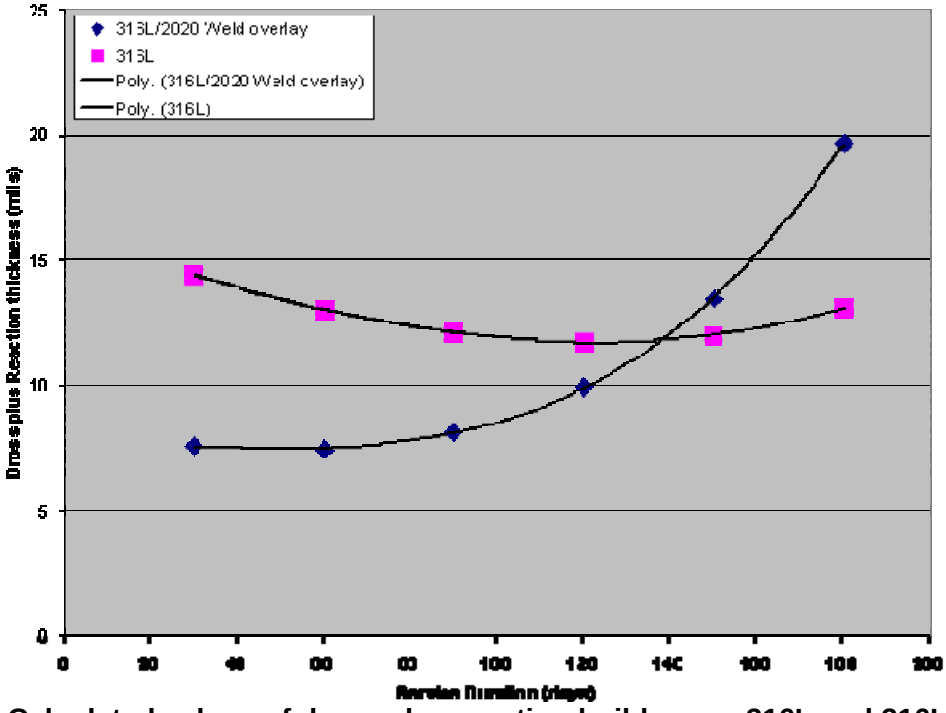

Figure 42: Calculated values of dross plus reaction build-up on 316L and 316L/2020 weld overlay

5.1.5 Component Testing

Three facilities were identified as sites for the testing of newly developed alloy 2020 weld overlay as the stabilizer roll coating: Nucor Steel – Crawfordsville, IN; Berkeley, SC; and Armoree, AK.

5.1.5.1 Fabrication

The stabilizer rolls for in-plant tests were donated by Nucor Steel Co. and the coatings were deposited and post-coating processes were conducted by ORNL and WVU, in collaborated with industrial partners (Metaullics, Duraloy, Specialty Welding, and Stoody Company). For the test at Nucor Steel – Crawfordsville, an 8-in.-OD roll of type 316L was weld overlaid with 2020 wire. Figures 43-45 show the progressive steps of the weld overlaying and Figure 44 shows the completed roll. The welding was carried out at Specialty Welding & Machining, Inc. The welded roll was shipped to Duraloy Technologies, Inc. for putting the ends on and machining the weld overlaid surface to achieve the desired surface finish. Figure 45 shows the partially machined roll. During machining, it was realized that there may be areas of the roll that would not clean up without needing some weld repair.

Figure 43: Nearly half of weld overlay of 2020 completed on 316L casting for stabilized roll application at Nucor in Indiana

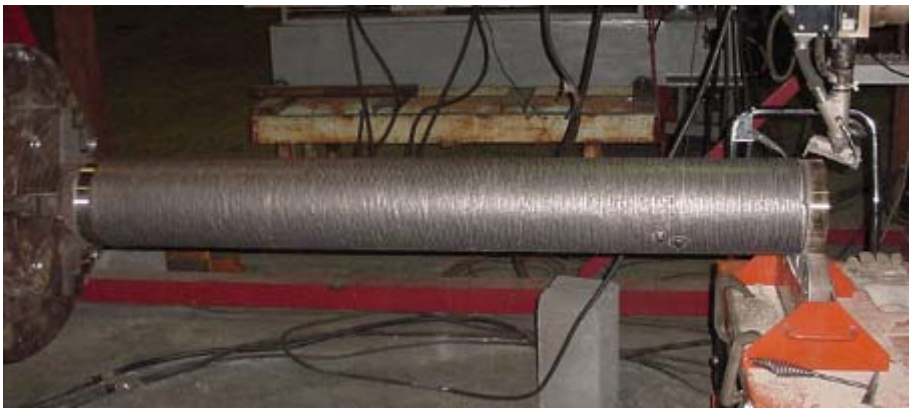

Figure 44: Completed stabilizer roll with 2020 weld overlaid on 316L casting

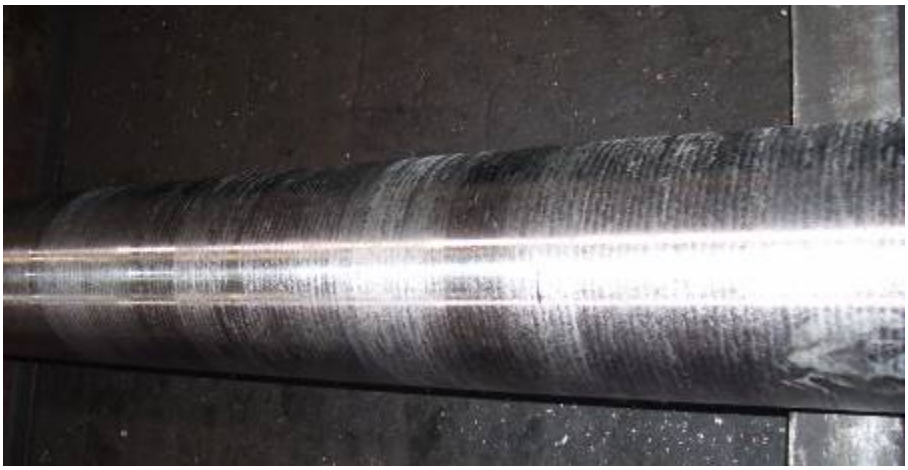

Figure 45: Partially machined roll surface of 316L/2020 weld overlay

The second layer of 2020 deposited with newly designed electrodes is shown in Figure 46. This figure shows the as-deposited second layer and the same layer after dye check. The dye check showed no defects in the second layer produced from the electrodes. This is a very significant accomplishment in light of always needing some weld repair while welding a large surface.

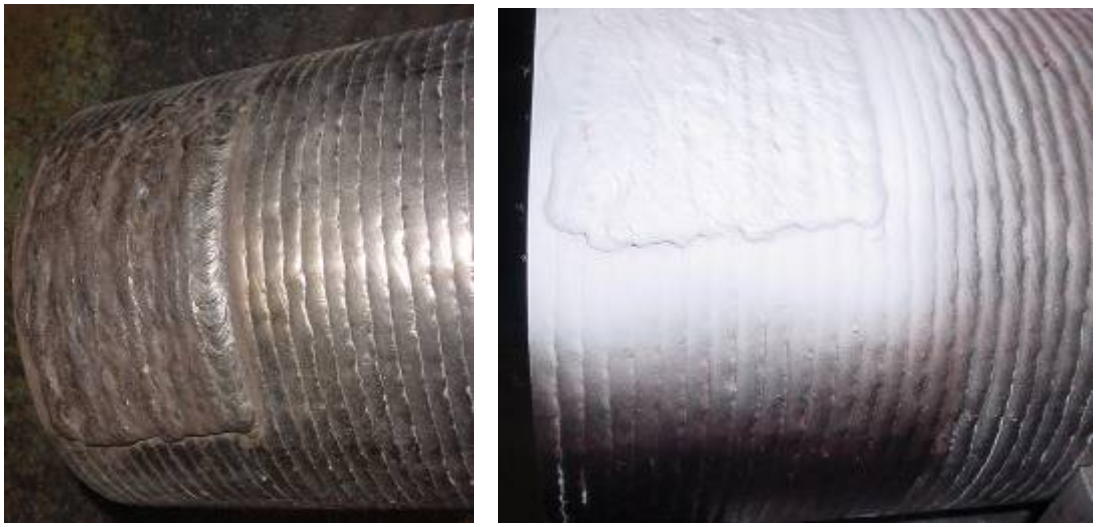

(a) **(b)**

Figure 46: Second layer of 2020 deposited with the newly developed electrode: (a) as-welded and (b) after dye check. No cracks were noted.

The fabrication of the rolls tested at Nucor Steel – Berkeley and Nucor Steel – Armoree were similar to the one at Crawfordsville, which is described above.

5.1.5.2 Testing at Nucor Crawfordsville

The roll, prior to going for in-line trial, is shown in Figure 47. Details of this roll's in-line trial are given below.

- 316L/2020 Weld Overlay
  - Installed on May 6, 2007
  - Removed on May 14, 2007, due to operation problem discussed below
  - Total number of days in-line: 7
  - Total feet of sheet production run on the new roll: 2,615,029
- Comparable 316L Removed from Service after Sheet Production Run of 5,773,911 ft

Rolls removed from the in-line trial are shown in Figure 48. This figure shows the sink roll and stabilizer rolls of 316L and 316L/2020 weld overlay. Close-up of stabilizer rolls of 316L and 316L/2020 removed from in-line trial are shown in Figure 49.

Figure 47: The 316L/2020 roll in maintenance stand prior to installation for in-line trial at Nucor's Crawfordsville, IN Plant

Figure 48: Rolls removed from service at Nucor's Crawfordsville, IN Plant: 316L/2020 (Alloy 2020) roll had a one-week in-line service with 2,615,029 ft of material processed

Figure 49: Close-up of 316L (28) and 316L/2020 (Alloy 2020) rolls: Alloy 2020 roll has approximately half the in-line time as compared to the 316L roll

It is to be noted that the 316L/2020 roll was taken out because of vibrations. The roll was in the bath approximately one-half the time as opposed to 316L. A visual inspection of the roll during the visit to Nucor showed that the journals on the end bells were badly worn from the wear process. This suggested that the in-line roll trial of 316L/2020 was shortened by the poor performance of the journals.

A visit to the machine shop used by Nucor was made on July 19, 2007 to determine the next step in cleaning the roll surface and improving the journal area for the follow-on in-line testing. Several methods were attempted on a trial basis to clean the surface of the weld overlay roll (316L/2020) that was removed from service. The purpose of trying various approaches was to find the best one that can be used without excessive removal of the 2020 weld overlaid surface. Methods that were tried include sandblasting, sand belt grinding, and grinding wheel. Among the three methods tried, the use of grinding wheel was found to yield the most control.

After the first trial cycle, a roll was finally machined by surface grinding. The machined roll surface was 7.975 in. and a surface finish of Ra60. With a starting roll diameter of 8.0 in., only 0.0125 in. of the weld overlay was removed at this stage. The as-machined roll after the first cycle is shown in Figure 50.

Figure 50: Machined roll surface after first cycle of in-line trial at Nucor's Crawfordsville, Indiana plant

The second trial started on December 5, 2007. The roll was removed after approximately 20 days on December 24, 2007 due to dross build-up.

The roll processed 7,310,210 feet of sheet for the second cycle and 2,616,462 feet during the first cycle for a total of 9,926,672 feet of in-line service and 26 days of in-line trial. The second trial at almost 20 days was the longest time a trial roll was operated in service.

5.1.5.3 Test at Nucor Hickman, AK

Nucor Steel – Armoree donated a stabilizer roll for the in-plant testing. The roll was machined at Duraloy, then coated by Specialty Welding, following the processing routes developed by ORNL, then was machined and shipped to Armoree. The coated roll was put in the bath on January 21, 2008 and removed on February 1, 2008. There were totally 11 days for the roll in service. The reason for taking out the roll was dross buildup, which was believed to relate to micro-cracks in the coating

5.2 Dross control and scraper design

A series of static and dynamic tests were carried out. After each test, the 309 stainless coupon sample of the roll (representing sink roll at CGL) was removed, cut and polished (to 0.3μ) using diamond paste on micro-cloth then ultrasonically cleaned with acetone for 5 minutes to remove any residual polishing agents. The cross-section morphology of each sample roll was subsequently analyzed using a Hitachi S-4700 Scanning Electron Microscope fitted with an EDAX Energy Dispersive X-ray Analyzer (EDS). Elemental analysis was carried out at the sample roll-bath interface to identify and measure the compositions in each region.

Roll-Bath Interface After 20 Minutes

Upon careful inspection of the cross sectional roll-bath interface (surface of the roll) after 20 minutes of immersion, a reaction layer of uniform thickness was observed (at 250X). However, at higher magnification (at 1000X), the reaction layer actually showed two distinct layers as displayed in Figure 51. EDS mapping (Figure 52) revealed the outward diffusion of iron (Fe) and a uniform layer of silicon (Si) on the sample roll surface.

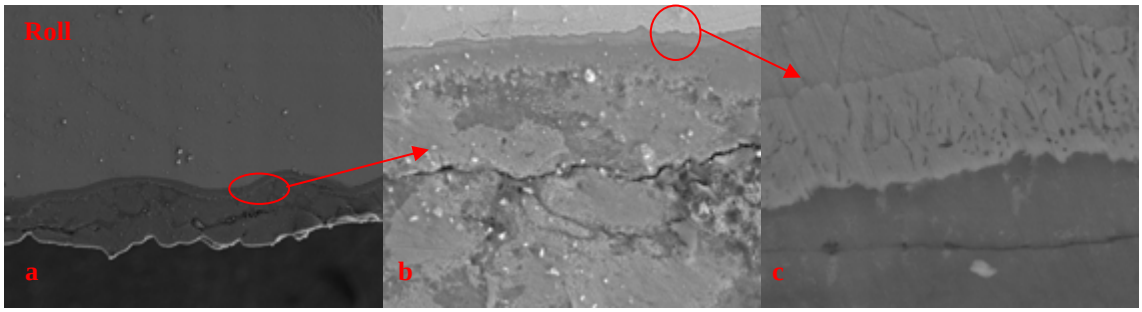

Figure 51: Micrographs of the roll-bath interface (surface of the roll) (a) 250X magnification, (b) 1000X magnification, (c) 8000X magnification

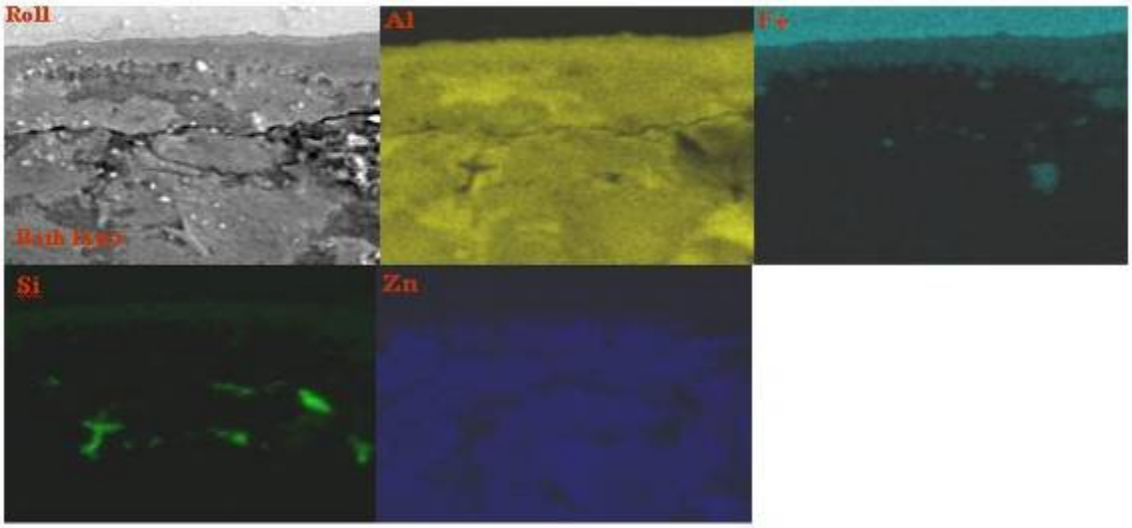

Figure 52: EDS map of the roll-bath interface (surface of the roll) at 1000X magnification

Sample roll-Bath Interface After 40 Minutes

As displayed in Figure 53, the surface of the rolls showed two main characteristic features subsequent to 40 minutes immersion:

(i) Micro-cracks in the reaction layer

(ii) Small discontinuous dross particles on the surface of the roll (bath side of the reaction layer) (average size = 12μm)

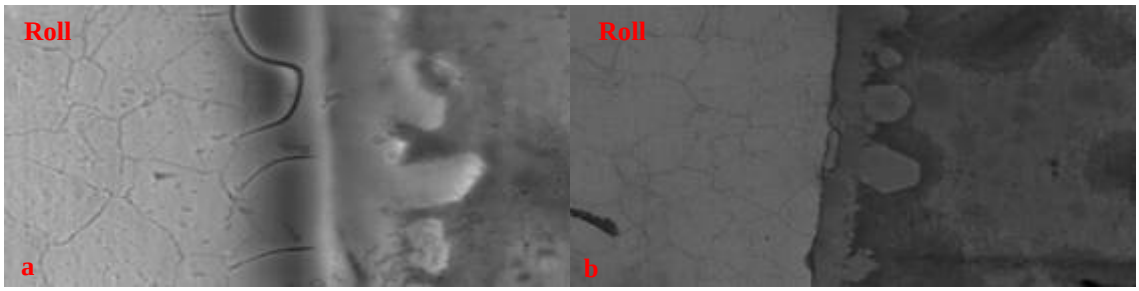

Figure 53: Sample roll-bath interface after 40 minutes (a) Microcracks on the roll-bath interface (2000X magnification), (b) Small dross particles (~12µm) (1000X magnification)

Sample Roll-Bath Interface After 60 Minutes

The sample roll-bath interface after 60 minutes of testing had a uniform layer of dross formation. Agglomeration of small dross particles over the dross layer was also observed in certain areas under higher magnification (1000X) (as shown in Figure 54). Average thickness of the dross layer at the end of 60 minutes was 40µm. The EDS spectrum of the dross layer and the bath is shown in Figure 55. In Figure 55-1 the composition of bath is Zn-Al-Si, while in Figure 55-2 the dross layer is composed of a Fe-Si-Al ternary intermetallic compound. From this analysis, a better understanding of the effect of silicon in forming stable ternary intermetallic compounds may be ascertained.

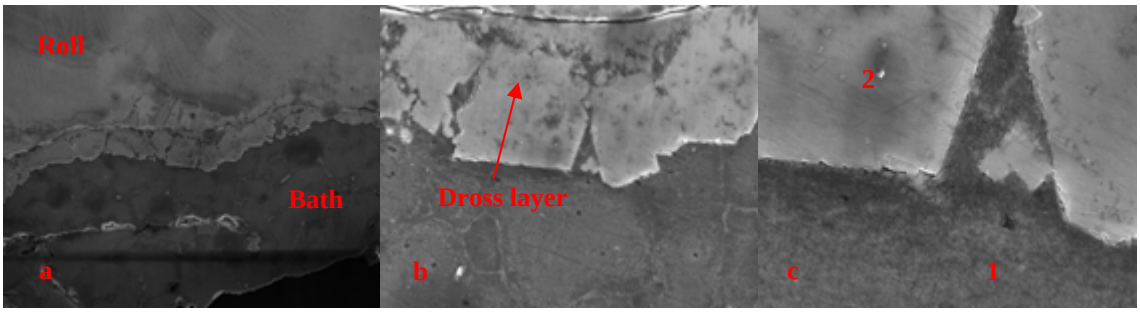

Figure 54: Sample-Bath interface after 60 minutes (a) structure of the dross layer formed at the interface (250 X), (b) 1000X magnification, (c) agglomeration of small dross particles on the continuous layer (4000X)

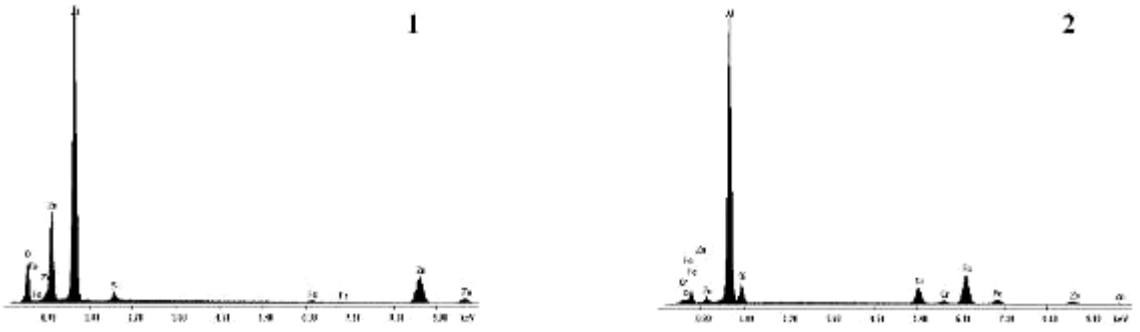

Figure 55: EDS Spectrum showing the composition of bath (location 1) and dross (location 2) as indicated in Figure 54 (c)

Sample Roll-Bath Interface After 80 Minutes

The micrographs of the 80 minute sample roll (Figure 56) showed two distinct layers of dross with slight changes in the aluminum and iron content. The inner layer (closest to the roll) was continuous and had uniform thickness, whereas the outer layer was irregular and contained small dross particles agglomerating to it.

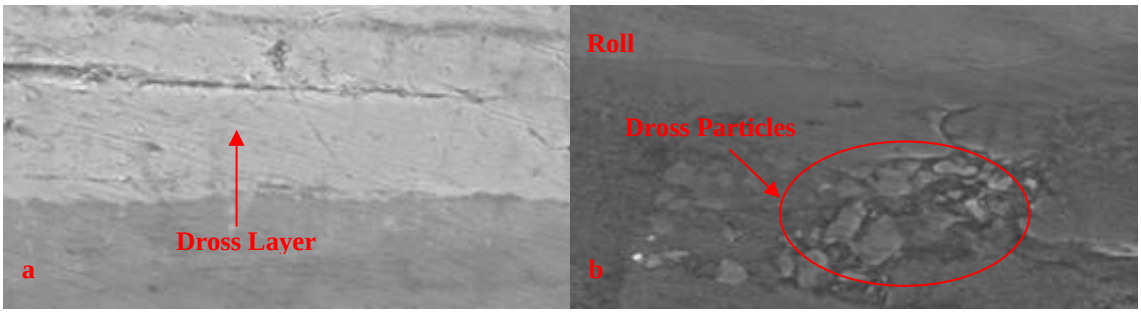

Figure 56: Dross layer formed on the roll surface after 80 minutes (a) 3000X magnification, (b) 1000X magnification

Sample Roll-Bath Interface After 100, 120 and 140 Minutes

After 100 minutes and beyond (Figure 57) the same mechanism of dross formation was observed as with the 80 minute sample roll except with increasing dross layer thickness. Discontinuity of dross layer towards the bath side was observed indicating agglomeration of the dross particles over time. The size of the dross particles on the outer layer were larger compared to the 40 minutes sample roll. This increase in size was possibly due to agglomeration of smaller dross particles formed in the bath and moving towards the sample roll as a result of the dynamic motion of the bath. In actual applications, these larger dross particles would make the overall roll surface rougher, leading to poor quality and surface imperfections on the galvanized sheets.

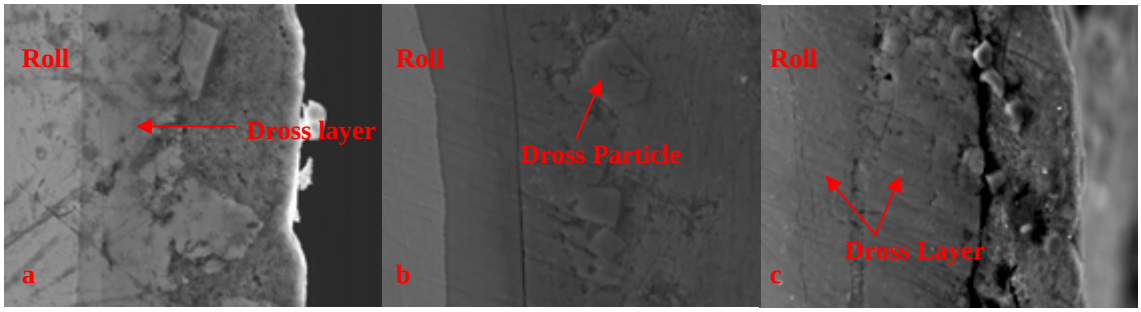

Figure 57: Sample Roll-Bath interface after (a) 100 minutes (1500X), (b) 120 minutes (1500X), (c) 140 minutes (1500X)

5.2.1 Discussion of Test Results

Based on the time series tests, the overall dross formation mechanism on the submerged pot hardware in galvalume can be schematically represented as shown in Figure 58.

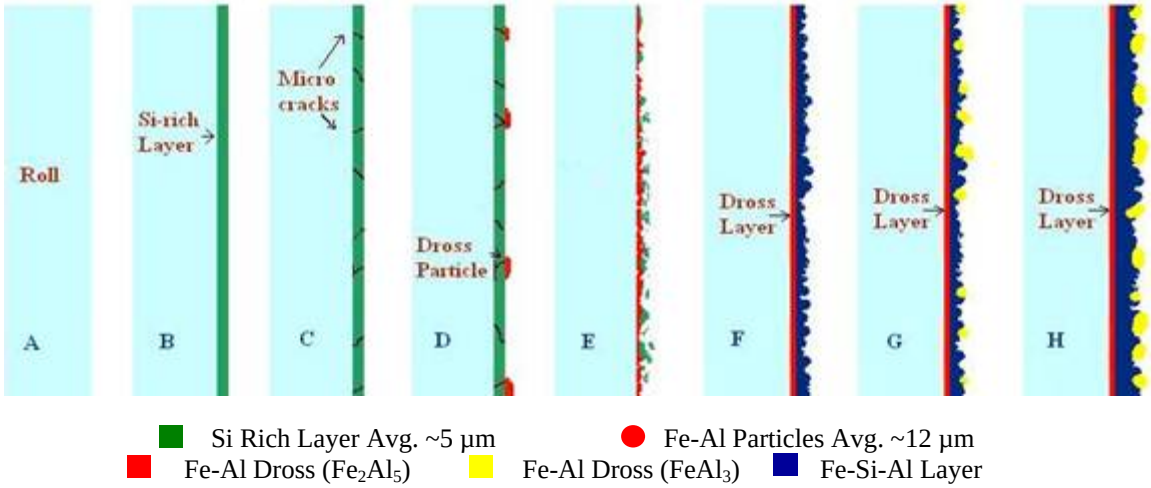

Figure 58: Schematic representation of dross formation on roll surface in galvalume bath

After 20 minutes, a uniform protective layer of silicon was observed between the sample roll and the bath interface (Figure 58-B). The source of Si-rich layer formed after 20 minutes may be due to either the Si atoms liberated from the roll surface as a result of dissolution of the steel or from solidification of the metallic phase silicon (about 0.5% Si in 309SS), which has a higher melting point (1414^{o}C) than that of the molten bath (649^{o}C) [20]. Subsequently after 40 minutes (Figures 58-C and 58-D), cracks were observed over the uniform layer of silicon and agglomeration of small dross particles were identified. These dross particles were probably formed elsewhere in the bath due to the reaction between the iron and aluminum and the dynamic motion of the bath caused the particles to agglomerate on the sample roll surface. After 60 minutes (Figure 58-E), a uniform dross layer was observed on the sample roll surface and silicon-rich areas were observed in the outer regions of the build-up. After 80 minutes (Figures 58-F and 58-G), two layers of dross were observed, the inner most thin layer consisted mainly of Fe and Al and the outer non-uniform layer contained Fe-Si-Al. At indeterminate locations, larger dross particles (Fe-Al) were observed. After 100 minutes (Figure 58-H) the dross layer and the dross particles observed were larger in size as compared to the 80 minutes sample roll.

It has been reported [21] that the silicon phase present in the bath converts the Fe-Al particles to a more stable ternary Fe-Si-Al intermetallic layer. Based on these tests, the mechanism of the dross formation can be categorized under three dominant stages:

1. Formation of dross (Fe, Al and Si) in the bath
2. Agglomeration of small dross particles on the roll surface due to the dynamic motion of the bath
3. Formation of continuous dross layer over the roll surface

Furthermore, EDS analysis of the sample-bath interface revealed the intermetallic compound formed was a ternary phase containing Fe, Al and Si in addition to the typical Fe_2Al_5 and $FeAl_3$ phases. The dross layer formation at each stage was measured and the layer thicknesses were plotted relative to time. As outlined in Figure 59, the initial growth was slower due to the formation of a silicon inhibition layer. However, after 60 minutes, the dross growth rate settled into a parabolic trend.

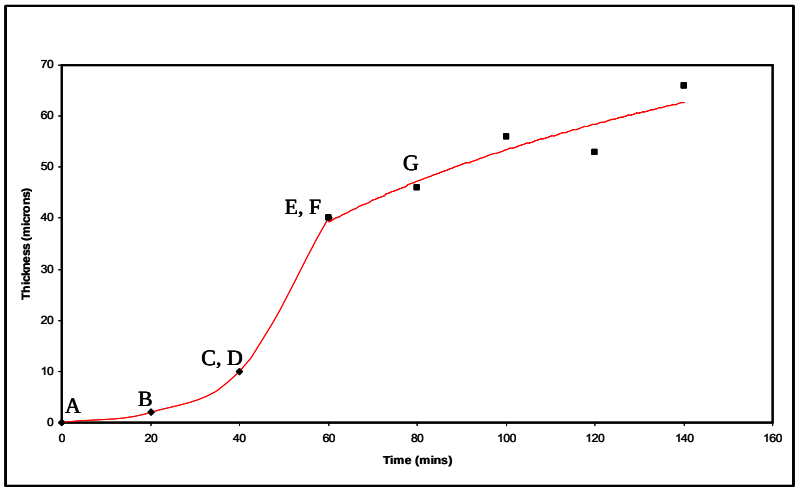

Figure 59: Dross layer growth pattern

5.2.2 Scraper Wearing Rate Test

As mentioned in the experimental setup part, three alloys were tested, initially with similar procedure, currently used in Wheeling Nisshin Inc. and the results indicated that Tribaloy T-401 has comparatively better performance.

5.2.3 Proposed New Scrapping Procedure

A new method (scraping procedure), which can still increase the efficiency of the scraper and the entire process of hot-dip was developed and test parameters are given below.

Once the bath temperature was stabilized at 600^{o}C (1112^{o}F) (see Table 11), the roll was immersed and held static in the bath for three hours, this is to simulate the actual industrial GL line where the sink roll stays in the bath for an average of three hours before the galvanizing process is started. After three hours the roll was rotated at the rated speed as mentioned in the test conditions and the load to the scraper blade was applied so that the scraping action starts once the roll starts to rotate. The new scrapping process would reduce scarper wearing rate significantly, based on the two main parameters.

A. **Lower contact pressure** for scraping action to reduce wearing rate

B. Scraper blade contact with **smoother hard dross layer.**

Table 11: Test condition for the continuous mode scraping process

Bath Chemistry	**Galvalume (GL)**
Roll RPM	108
Roll	309 Stainless steel
Bath Temperature	**600^{o}C (1112^{o}F)**
Duration	12 hours
Scraper Tip Material	Stellite 21, Stellite 6B and Tribaloy T-401
Scraping Process	**Continuous mode**
In bath idle time before testing	3 hours

After the tests were completed, the scraper blades were removed cleaned and the exact dimensions were measured using dial gauge and the measurements are shown in Table 12.

Table 12: Wearing rate of the scraper blade (Observed and Forecast values)

Material	Initial Length (Lo) (inches)	Wearing (ΔL) (Inches) Observed	% Wearing (ΔL/ Lo)*100 Observed	% Wearing (ΔL= Lo) (Days) Forecast
Stellite 21	1.635	0.074	4.544	~11

5.3 GEPDSS

The data that were obtained from the existing galvanizing lines were entered into GEPDSS and the output was analyzed. One of the major parameters that profoundly impact the energy consumption is the campaign period and the hours of downtime between campaign periods. Figure 60 shows the variation in energy consumption per ton (MMBtu/ton) with changes in production weeks and downtime (DT) hours simultaneously. Figure 59 shows that that there is a non-linear decrease in the MMBtu/ton when there is a decrease in downtime hours and increase in campaign period.

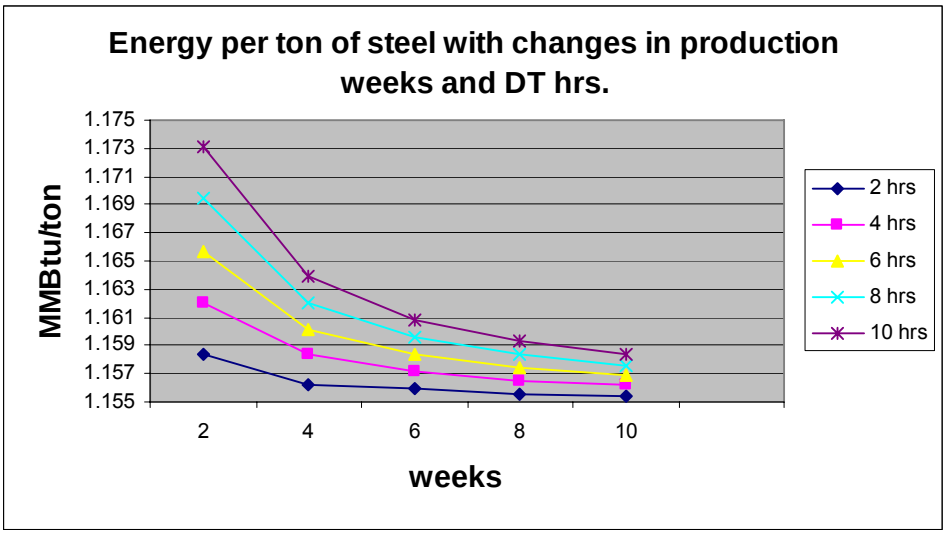

Figure 60: Change of MMBtu/ton with changes in production and DT

The graph in Figure 61 shows the annual energy consumption during production hours for eight galvanizing lines when the campaign period and hours of downtime are changed to various levels. It is seen from Figure 61 that each line has different annual energy consumption, however the change in magnitude of energy consumption for every line at different levels are the same. In other words, the figure yields a set of parallel curves.

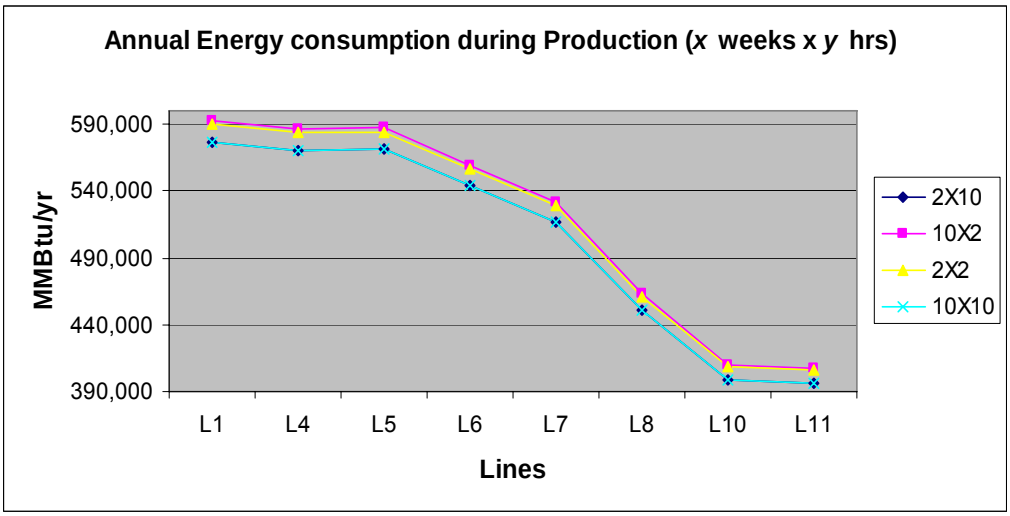

Figure 61: Annual energy consumption by lines at various campaign period and downtime

Figure 62 shows the cost incurred per ton for each line for electricity and natural gas (NG) during the hours of production. It is evident from the figure that line six (L6) pays the least electricity as well as natural gas cost per ton.

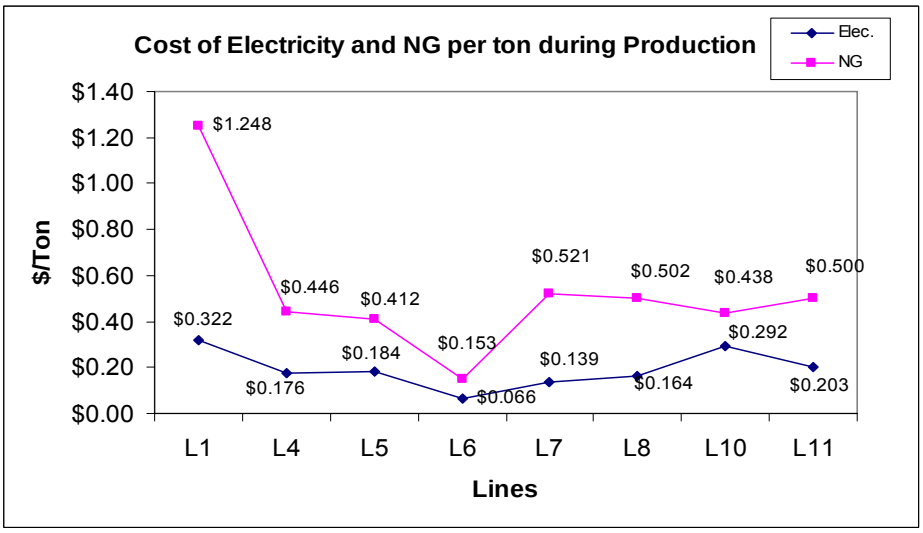

Figure 62: Cost incurred per ton for individual lines during production

5.4 Refractories

5.4.1 Survey

The results from the industrial survey are summarized below (focused on aluminum and super-alloy production which was decided to be the initial focus of the project):

Average metal processing temperatures:

730-845^{o}C (1350-1550^{o}F) for aluminum production

1150-1700^{o}C (2100-3100^{o}F) for super alloy production

Total cost of refractory materials consumption (over aluminum and super-alloy industries):

$5.72M/year

Cost of energy consumption (across aluminum and super-alloy industries):

$15.34M/year

Most common refractory problems encountered

Thermal – cycling, shock (especially in Al melters)

Chemical – attack (Cl), absorption into melt (Cr, Na, C, Ca), erosion/corrosion

Mechanical – fracture due to impact, vibration, bending loads, and wear

Processing – refractory inclusions

5.4.2 Post-mortem Analysis

The first set of refractory samples analyzed was from Sturm Rapid Response Center, Barboursville, WV. Samples were received from both a ladle and locations in various refractory linings, along with supporting information. Analysis revealed routes for refractory penetration, corrosion products, and gave insight into how to improve refractory performance. Following analysis at ORNL, samples were sent to UMR for additional analysis.

Additional samples were received from Sturm Rapid Response Center, Barboursville, WV. These samples were from a crucible used for melting various metals and from material used for repair patches on crucibles. Analysis revealed routes for refractory penetration, corrosion products, and gave insight into how to improve refractory performance in new materials developed through the project. As before, following analysis at ORNL, samples were sent to UMR for additional analysis.

Analysis of the spent castable refractories obtained from the natural gas fired reverberatory aluminum alloy melting furnace (small engine manufacturer after 3 years of service processing a 3000 series aluminum alloy) led to the following findings. Samples were found to be primarily composed of mullite ($3Al_2O_3$•$2SiO_2$) with calcium aluminate binder phases and calcium fluoride (CaF_2) anti-wetting agents commonly found in refractories for aluminum melting. From the chemistry of the calcium aluminate phase, the temperature of the lining was estimated at 900-1100^{o}C at the hot face and 800-900^{o}C further back in the lining. High amounts of kyanite (Al_2O_3•SiO_2) were found in the metal penetrated zones and calcium aluminate and calcium fluoride phases were not observed in these areas. In these zones, it was also found that an impermeable black layer formed at the hot face in which the mullite phase had been converted to corundum embedded within a continuous silicon matrix. Original alumina refractory aggregates were also found to be destroyed by the metal penetration and interaction with silica from the matrix phase. Converted alumina was not, however, found to be reduced by molten metal penetration. Grain growth of the alumina was observed in all of the sintered refractory

alumina aggregates in the metal penetrated zone and only kyanite grains were found to be unaffected by metal penetration. This may be due to the fact that kyanite is present as single crystals.

Analysis of surface deposits revealed that both “alumina mushroom” and alumina concretion structures were formed in thin layers. Adjacent to this metal penetrated zone, large quantities of anorthite ($CaO•Al_2O_3•2SiO_2$) formation in the form of a “ring” structure was observed in the matrix of the refractory. This suggests that the anorthite formed from CaO containing compounds, for example calcium aluminate cement clinkers or the calcium fluorite anti-wetting agent and silica containing compounds such as fumed silica, silicon metal or silica from the refractory mullite grogs.

Based on the characterization of currently used materials, several degradation mechanisms were identified in the refractory both above and below the melt line as shown schematically below in Figure 63.

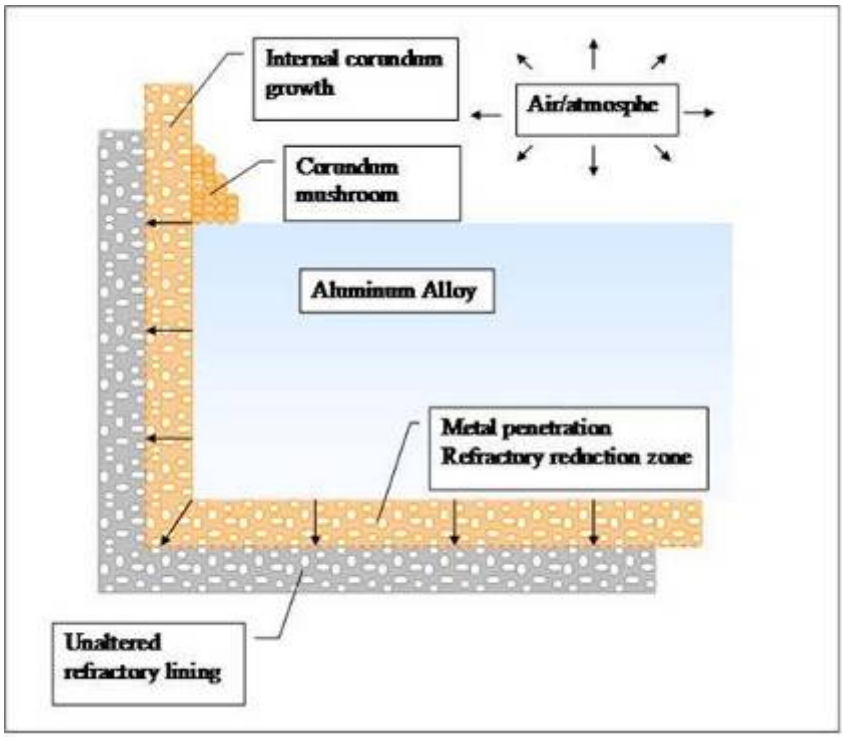

Figure 63: Degredation Mechanisms Identified in the Refractory (both above and below the melt line)

The most severe reactions were found to occur at the metal line triple point where solid refractory was in contact with the molten metal (liquid) and the gaseous species above the melt. At this location, formation of the corundum mushroom on the wall above the molten metal leads to spalling of the refractory wall as stresses are created by the alumina surface concretion and creation of porosity in the castable structure through internal corundum growth within the castable wall. Above the corundum mushroom, the refractory lining does not appear to be affected since it is only in contact with gaseous species from the melt. The integrity of the refractory lining below the metal line was degraded by metal penetration, as described below, leading to reduced thickness of the refractory wall and floor. This reduces the thermal efficiency

of the castable lining leading to greater heat losses and less heat retained in the process and can result in catastrophic failure of the aluminum containment vessel.

As a case study of the analysis of tested materials, the microscopy analysis of one characteristic sample is presented. SEM analysis of the penetrated zone does not reveal much information since the refractory is alumina based and the corrosion product is also alumina based. See Figures 64 and 65 below.

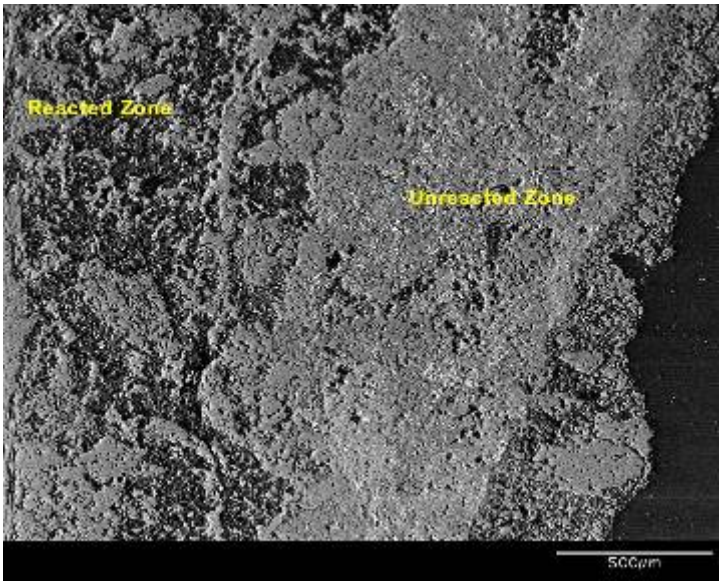

Figure 64: SEM image of penetration interface in sample SC-B

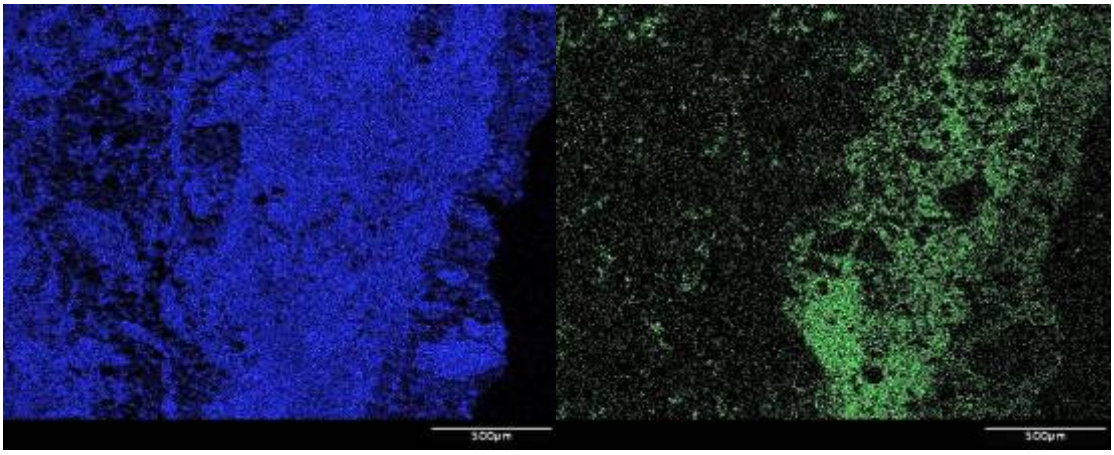

Figure 65: EDS elemental map showing Al (blue) and Si (green) in the area in Figure 64 (Note that the Si content was depleted in the penetrated zone)

SEM and EDS analysis are based on atomic weight of elements and do not help in identifying the mineral phases present in the refractory. Cathodoluminescence microscopy is thus an invaluable tool to have for such an analysis. It provides a low magnification view of the sample and hence gives a good idea of the chemical interactions that may have occurred in the sample. See Figure 66.

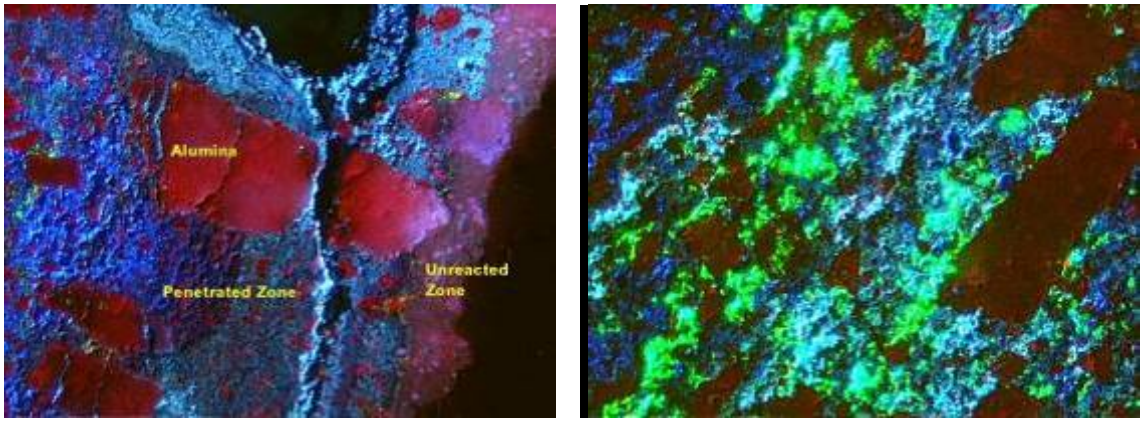

Figure 66: CLM image of penetrated refractory showing different colors based on mineral composition
(Note green layers of spinel are seen here, but not available through the SEM.)

Post mortem analysis through Scanning Electron Microscopy (SEM) and Energy Dispersive Spectroscopy (EDS), in conjunction with Cathodoluminescence Microscopy (CLM) was used to identify the chemical reactions occurring during molten aluminum penetration. Further, the penetration interface for each reaction was identified using EDS. From this analysis, it was found that the major problems associated with refractory degradation involved poor anti-wetting additives, poor refractory quality, reaction of silica, and poor furnace maintenance practices. Therefore, this project focused on the use of kyanite in place of fumed silica, the use of higher purity aggregates, and the identification of materials better suited for current maintenance procedures.

5.4.3 Materials Testing

New formulations of Fireline materials were designed based on test data generated from this project. Samples were supplied to ORNL and UMR for evaluation by strength and thermal shock testing to validate them for use in molten metal applications. Strength was evaluated through modulus of rigidity (MOR) testing and thermal shock was characterized by carrying out MOR testing at room temperature before and after thermal cycling. Results from testing are shown in Figure 67 below compared to previous TCON® Materials tested (TC2 is a new material, values following sample identity were test temperature in degrees Celsius, RT-room temperature/TC-thermal cycled).

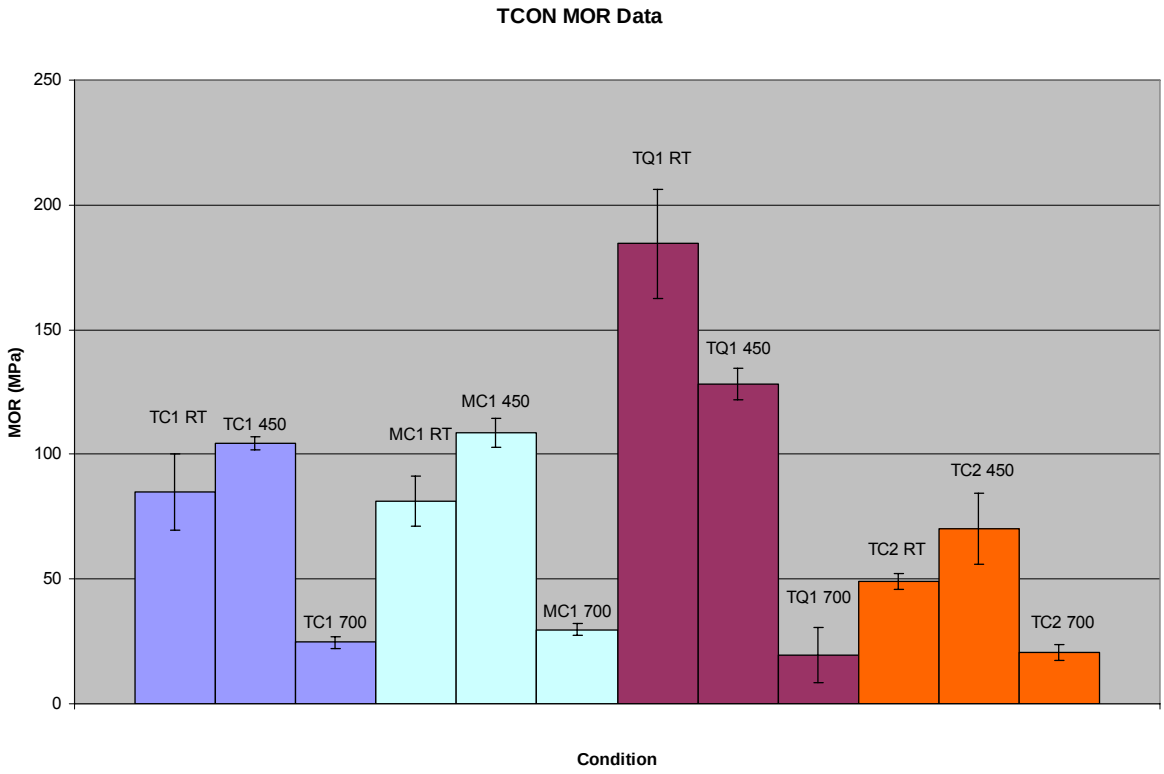

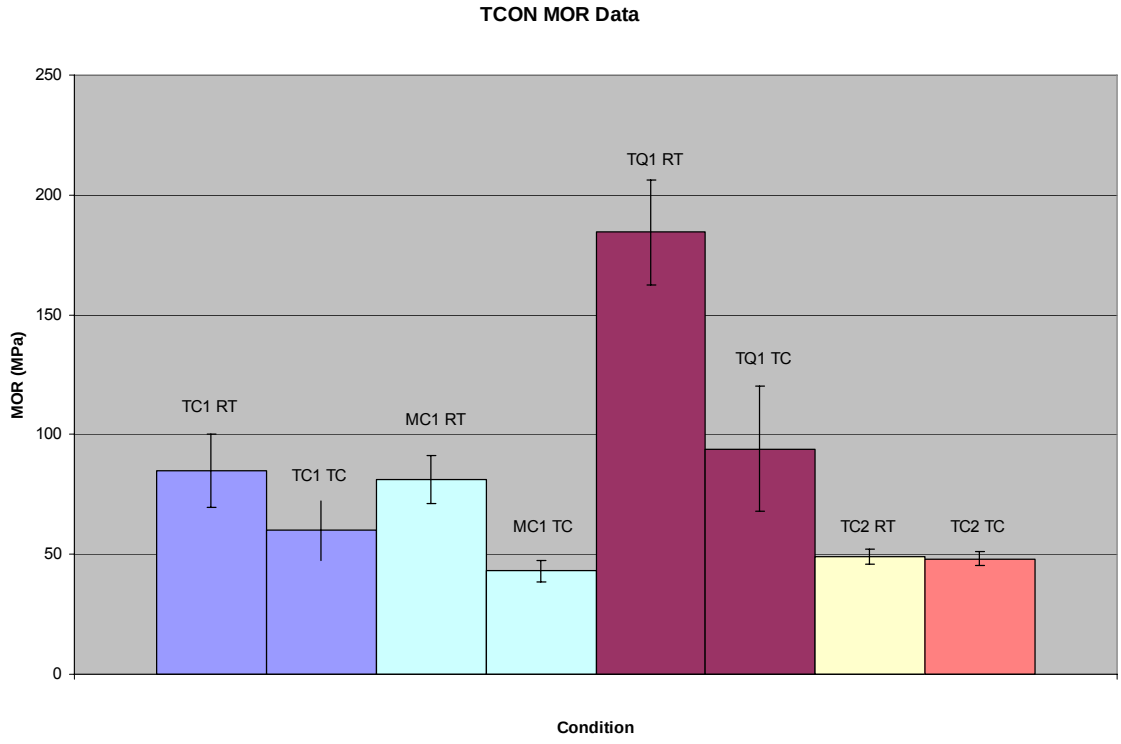

Figure 67: Results of TCON® MOR Testing for Various TCON® Formulations at Room Temperature (RT), 450oC (450), 700oC (700), and After Thermal Cycling (TC)

Results from testing indicated that the newly developed materials have lower strength than the previously developed materials, but greater thermal shock resistance. Although the strength was lower as compared to previous TCON® materials tested, it is still far superior to most refractory materials used in this application.

Testing was also carried out to evaluate adhesion between the bonite castable and the TCON® material developed for the integrated lining structures utilized for this project. TCON® TC2 samples were cut in half longitudinally and a 1" thick layer of bonite castable was cast between the two halves. Following air drying over night, the samples were taken through an extended dry out cycle consisting of ramp and hold segments resulting in heating to 1000°C over a 26.5 hour period. After natural cooling, MOR testing was performed at room temperature, 450°C, and 700°C. Results of testing are shown below in Figure 68, which also shows comparative values to those previously determined for TCON® TC-2 samples.

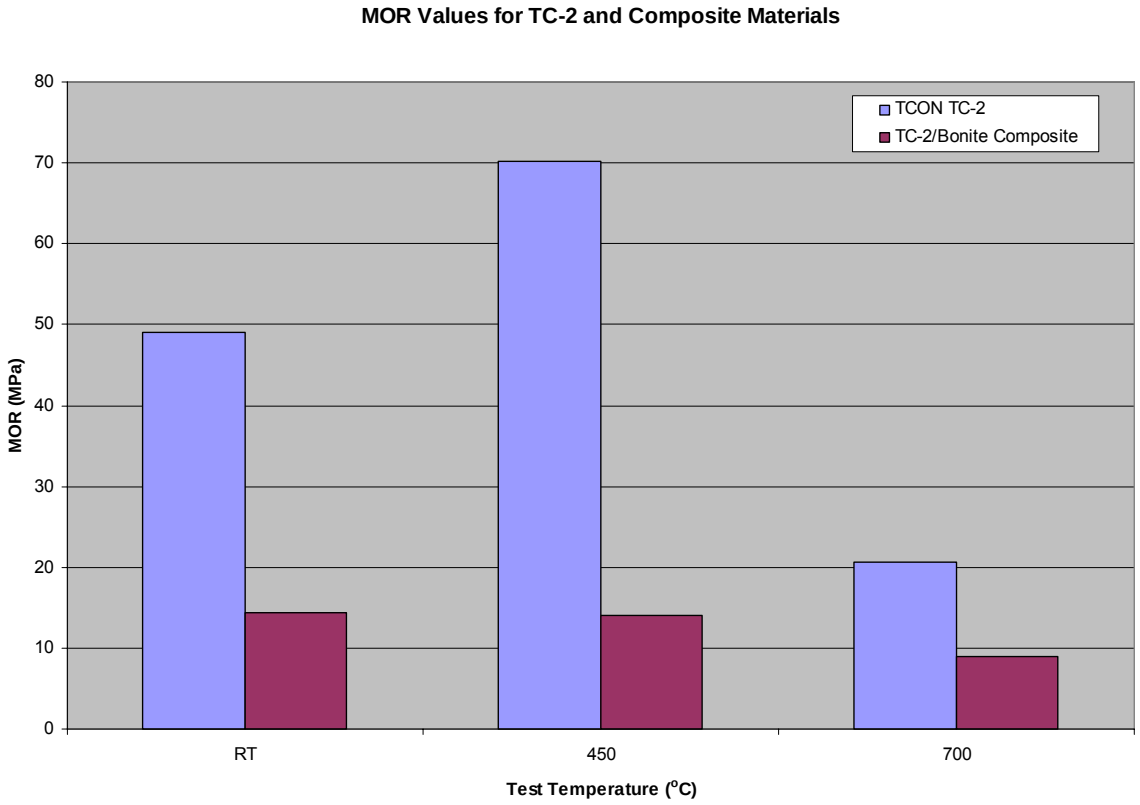

Figure 68: Results of MOR Testing Performed at Room Temperature

It was found that there was a drastic decrease in strength at all temperatures for the composite samples, as compared to the original TC-2 samples. This drop off in strength was partly due to the fact that the castable is physically weaker than the TCON® material. The large drop off in strength also indicated that there was poor adhesion between the TCON® material and the castable. This was further confirmed by visual inspection of the samples after testing, which revealed separation of the TCON® plate from the castable.

Simulative static corrosion testing was conducted at UMR by standard cup testing as described earlier.

Material 1:

A Hibonite (calcium hexa-aluminate) based castable refractory was developed at UMR with optimized water content. Initial observations of the material showed that it performed exceptionally well in the static cup test. As seen in Figure 69, there was no visible penetration of molten alloy and no trace of aluminum oxidation either. These favorable results were confirmed through analysis by SEM, optical and cathodoluminescence microscopy.

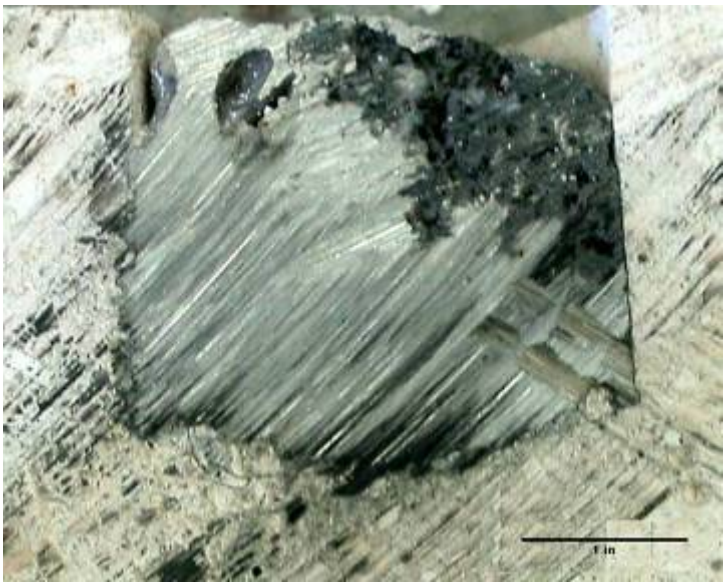

Figure 69: Bonite Material Cup after Testing

Scanning Electron Microscopy (SEM) and Cathode Luminescence Microscopy (CLM) were performed on each tested sample. Figure 70 shows a CLM image of a penetration interface. The refractory remained unchanged with a very thin layer of penetration (a few microns in thickness) which, appears as a bright line at the metal-refractory interface in Figure 70.

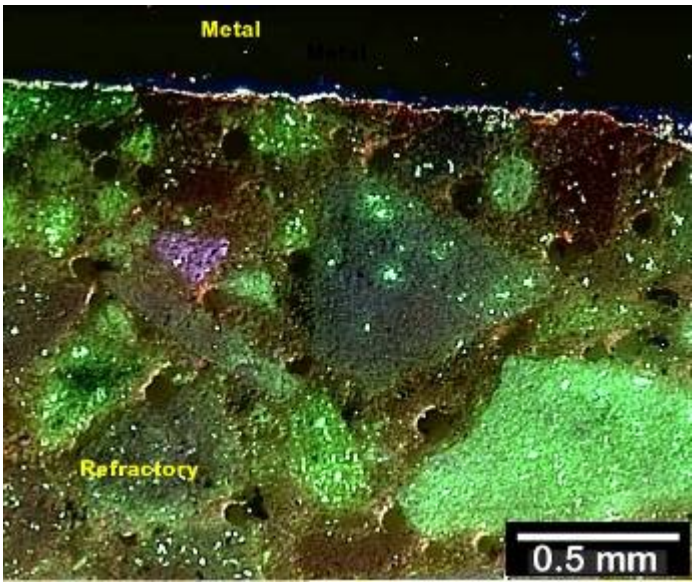

Figure 70: CLM Image of Penetration Interface after Static Cup Testing

Higher magnification SEM images showed that some metal had indeed penetrated. As noted in Figure 70, the layer is approximately 50µm thick. Energy Dispersive Spectroscopy showed that the magnesium and aluminum from the molten alloy had penetrated into the refractory. There was also a visible densification of the matrix in the penetration zone as is seen in Figures 71 and 72.

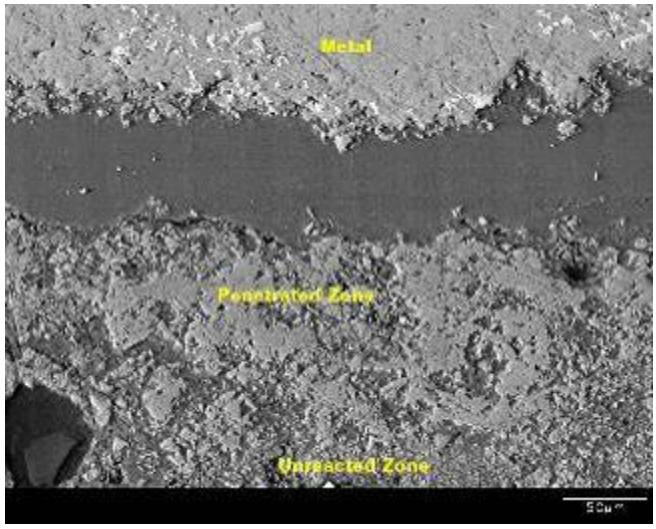

Figure 71: SEM Image of Penetrated Zone after Static Cup Testing

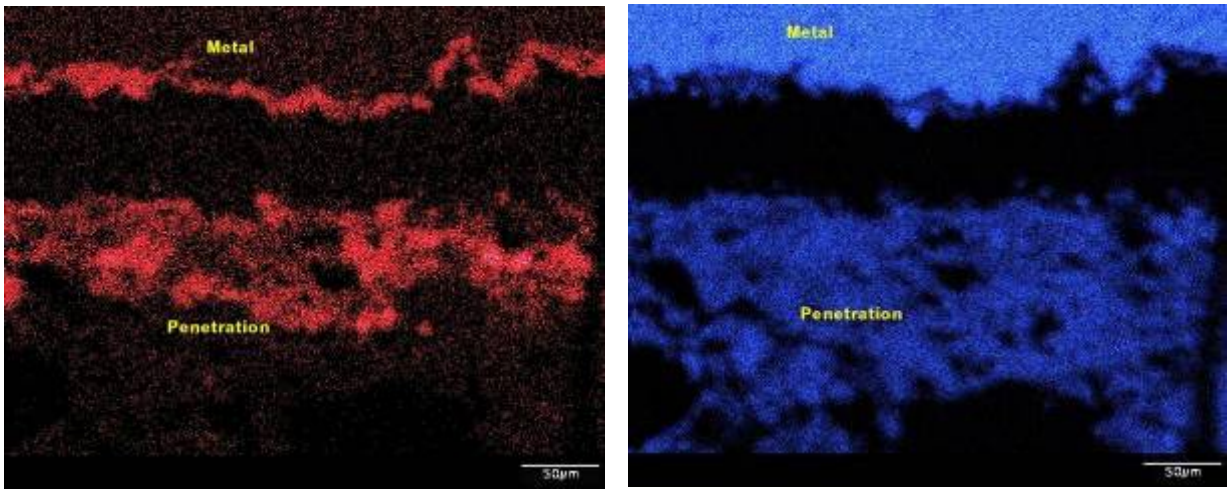

Figure 72: EDS Image of Penetration Layer showing Magnesium in Red and Aluminum in Blue

Material 2:

An alumina/SiC composite material was also tested. Figure 73 shows the cross section of the cup after static cup testing.

Figure 73: Material EH after static cup testing

Observations showed that the material provided excellent resistance to penetration. However there was a small corrosion layer present which was further investigated using microscopy techniques.

The first observations made were in regard to the silicon enrichment into the molten alloy. Microscopy showed that eutectic silicon metal was present in the molten alloy near the metal-refractory interface. This is in accordance with the well known reaction known to occur between molten Al and silica. Figure 74 shows the Silicon formation in molten alloy.

$$4Al + 2SiO_2 = 2Al_2O_3 + 2Si \qquad \textbf{Equation 8}$$

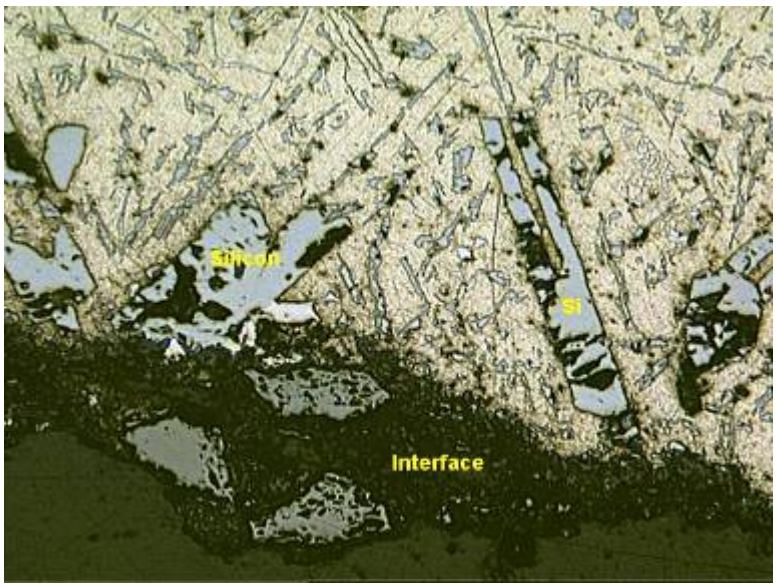

Figure 74: Eutectic Silicon Dendrites in Molten Alloy after Testing

Observations showed that the molten alloy had no effect on the structural integrity of the test cup since there were no visible signs of thermal stress or specific corrosion attack. There also appeared to be some stratification within the cross section of the test cups. This may be attributed to metal penetration and was further investigated by microscopy as this was the only visible change in the material after testing.

CLM analysis of this material showed a silicon carbide aggregate in an alumina matrix. Figure 75 shows the CLM image of the sample that was not affected by molten alloy. Note the similarity in Figures 75 and 76 respectively. This shows that the refractory aggregates (SiC) have not been damaged by the penetration process. The previously described silicon enrichment of the molten alloy has occurred by the reduction of any free silica that may be present in the refractory matrix.

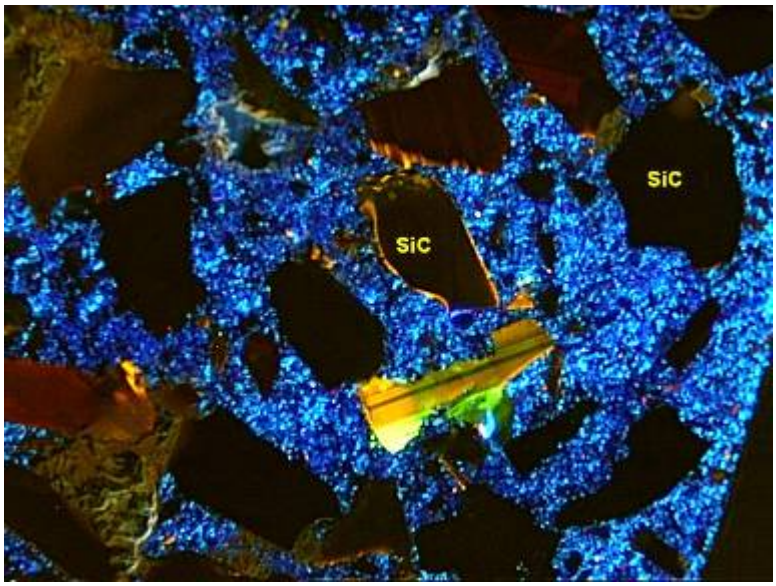

Figure 75: CLM Image of Virgin Material EH

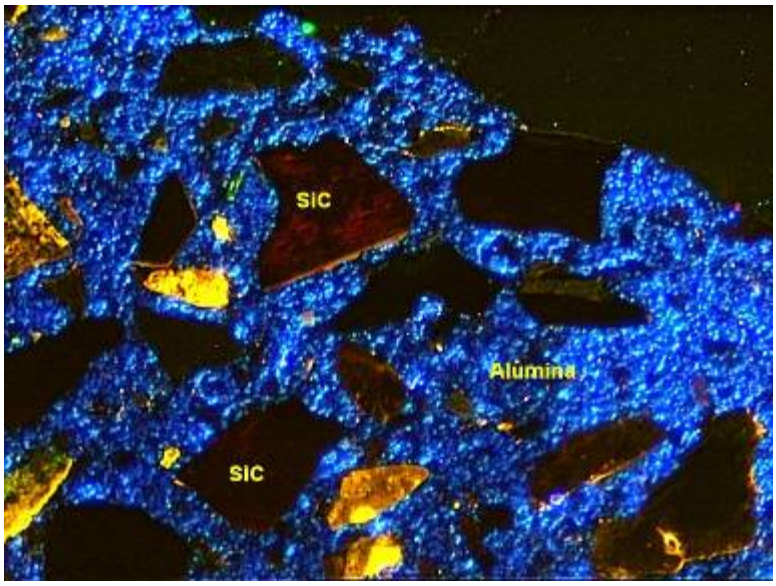

Figure 76: CLM Image Of Contact Area of Material EH After Testing

For the material tested, there was no structural damage to the test specimens although the reduction of silica to elemental silicon had occurred. The silicon had formed globules of metal within the material matrix and the silicon closer to metal alloy had dissolved into the alloy.

Analysis was performed on experimental materials from Fireline, Youngstown, OH. These samples were studied after exposure for 100 hours in molten aluminum. Analysis revealed lack of penetration and good corrosion resistance of these materials in the molten metal bath. Thermal shock resistance was found to be an issue for these materials and warranted further development activities by Fireline.

Analysis was next performed on the previously analyzed materials from Fireline, Youngstown, OH which had been exposed to molten aluminum for 1,000 hours. Additionally, analysis was performed on new refractory samples designed by Fireline based on previous testing results at ORNL and exposed for 100 and 500 hours in molten aluminum. Analysis revealed lack of penetration and good corrosion resistance in all of these materials during exposure to the molten metal bath. Thermal shock resistance was still found to be an issue, though for the modified materials received, it was improved over the materials tested earlier. Testing of subsequently modified materials showed even further improvement in thermal shock resistance. Analysis was also performed on TCON® samples which were subjected to Modulus of Rupture Testing (MOR) and thermal shock testing as part of another project. Results from this analysis were used to aid in identification of failure mechanisms and material life prediction under thermo-mechanical stresses.

Subsequently produced TCON® materials were subjected to a more aggressive aluminum alloy (5083) containing magnesium. Samples were analyzed after 1000 hours of exposure with these materials still showing promising resistance to corrosion by molten aluminum with sharp corners retained on samples and non-wetting behavior exhibited (see Figure 77). Thermal shock was still found to be an issue for these materials.

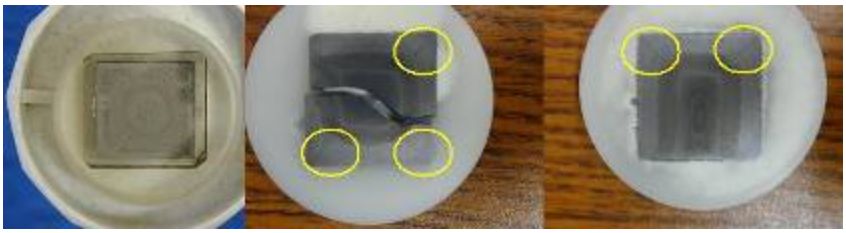

Figure 77: Cross-sectional mounts of TCON® materials subjected to corrosion testing in molten aluminum showing sharp edges of samples maintained, significant non-wetting behavior, and cracking indicating thermal shock

TCON® materials were also subjected to dynamic corrosion testing and samples were analyzed after 100 and 500 hours of exposure. Similar to previous analysis discussed above, a lack of penetration, indication of good corrosion resistance, was seen in all materials during exposure to the molten metal bath. Thermal shock resistance was also found to be improved for this latest round of materials, but was still an issue along with hot strength.

Microstructural analysis of TCON® materials was performed by SEM with chemical analysis of materials being performed by EDS. Examples of material microstructures and chemistry are shown below in Figure 78.

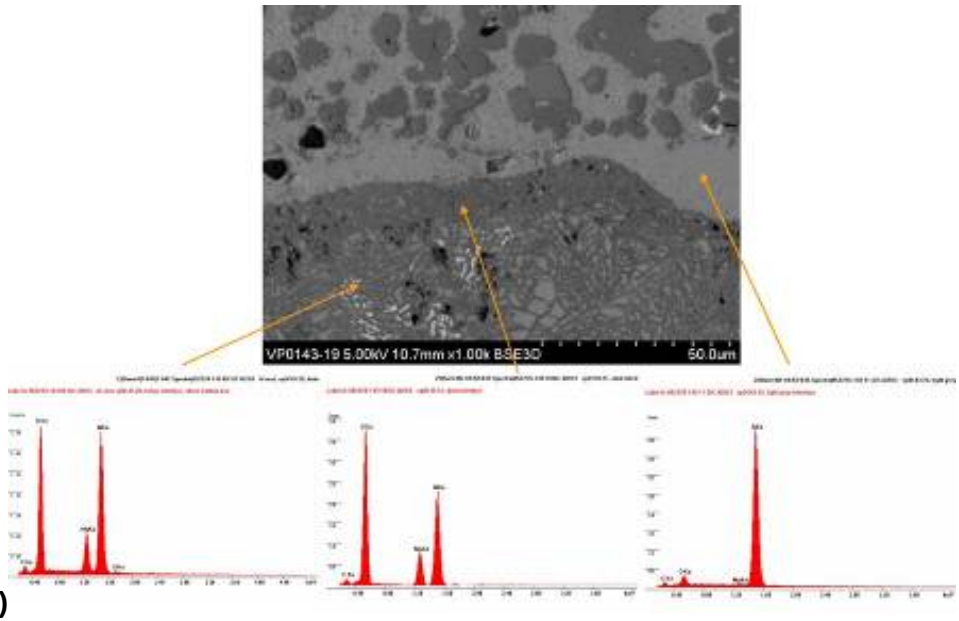

a)

Figure 78a: Microstructural and X-ray analysis results for early TCON® version (MC) sample after 100 hour exposure in molten aluminum for edge region

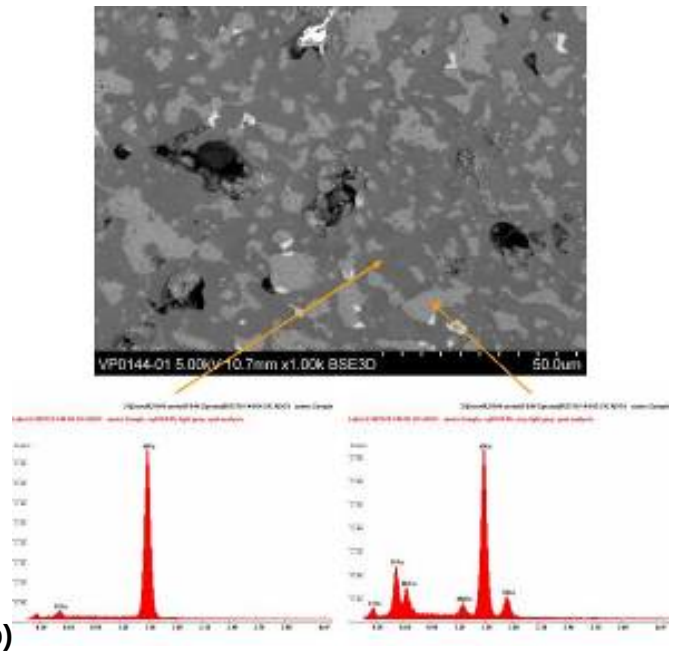

b)

Figure 78b: Microstructural and X-ray analysis results for early TCON® version (MC) sample after 100 hour exposure in molten aluminum for edge region (a) and center region

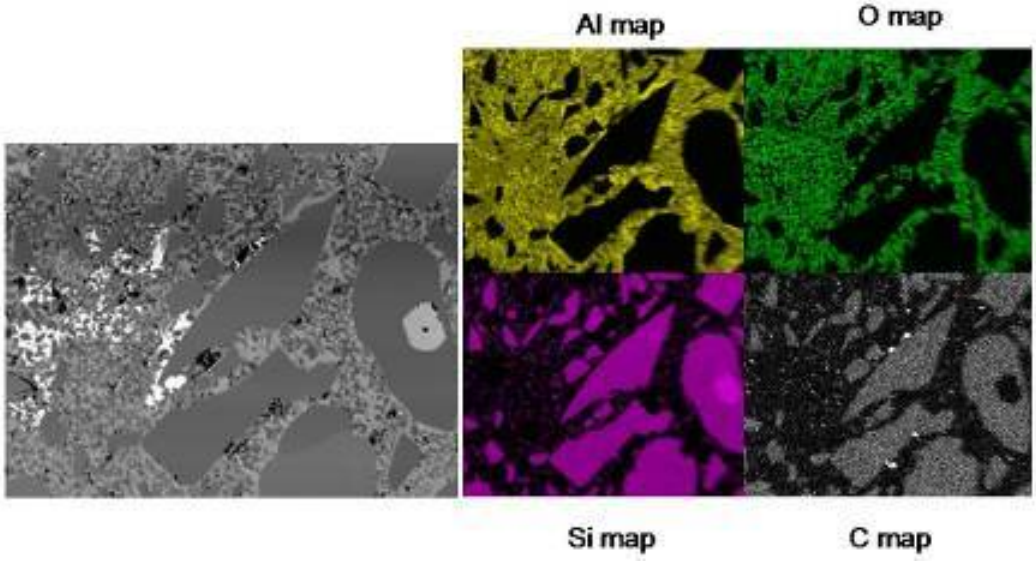

c)

Figure 78c: Microstructural and chemical analysis results for later TCON® version (TC) sample after 100 hour exposure

Further microstructural analysis of TCON® samples subjected to dynamic corrosion showed signs of wetting between the refractory and molten aluminum. Contrary to previously reported results discussed previously, signs of wetting between the SiC particles of the TCON® refractory and the aluminum metal were found as shown in Figure 79 below. The refractory matrix (primarily alumina) was found to still be non-wetting. In addition, a reaction layer between the molten aluminum and the refractory surface was found at locations at and below the metal line as shown below in Figure 80.

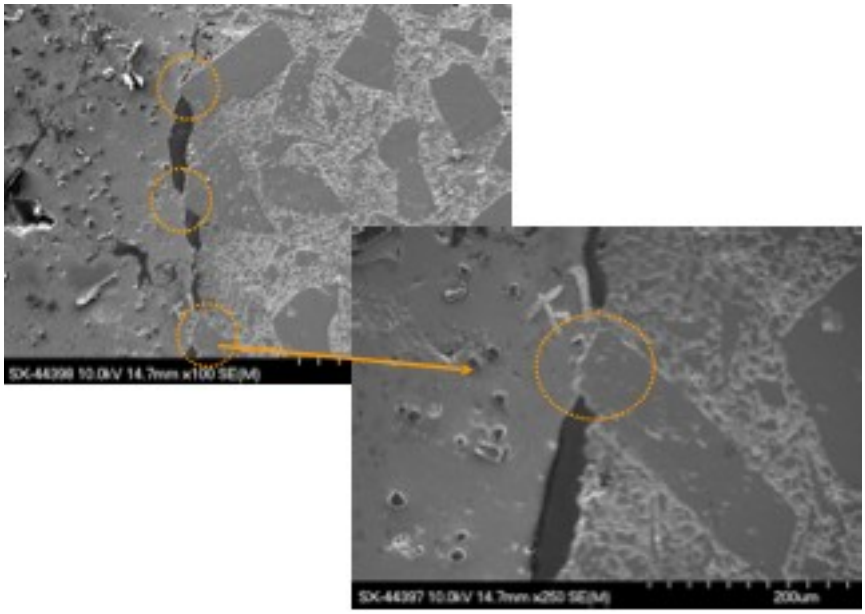

Figure 79: Wetting of SiC particles in TCON® refractory material by 5083 aluminum (circled regions) - Gaps seen between alumina refractory matrix and 5083 aluminum

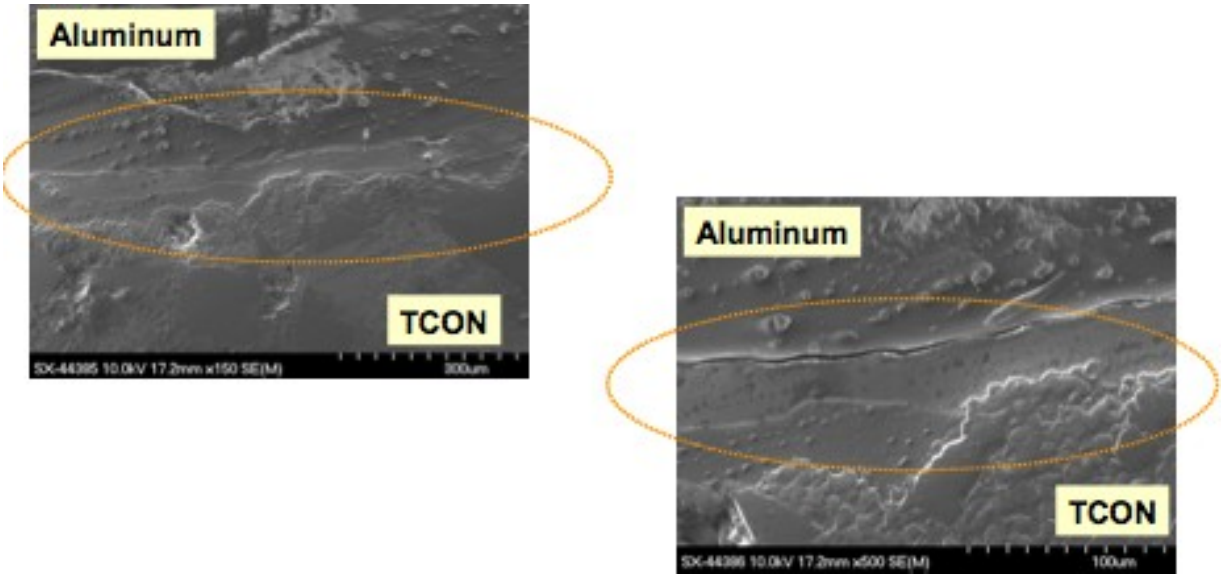

Figure 80: Presence of reaction layer between TCON® refractory material and 5083 aluminum

This indicated that the previously reported conclusion of the TCON® materials being completely non-wetting was false, although these materials showed far less wetting behavior than other currently used refractory materials studied from the aluminum industry. To further evaluate the wetting behavior of the TCON® material, static sessile drop testing was performed. Through this study, molten aluminum was found to be initially non-wetting to TCON® refractory substrates, but was then found to react with time leading to a wetting condition between the

molten aluminum and the substrate as shown in Figure 81. Further detail on this testing can be found in the work published in the *International Journal of Applied Ceramic Technology* [7].

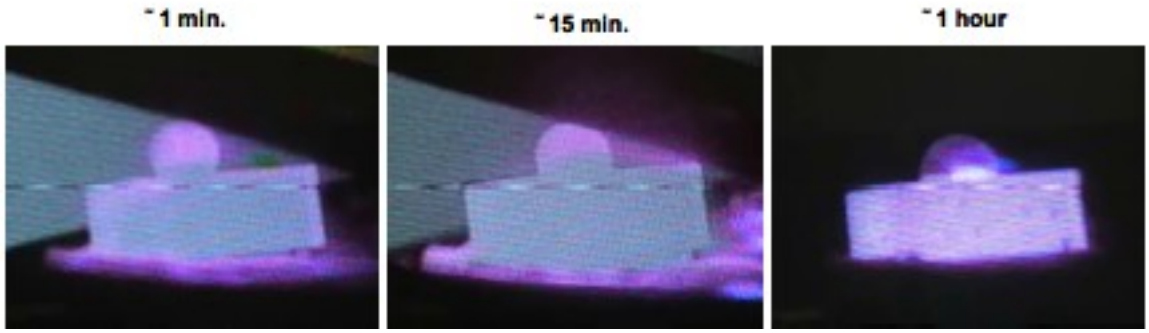

Figure 81: Static sessile drop testing of TCON® TC refractory with 50835 aluminum

The metal was found to be initially non-wetting to the refractory substrate as indicated by the high wetting angle exhibited by the ball of molten metal. The metal was then found to begin reacting with time, leading to a wetting condition between the metal and the substrate as indicated by the decease in wetting angle. Although wetting was seen in these tests, no significant reaction was observed between the metal and the refractory. Further, it was found that the SiC did not wet during the one hour test, but there was evidence that it might under longer duration interaction. The matrix phase (Al_2O_3) was found to wet, but not to react with the metal. Examples of this are shown in Figure 82.

a)

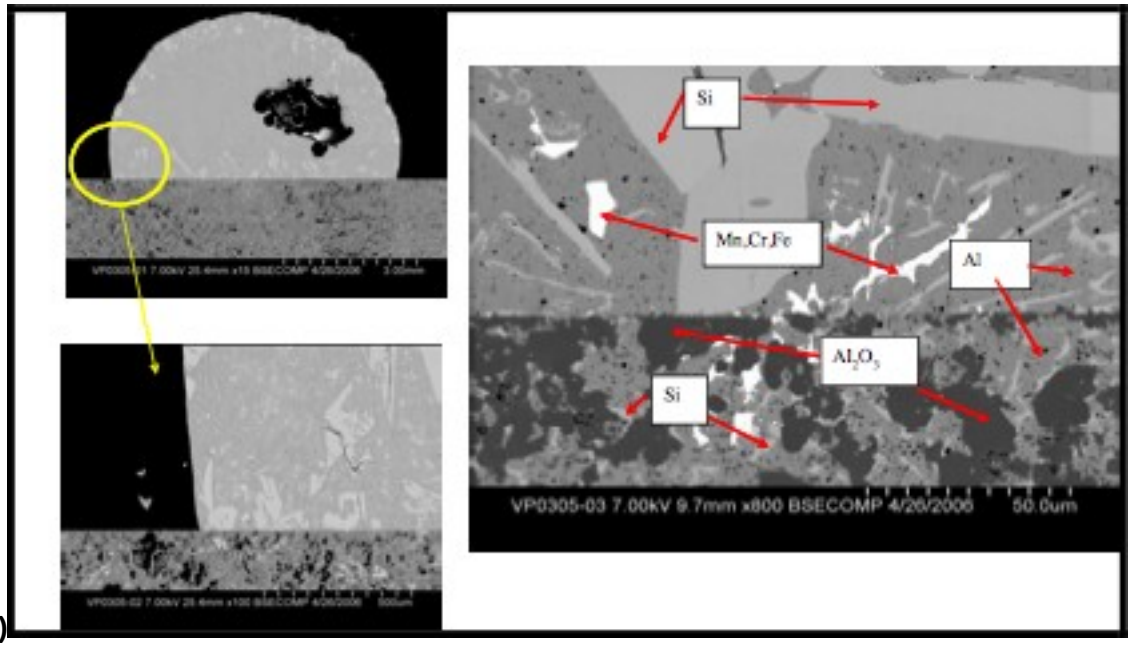

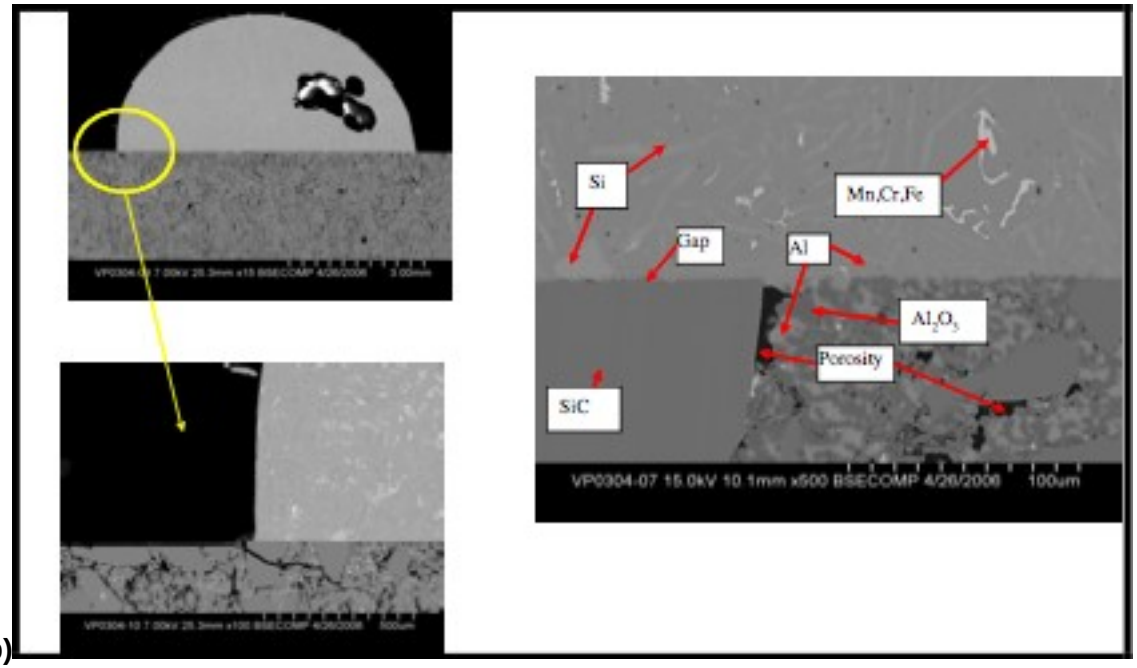

b)

Figure 82: Micrographs of TCON® TC refractory static sessile drop specimens with aluminum alloy

It was observed that although evidence of wetting was seen, no reaction was present between the ceramic substrate and the molten metal (a). Further, it was observed that the SiC does not wet, while the matrix shows signs of wetting but not of reaction (b).

Microprobe mapping of the molten metal/refractory interface was also performed and the results are shown in Figure 83. This mapping revealed the diffusion of silicon from the refractory substrate into the molten aluminum droplet. Low levels of Mn, Cr, and Fe were also detected on both sides of the interface.

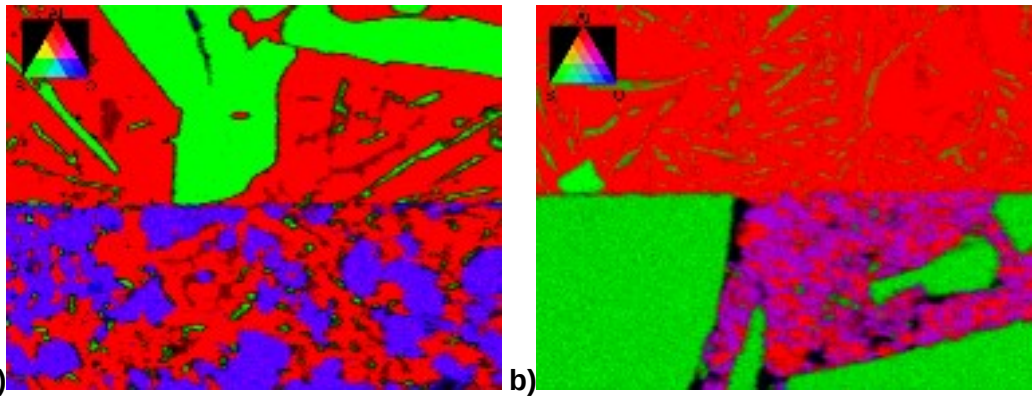

a) b)

Figure 83: Microprobe images of TCON® TC refractory static sessile drop specimens with aluminum alloy

It was observed that silicon diffused from the refractory substrate into the molten aluminum droplet and that various impurity elements were present on both sides of the interface. A sharp interface was present though indicating lack of reaction.

Based on previous test results, additional TCON® samples were developed and received from Fireline representing improved grades of material expected to provide better thermal shock resistance, while maintaining the good corrosion/erosion/wear resistance of the previous formulations. Samples exposed to both static and dynamic corrosion testing with immersion times of 250 and 500 hours in molten aluminum alloy were analyzed with results found to be similar for both immersion times. Observation of test samples showed minor adherence of metal to the refractory surface, but no sign of corrosion. Samples were sectioned and examined using optical microscopy which revealed interaction of the metal with the test sample, as indicated by a reaction zone on the exterior of the sample, which extended approximately 1/8" into the sample. This reaction zone was similar in thickness for both the 250 and 500 hour samples, leading to the conclusion that this layer may be static and will not increase with further exposure time. Such behavior is often seen in refractory materials subjected to molten metal or glass exposure, as the reaction occurring at the refractory/molten materials surface forms an in-situ passivating layer that acts to protect the refractory after initial reaction. If this is the case, then this material would be expected to exhibit excellent corrosion resistance in the molten aluminum environment. Further, these results would support those obtained earlier on the original TCON® material through static, dynamic, and sessile drop testing as previously presented.

To address concerns regarding dross formation and interaction with refractories above the metal line with air, dynamic corrosion testing was performed with argon above the molten metal for 250 and 500 hours in molten aluminum alloy. Analysis of samples from this testing found that below the metal line, behavior was similar to what was previously seen with significant adhesion of metal to the refractory surface, but little apparent penetration or reaction of the metal with the refractory. Cross sectioning of samples revealed interaction of the metal with the test sample, as indicated by a reaction zone on the exterior of the sample which extended approximately 1/8-1/4" into the sample. This is similar to what was found previously for static corrosion samples. Above the metal line, the solidified dross layer previously seen on dynamic test samples was absent for the 250 hour samples and minimal for the 500 hour samples (1/8" or less). X-ray diffraction and SEM/EDS revealed that the reaction layer seen on these samples was composed largely of silicon metal indicating that the silicon is diffusing from the refractory substrate into the molten Al during the exposure. In addition, aluminum metal was found in the reaction zone indicating that Al is diffusing into the pores of the refractory substrate. The diffused liquid Al joins with the existing residual Al metal present in the composite refractories, inhabiting both the pores as well as positions vacated by the diffusing silicon.

Initial static and dynamic corrosion testing of the TCON® material, along with sessile drop testing, showed this material exhibited non-wetting behavior on the macroscopic level and only slight wetting behavior on a microscopic level. Additionally, exposures of up to 500 hours in contact with molten aluminum showed only minimal interaction of the material with the molten metal and the formation of a passivation layer on the refractory surface which served to protect the refractory from further reaction.

5.4.4 Thermal Conductivity

Results have been achieved to validate the method and to measure the properties of experimental materials from this project as follows:

Initial measurements were made on a high purity alumina sample (Coors AD98) previously measured by multiple techniques in a previous study [8]. This sample represents a homogeneous, small grain sized material that should not present difficulties in measurement due to grain size or heterogeneity effects. The thermal conductivity values previously measured for this sample by hot wire, calorimetry and laser flash are shown below showing the variation in

measured values by technique and even within technique in the case of calorimetry. It was expected that since the measurements of this sample should not be affected by grain size or heterogeneity concerns, results obtained by the new IR technique should compare well with those obtained by the laser flash diffusivity technique. This was in fact the case as seen in Figures 84 and 85 below.

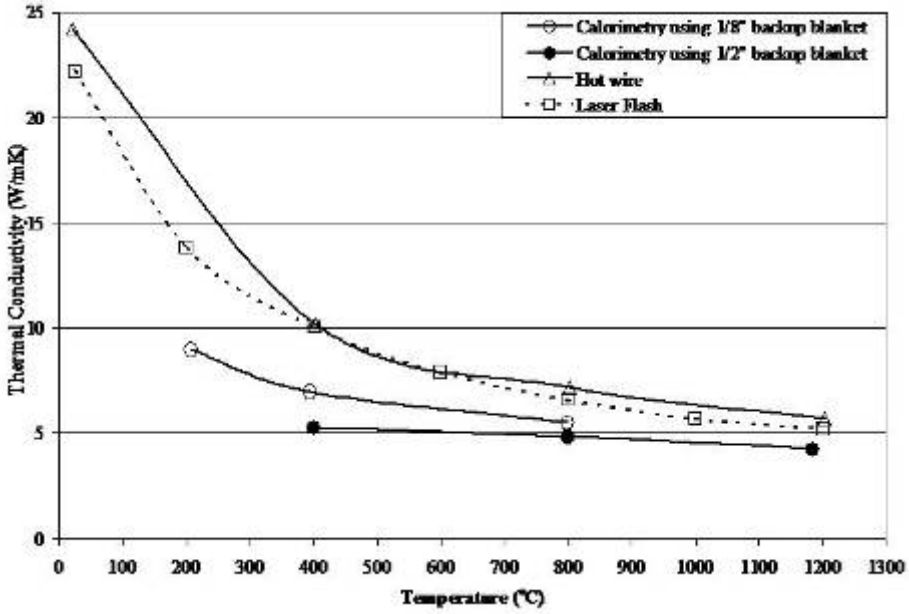

Figure 84: Thermal Conductivity Values for High Purity Alumina (Coors AD98) as Measured by Various Techniques[2]

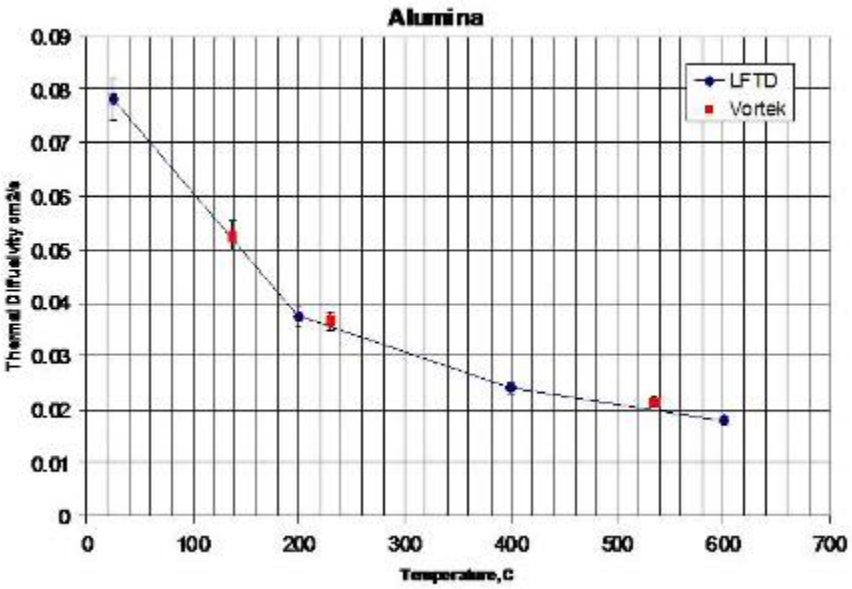

Figure 85: Comparison of Laser Flash and IR Thermal Conductivity Measurements on High Alumina (Coors AD98) Material (LFTD – Laser Flash Diffusivity Technique, Vortek – IR Technique)

Measurements were also made on a number of commercial refractory materials with published conductivity results. Results for two such materials, Harbison Walker Clipper DP brick and ArmorKast 65AL castable, are shown below in Figure 86. These materials were chosen to represent two standard refractory materials; an insulating fire brick (IFB) and a traditional metal contact castable.

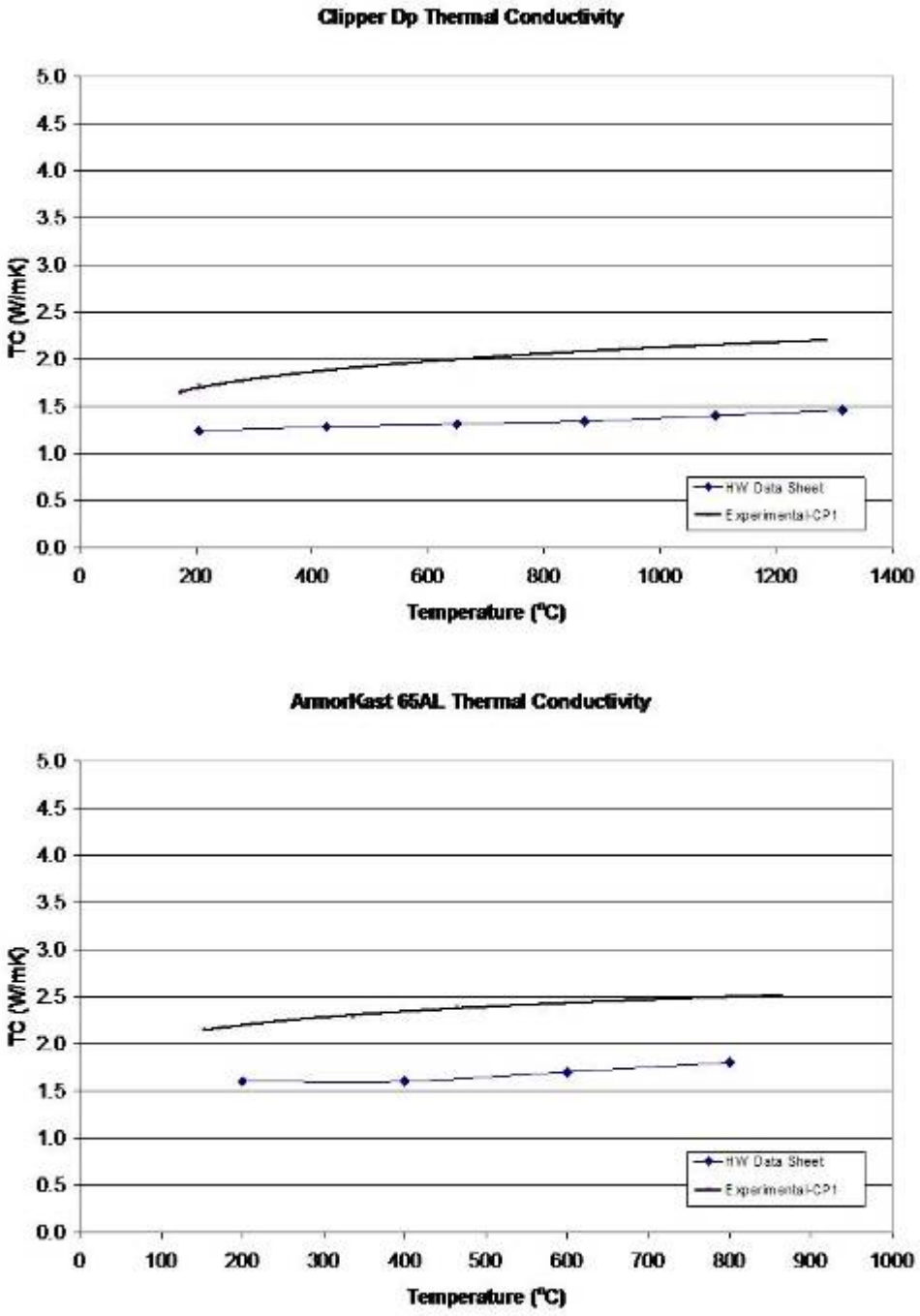

Figure 86: Experimental and Published Thermal Conductivity Values for Clipper DP and ArmorKast 65AL Refractory Materials

Thermal diffusivity measurements were also made on two grades of TCON® experimental material with unknown conductivity values. These materials, TC1 and TC2, were under consideration for use as primary hot-face lining and wear resistant lining materials. Conductivity of the TCON® materials was seen to decrease with temperature, as often is seen in bulk ceramic materials. Values were similar between the two formulations with the TC1 material being slightly more thermally conductive than the TC2 material.

Since no literature data exists for this material, experimental data in Figure 87 was compared to theoretical data for the refractory's components. Data is shown for alumina (Al_2O_3), silica (SiO_2), silicon carbide (SiC), aluminum metal (Al), and silicon metal (Si) is shown in Figure 88. Experimental results were shown to compare favorably with this theoretical data in Figure 89.

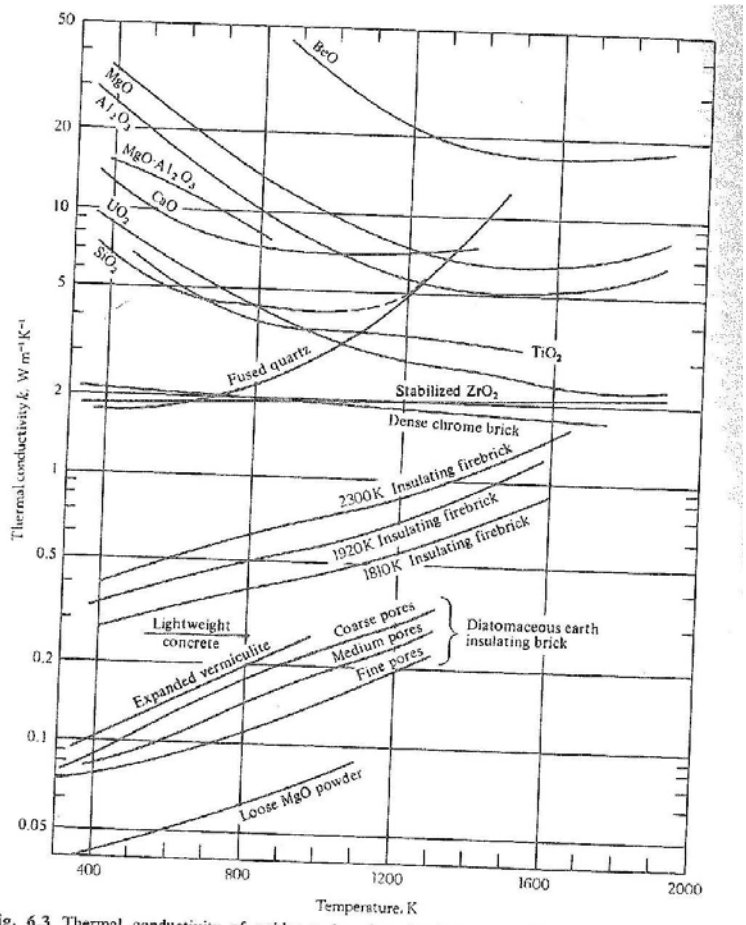

Fig. 6.3 Thermal conductivity of oxides and various insulating materials. (From A. Schack, *Industrial Heat Transfer*, Wiley, New York, NY, 1965, page 189.)

Figure 87a: Theoretical Thermal Conductivity Curves for Oxides such as Alumina and Silica

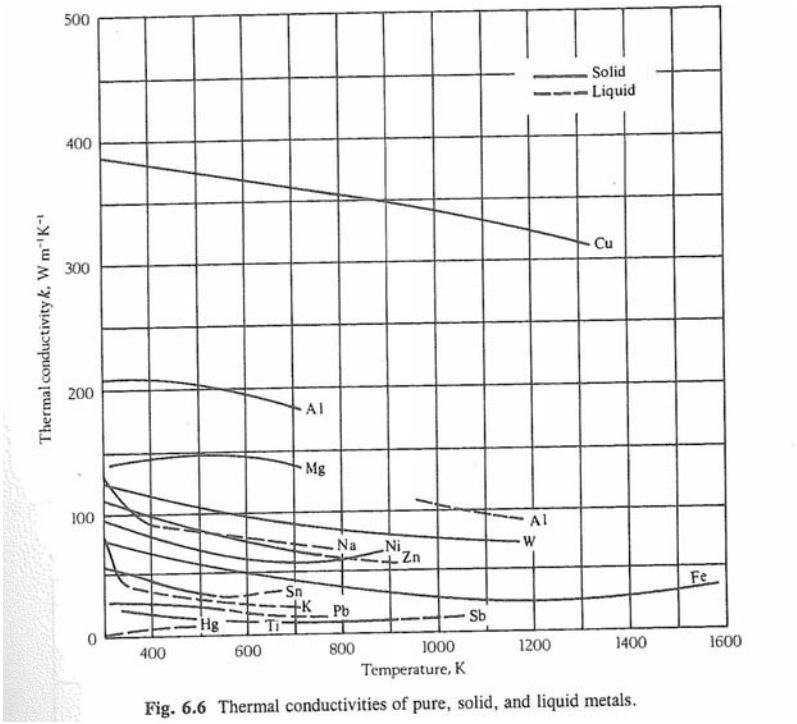

Fig. 6.6 Thermal conductivities of pure, solid, and liquid metals.

Figure 87b: Theoretical Conductivity Curves for Metals such as Aluminum and Silicon

Figure 87: Theoretical Data for Refractory Components

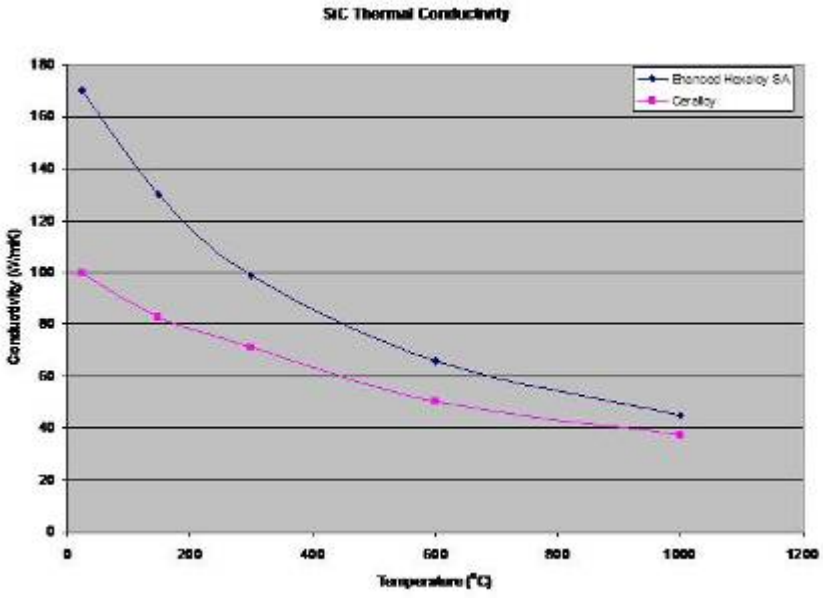

Figure 88: Experimental Data for SiC Thermal Conductivity

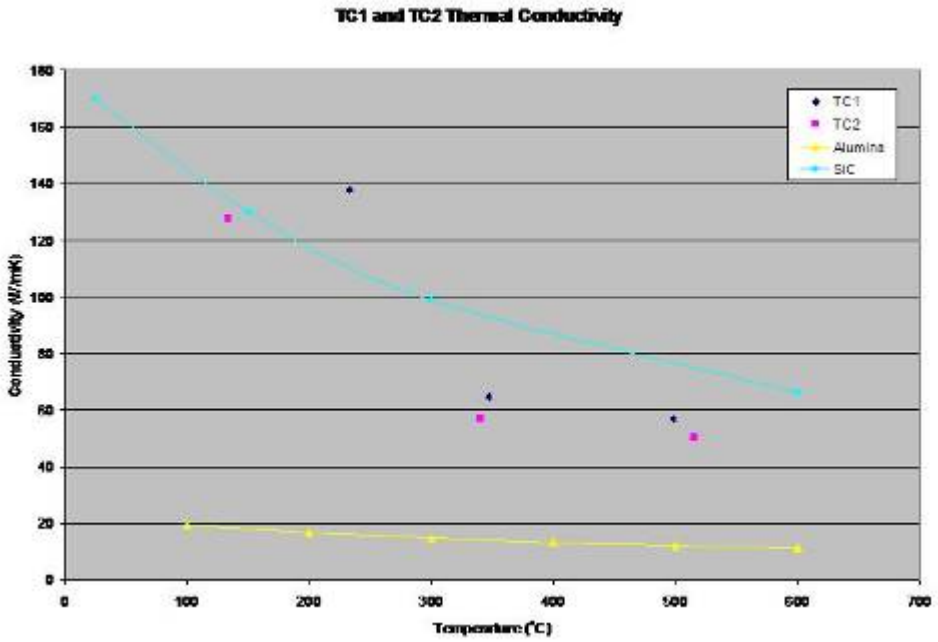

Figure 89: Experimental Data for TC1 and TC2 Thermal Conductivity

Testing was also conducted on the experimental bonite material that was developed under this project. Results of testing with the projected trend in data are shown in Figure 90. No “literature data” for this material currently exists. Measurements were only made at lower temperatures due a blown lamp tube. Higher temperature measurements were planned, but never carried out.

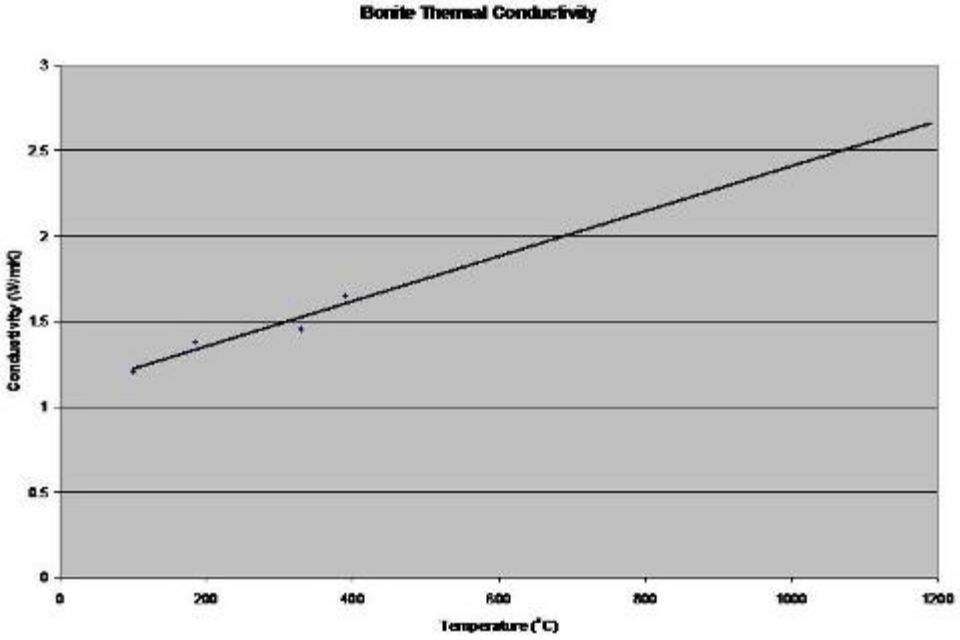

Figure 90: Results of Bonite Thermal Conductivity Testing with Projected Trend in Data

The TCON® material was found to exhibit high conductivity values dictated by the SiC content at lower temperatures and by the Al_2O_3 content at higher temperatures. The bonite material was found to have low conductivity, as would be expected for an insulating castable. The use of these two materials together may be sufficient to produce a suitable refractory lining for molten aluminum containment since a lining could be produced with both abrasion/wear resistance and thermal efficiency.

5.4.5 Development of Refractory Corrosion Model

Refractories for molten aluminum container applications serve two major purposes:

- To preserve energy during operation, i.e. minimize heat losses. Maintaining the aluminum in its molten state prior to casting is an energy intensive process. It is vital to maintain high enough temperature for smooth flow of molten alloy. The basic purpose of the refractory material is to insulate the holding vessel so as to minimize heat losses from the molten alloy into its surroundings. This type of refractory is usually a thermal insulation material, with low mechanical strength and poor chemical resistance to the molten alloy.
- To protect the insulation material and outer steel casing of holding vessel. The molten metal is highly corrosive. It will react with the thermal insulation and the outer steel shell causing severe damage to the mechanical integrity of the holding vessel and at the same time cause loss of molten alloy due to contamination as a result of reaction with these insulation layers. Thus the contact surface between molten metal and refractory should be a dense material with high chemical resistance to molten metal and good mechanical strength to resist wear and erosion caused by the flow patterns of viscous molten metal.

In the case of refractories for aluminum contact applications, alumino-silicate based castables have been traditionally used. These materials exhibit good mechanical properties at the service temperature and good thermal shock resistance as well. In addition, they are widely available and hence inexpensive. However, these have been found to be susceptible to chemical reaction with molten aluminum and consequent mechanical damage. Corundum formation by reaction of aluminum with refractory oxides (mainly silica) is detrimental to the service life of refractory linings. Such degradation of refractory is more pronounced when aluminum contains alloying elements such as magnesium and zinc.

The conversion of alumino-silicate refractories into corundum has a three pronged damaging effect. First, it leads to a sharp decrease in mechanical properties of the refractory lining. The corundum formation leads to volume expansion followed by spalling, induces stresses and crack formation and eventually aids in further penetration of alloy. Initially the conversion of alumino-silicate to corundum results in a volume expansion. This opens up the structure of the refractor and leads to spalling. This effect compounds damage and ultimately leads to mechanical failure of the refractory lining. Figure 91 shows a typical alumino-silicate castable in contact with molten aluminum alloy after cup testing. Note the severe cracking caused by corundum formation.

Figure 91: Expansion cracking in alumino-silicate castable after aluminum penetration

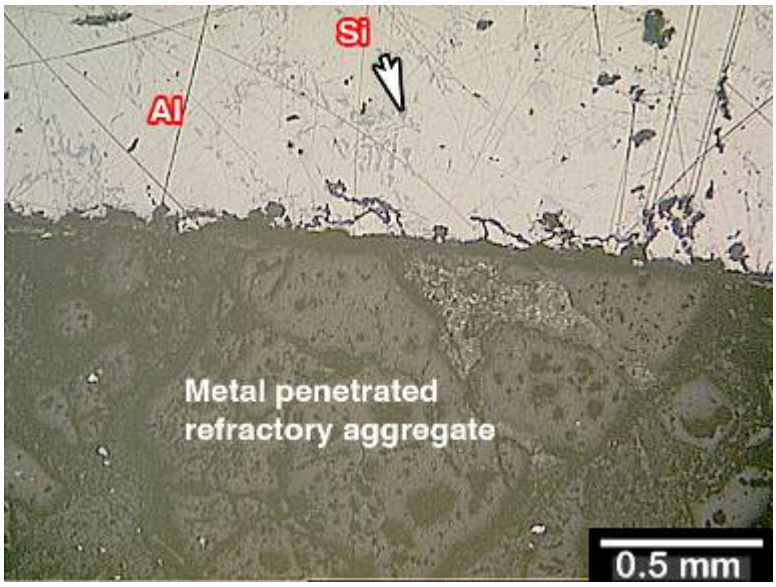

Figure 92: "Silicon Pickup" in aluminum after testing with alumino-silicate refractory

The second impact occurs on the molten aluminum itself. The reaction with refractory oxides leads to corundum formation by reduction of these oxides. The metals in their reduced state contaminate the molten aluminum. The most typically seen case of such behavior is that of silicon metal addition into aluminum caused due to reduction of silica. This phenomenon is so widely seen, that it is commonly referred to as "silicon pickup". Figure 92 shows a typical example of such an occurrence.

The third impact is a kind of contamination that will be caused due to mechanical factors. The weakened refractory tends to crack and loosen. Pieces of refractory material will fall into the molten aluminum causing further contamination.

Corrosion Mechanism:

In order for aluminum to corrode a refractory surface, two basic conditions must exist:

- There should be physical contact between the two species. The refractory surface should be wet by molten aluminum to cause extensive damage.
- Upon contact, there should be a chemical driving force for reaction to occur. The reaction should be thermodynamically feasible and kinetically aggressive to cause corrosion damage.

These two conditions have been the focus of extensive research and have lead to two parallel approaches in alleviating the issue of refractory corrosion by molten aluminum.

Physical Contact:

The first step in the corrosion process is for wetting to occur. Molten aluminum must first wet the refractory surface in order for the corrosion reaction to occur. This issue has been at the forefront of recent development work and has lead to the addition of "anti-wetting additives" into refractory mixes. Wetting angle measurements, sessile drop testing and pore size distributions are carried out extensively to develop a surface that is not wet by molten aluminum [14, 15, 16). Based on literature review, it can be stated that generally all refractory oxides are wet by molten aluminum. A decrease in wetting angle is usually observed with increasing temperature and exposure time. This means that a reaction induced wetting occurs; leading to more corrosion once the refractory surface is further wet. The process of wetting is a balance between various surface energies at the solid liquid interface. It may be mathematically represented as:

$$\cos\phi = \frac{\left(\gamma_{sv} - \gamma_{sl}\right)}{\gamma_{lv}} \qquad \textbf{Equation 9}$$

Where: γ_{sv} = surface tension of the refractory surface
γ_{lv} = surface tension of the liquid metal
γ_{sl} = interfacial tension between the refractory surface and liquid metal

The wetting angle, given by Φ, if lower than 90°, indicates that a material is wet by the liquid.

As stated earlier, molten aluminum will wet most alumino-silicate materials and other common refractory oxides. Upon wetting, the metal may penetrate into the surface of the refractory through pores and cracks. The nature of these pores and cracks will provide additional surface for metal-refractory contact, making way for more aggressive chemical reaction between the two. If the open pores are superficial; i.e. not very deep, then the penetration may be dependant on hydrostatic pressure balance between infiltrating material and trapped atmosphere in the pore. Such penetration will be a function of metal viscosity and pore radius. On the other hand, if the pores form a network of open channels and extend deeper into the refractory, these pores will contribute more extensively to refractory damage. The penetration will then be dependent on pore radius and metal viscosity. Penetration can be reduced by having a higher viscosity and lower pore radius.

Literature review [17] indicates that the viscosity and surface energy of molten aluminum will decrease as a function of increasing temperature. Thus, at higher service temperatures, a refractory surface will tend to wet more easily as a result of less viscous metal. It was also seen that addition of alloy components does not contribute drastically in reducing the viscosity or surface energy of aluminum. Since it is not possible to control the alloy composition just for the

sake of increasing viscosity and refractory life, the other factor available is pore radius and pore size distribution.

From the refractories perspective, pore size and wetting angle are important factors that govern the metal penetration into an open pore structure. Literature review has suggested that alumino-silicate refractories perform much better with a mean pore diameter of 1-2 micron [17].

Chemical Reaction:

The second fundamental requirement for refractory corrosion is a chemical driving force for reaction between molten aluminum and refractory oxide. There are two aspects to this process. First is a negative free energy change that will indicate the thermodynamic feasibility of the reaction. The second part is to sustain a reaction rate that will lead to the formation of corrosion products, sufficient to cause mechanical damage.

The most common of such reactions is the reduction of silica by aluminum. It has a very high negative free energy change

$$Al + 0.75SiO_2 \rightarrow 0.5Al_2O_3 + 0.75Si \qquad \Delta G_{1273K} = -132kJ/mol \qquad \textbf{Equation 10}$$

Alumino-silicates such as kyanite and mullite also lead to the formation of corundum, which is the major contributor to refractory damage. The corundum formation process is accompanied by a volume change. There is also a corresponding difference in thermal expansion behavior, which leads to mechanical damage during thermal cycling. The corundum growth in refractory linings occurs by two commonly accepted processes.

- Internal corundum growth:

  Corundum formation occurring as a result of reduction of refractory oxides by aluminum metal penetrating through the pore system is referred to as internal growth. Some direct oxidation may also occur initially due to air present in the pores. Internal corundum growth is further aggravated by reducing the partial pressure of oxygen. Molten aluminum attack is then focused on reducing the refractory oxides. It is also accelerated by increasing operating temperatures, which lead to reduction in metal viscosity and higher penetration rates.

- External Corundum Growth:

  This occurs at the triple point junction of the aluminum, refractories and atmosphere. Molten aluminum is directly oxidized by atmospheric oxygen. Some aluminum penetrates the refractory and moves up into the refractory by capillary action. The penetrated metal is then exposed to an open atmosphere, where it oxidizes to form more corundum. If magnesium is present, the corundum growth is accelerated by the direct metal oxidation process on the surface of the molten alloy as increasing oxygen partial pressure provides excess oxygen to promote the corundum “mushroom” growth. Presence of fluxing agents and salts also enhances corundum growth.

Generally, resistance to aluminum penetration increases with increasing alumina content in alumino-silicate materials. This statement finds support in the calculations for mullite, kyanite and silica, as presented in Section 5.4.6 “*Thermodynamic Refractory Calculations”*. The tendency of the reactions occurring between these materials should not be read as a shift towards higher alumina content, rather towards lowering the silica content in refractory mixes. Also, materials such as silicon carbide, calcium aluminate and phosphate have been shown to lower the chemical driving force for reaction and can also lead to reducing the damage caused

by molten aluminum. Materials such as zirconia do not react with aluminum, but are not used due to economic considerations.

Anti-wetting additives:

Due to its high affinity for oxygen, molten aluminum reduces common refractory oxides upon contact. In order to minimize this reaction, there should be minimum physical contact between the refractory and molten alloy. This has shifted the focus in refractories development towards non wetting additives. Additives such as $BaSO_4$, AlF_3, CaF_2 or $AlTiO_3$ have been employed as non wetting additives in order to minimize aluminum attack. Although these and similar additives are widely used in industry, their performance has not been consistent; especially at higher operating temperatures. The protection mechanism associated with these additives is not yet well understood and remains a topic for further investigation. These additives have been included in the matrix of the refractory mix and are believed to form glassy phases with non wetting properties. The glassy phases then prevent penetration of aluminum into the refractory grain boundaries as a result of their non-wetting behavior. It may be speculated that the glassy phase also reduces porosity and closes channels for metal penetration. It may also confine free silica into the glassy phase, thus reducing the chemical driving force required for chemical reaction with aluminum.

As discussed in section, 4.4 static cup testing was performed on materials provided by in-kind partners. Data from these tests are presented in following sections. A qualitative "ranking" of the tested materials' resistance to aluminum is presented in Table 13.

Table 13: Penetration data for all materials tested in Task 2

RANK	SAMPLE	PENET'N	COMP	REMARKS
1	BE	< 1 mm	SiC	• Negligible penetration • CLM shows NO major corrosion products
2	BD	< 1 mm	SiC	• Negligible penetration
3	TM	< 1 mm	SiC	• Negligible penetration • NO reaction visible to naked eye
4	TT	< 1 mm	SiC	• Negligible penetration • NO reaction visible to naked eye
5	CN	< 1 mm	Al_2O_3	• Negligible penetration • Slight discoloration
6	CO	< 1 mm	Al_2O_3	• Phosphate bond • Negligible penetration
7	BC	< 1mm	SiC	• Negligible penetration • Protective spinel layer
8	BB	< 1mm	SiC	• Negligible penetration
9	SCA	< 1mm	Al_2O_3	• Negligible penetration
10	SCC	< 1mm	Al_2O_3	• Negligible penetration
11	BA	< 2 mm	SiC	• Bellyband zone observed • Minor penetration in some areas
12	BF	< 2 mm	Al_2O_3	• Matrix dissolution in some areas • Fused silica spheres in matrix are reacted.

RANK	SAMPLE	PENET'N	COMP	REMARKS
13	CB	< 2 mm	Al_2O_3	• Negligible penetration • Attack is on specific grains in aggregate
14	CF	< 2 mm	Al_2O_3	• Uniform penetration
15	CP	< 2 mm	Al_2O_3	• Phosphate bonded • Minor uniform penetration
16	CC	< 2mm	Al_2O_3	• Uniform penetration • Attack is on specific grains in aggregate
17	CE	< 2mm	Al_2O_3	• Small bellyband zone observed • Specific grains attacked • Stress-cracking near corroded grains
18	CA	3-5 mm	SiO_2	• Uniform penetrated zone • Stress-cracking at interface • Aggregate particles are corroded
19	KK	3-5 mm	Kyanite	• Uniform penetration • Aggregate particles corroded
20	KM	3-5 mm	Kyanite + mullite	• Uniform penetration • Attack is on specific grains in aggregate
21	CD	5-7 mm	SiO_2	• Uniform penetration • Stress-cracking at interface • Silica spheres are corroded
22	SCB	5-7mm	SiO_2	• Uniform penetration • Aggregate unreacted • Extensive stress-cracking
23	KF	5-7mm	Kyanite + Silica	• Uniform penetration • Specific aggregates attacked • Extensive stress-cracking
24	SCD	5-7mm	Al_2O_3	• Uniform penetration • Extensive stress-cracking
25	SCE	5-7mm	Al_2O_3	• Uniform penetration • Extensive stress-cracking

Apparent porosity was measured for all the tested materials. The measurement was done using ASTM standard C 830. From the data in Figure 93, it can be determined that there is no correlation between penetration and open porosity.

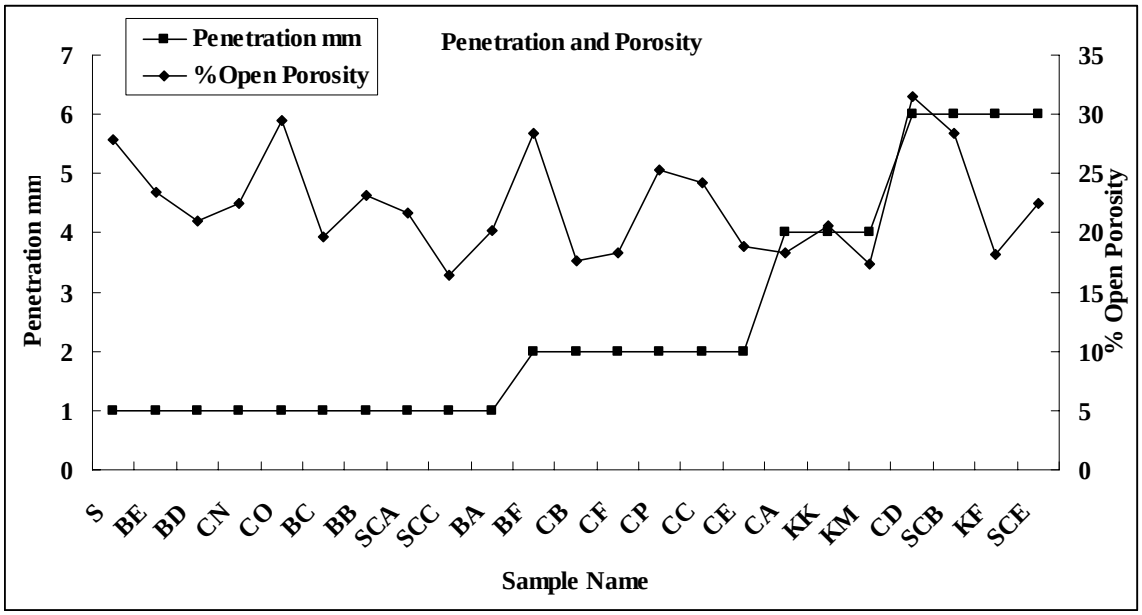

Figure 93: Graphical comparison of Penetration with Porosity

Hence, apparent porosity is not an important guiding factor in predicting the performance of refractory. As cited in earlier sections, the average pore size and pore size distributions are much more important parameters. Controlling the mean pore size to a range of 1-2 micron has been suggested in literature.

For alumino-silicate based castables, the penetration depth was compared to free silica present in the refractory mix. As seen in Figure 94 the penetration depth increased with an increase in silica content. The graph in Figure 94 includes materials with only alumina and silica as the major constituents of the refractory aggregate and matrix.

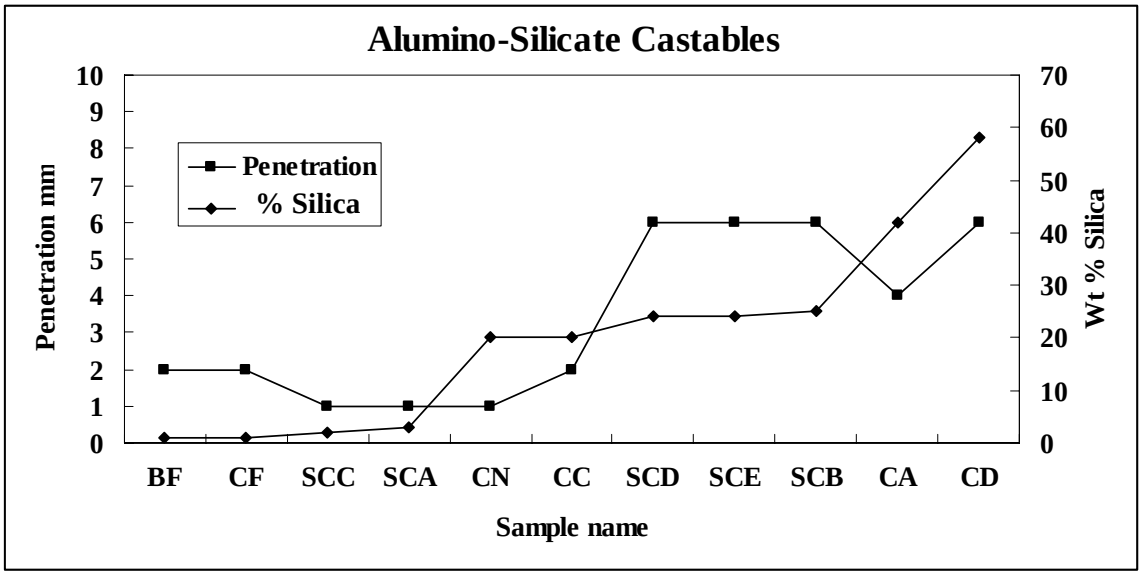

Figure 94: Relationship between Penetration Silica content for alumino-silicate castable

When comparing the penetration with the type of aggregate in use the trend is similar. Silicate based materials have shown higher penetration by molten aluminum than the other materials as seen below in Figure 95. Materials with high resistance to aluminum have very little or no silica present.

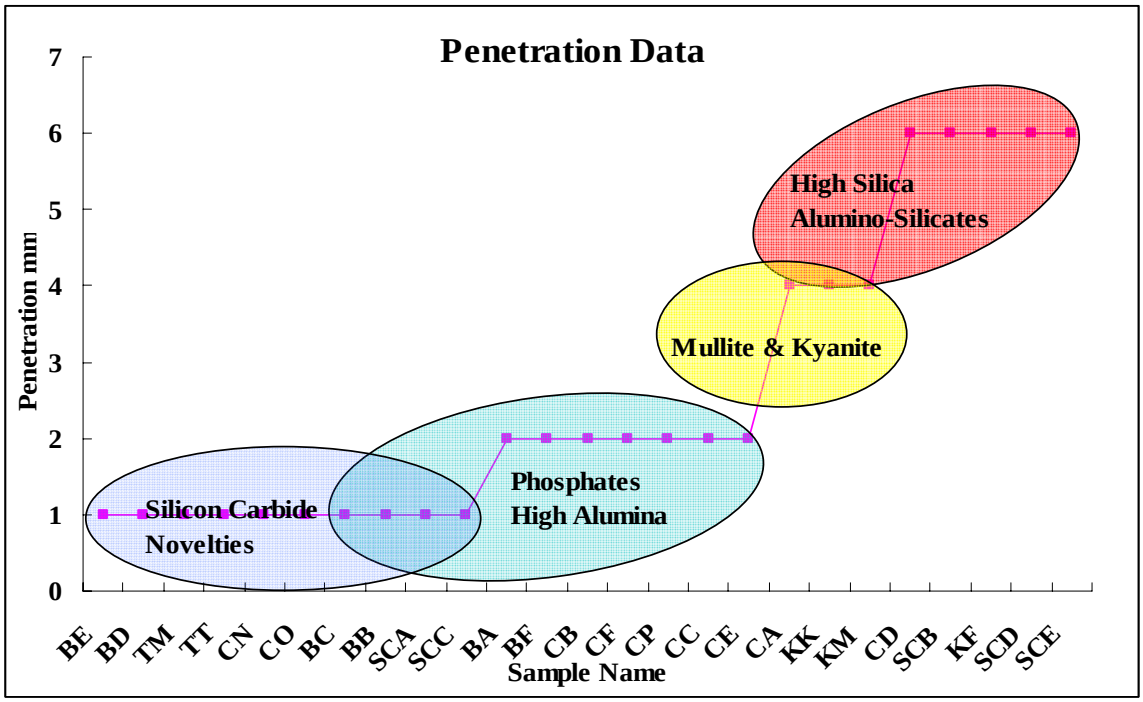

Figure 95: Penetration Data for all materials tested in Task 2

5.4.6 Thermodynamic Refractory Calculations

Hypothetical improvements in wall losses through better insulation were predicted by the DOE PHAST tool as shown in Table 14 below. The baseline case was based on current refractory practices. Subsequent improvements were based on improved thermal efficiency through better furnace insulation.

Table 14: Improvements in wall losses through better insulation

Improvement	Surface Temperature	Wall Losses
Baseline	275°F	748,515 Btu/hr.
9%	250°F	610,727 Btu/hr.
18%	225°F	491,153 Btu/hr.
27%	200°F	389,794 Btu/hr.

Improvements in net and gross heat required by the furnace, energy used and thermal efficiency predicted by the DOE PHAST tool are shown in Table 15 below.

Table 15: Improvements in net and gross heat required by the furnace, energy used and thermal efficiency

	Current	9% Improvement	18% Improvement	27% Improvement
Surface Temperature (ºF)	275	250	225	200
Net Heat (Btu/hr.)	7,835,426	7,697,638	7,578,064	7,476,705
Gross Heat (Btu)	17,599,789	17,290,292	17,021,707	16,794,036
Energy Used (Btu/lb.)	1,173	1,153	1,135	1,120
Thermal Efficiency (%)	39.17	39.87	40.50	41.05

(thermal efficiency = % gross Btu input that is realized as useful Btu output of furnace)

Examples of thermal profiles through hypothetical refractory wall constructions, along with heat flux values predicted using basic heat transfer theory are shown below in Figure 96.

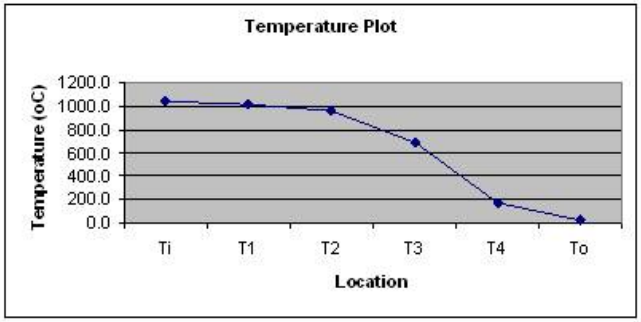

1.83, 0.31, 0.08

	(K)	(°C)
Ti	1308.0	1035.0
T1	1278.3	1005.3
T2	1232.8	959.8
T3	964.3	691.3
T4	444.0	171.0
To	298.0	25.0

$Q = 830\ W/m^2K$

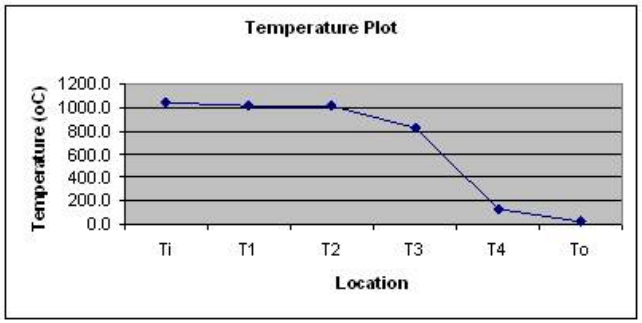

25, 0.75, 0.1

	(K)	(°C)
Ti	1308.0	1035.0
T1	1286.3	1013.3
T2	1284.4	1011.4
T3	1099.2	826.2
T4	404.6	131.6
To	298.0	25.0

$Q = 600\ W/m^2K$

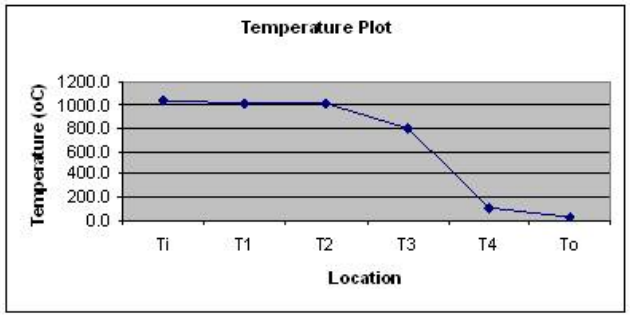

25, 0.5, 0.08

	(K)	(°C)
Ti	1308.0	1035.0
T1	1290.8	1017.8
T2	1289.4	1016.4
T3	1069.5	796.5
T4	382.4	109.4
To	298.0	25.0

$Q = 480\ W/m^2K$

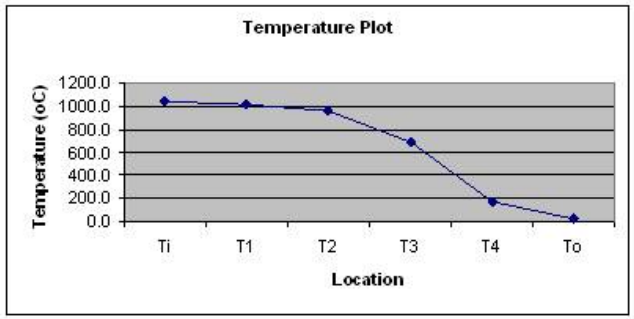

1.83, 0.31, 0.08

	(K)	(°C)
Ti	1308.0	1035.0
T1	1278.3	1005.3
T2	1232.8	959.8
T3	964.3	691.3
T4	444.0	171.0
To	298.0	25.0

$Q = 830\ W/m^2K$

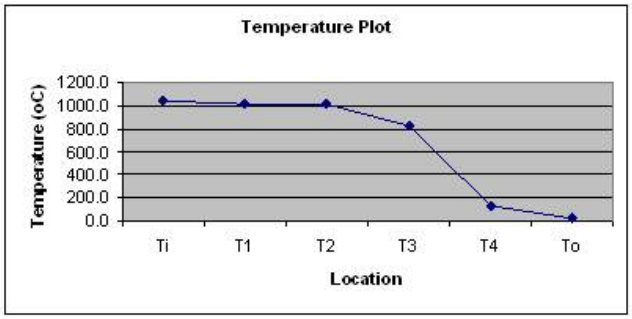

25, 0.75, 0.1

	(K)	(°C)
Ti	1308.0	1035.0
T1	1286.3	1013.3
T2	1284.4	1011.4
T3	1099.2	826.2
T4	404.6	131.6
To	298.0	25.0

$Q = 600\ W/m^2K$

Figure 96: Examples of Thermal Profiles
(five cases with various conductivity refractory layers)

Initial results of the 3E Plus analysis using measured TCON® conductivity values and estimated bonite conductivity values for three scenarios are shown in Table 16 below.

Table 16: Results from Initial Analysis (using experimental TCON® values and estimate bonite values)

	Scenario 1	Scenario 2	Scenario 3
Furnace Surface Temperature (^oC)	129	275	128
Heat Loss (Btu/ft/yr)	1.6217×10^6	2.7139×10^7	1.2099×10^7
Thermal Efficiency (%)	95	77.24	89.85

Scenario 1 represents an example of a currently used refractory lining that is subject to corrosion and erosion damage during its lifetime. These values are valid for the initial thermal performance, with the performance expected to decrease with time. Scenario 2 represents a modified refractory lining with TCON® used on the hot face to increase corrosion/erosion resistance, and 1.5" of bonite castable used behind the TCON®. It is evident that the thermal performance is much poorer for Scenario 2 than for Scenario 1. Scenario 3 represents a further modified refractory lining with TCON® used on the hot face and 5.0" of bonite castable used behind the TCON®. This scenario now gives thermal performance very similar to Scenario 1 in thermal efficiency and only slightly worse in heat loss/year. The advantage of Scenario 3 is that the thermal performance should not degrade with time as it is expected to for Scenario 1. The performance could also be further improved for Scenario 3 by using a thicker layer of bonite or by improving the insulating properties of the bonite.

Results from the additional analysis carried out using the DOE software tool, 3E Plus using experimental values generated for both the TCON® materials and the bonite castable conductivity are shown in Table 17 below. These results are for the same three scenarios previously examined and were found to correlate well with the previous analysis above.

Table 17: Results from Additional Analysis (using experimental TCON® and bonite values)

	Scenario 1	Scenario 2	Scenario 3
Furnace Surface Temperature (^oC)	129	248	130
Heat Loss (Btu/ft/yr)	1.6217×10^6	2.2354×10^7	1.1156×10^7
Thermal Efficiency (%)	95	80.47	90.84

The results of the thermodynamic modeling to predict phase formation was as follows:

Silicon Carbide:

Silicon Carbide (SiC) was the key aggregate ingredient in many materials considered under this project In the absence of oxygen or oxide materials, SiC will react with the alloy to form minor amounts of aluminum carbide and di-magnesium silicide.

$$1.5Mg + Al + 0.75SiC \rightarrow 0.75Mg_2Si + 0.25Al_4C_3 \qquad (\Delta G_{1273K} = -28.8kJ/mol)$$ **Equation 11**

However, in the presence of an oxide such as silica, the SiC remains completely unaffected. and the reaction between alloy and silica shows the formation of spinel and silicon metal.

$$0.5Mg + Al + SiO_2 \rightarrow Si + MgAl_2O_4 \qquad (\Delta G_{1273K} = -199kJ/mol)$$ **Equation 12**

Such a reaction was found to occur in the matrix phase of silicon carbide based castable materials analyzed under this project. Microscopy analysis revealed that the SiC grains indeed remained unaffected by molten alloy, while the matrix phase formed spinel. The excess aluminum in the alloy leads to the formation of corundum by the famous "Brondyke reaction [1]. Some mullite formation may also occur as a result of reaction between alumina and silica present in the matrix.

It may be concluded from the microscopy observation and thermodynamic data presented here, that an oxide free material may be better suited for molten aluminum contact applications. Addition of free silica should also be avoided as much as possible.

Hibonite:

Calcium hexa-aluminate (CA6), known as Hibonite, was one material used as an aggregate material for materials developed under this project since it has been shown to exhibit excellent resistance to molten alloy penetration. An equilibrium model was built in FactSAGE, to predict the products of reaction between one mole of aluminum and one mole of Hibonite. It showed the formation of corundum, calcium aluminum and calcium aluminate.

$$Al + CaAl_{12}O_{19} \rightarrow 0.65CaAl_{12}O_{19} + 0.35CaAl_2 + 2.25Al_2O_3$$ **Equation 13**

The reaction by which Hibonite decomposes to alumina and calcium aluminum was investigated further using FactSAGE. In the presence of excess Al (as in an industrial application), the reaction with silica will be preferred but, unless the reaction with silica shields the remaining excess Al from the Hibonite, the reaction with Hibonite will still occur. Even in a situation with a deficiency of Al, since both equations are thermodynamically favorable, the Al will react with the first species it encounters. Since both reactions generate solid Al2O3, the reacted aluminum is no longer available to react with the other species and both the Hibonite and silica reactions will be present after the Al is fully reacted. Even with 1 mol of Al, some of each reaction will occur. The presence of the calcium aluminum compound was also seen in thermodynamic calculations cited by other authors.

$$Al + 0.375CaAl_{12}O_{19} \rightarrow 0.375CaAl_2 + 2.375Al_2O_3 \qquad \Delta G_{1273K} = -17kJ/mol$$ **Equation 14**

The reaction, although feasible thermodynamically as indicated by the negative free energy value, is highly improbable due to kinetic reason. The presence of any oxides such as silica will cause the aluminum to preferentially reduce and Hibonite will remain unreacted. The example of this is given by the reaction:

$$Al + 0.75SiO_2 \rightarrow 0.5Al_2O_3 + 0.75Si \qquad \Delta G_{1273K} = -132kJ/mol$$ **Equation 15**

Mullite:

Mullite ($3Al2O_3.2SiO_2$) is a commonly used aggregate material for refractories. It was the key aggregate ingredient in several materials investigated under this project. Molten aluminum is

capable of attacking the silica within the mullite structure; resulting in the formation of corundum and silicon metal.

$$Al + 0.375Al_6Si_2O_{13} \rightarrow 1.625Al_2O_3 + 0.75Si \qquad \Delta G_{1273K} = -117kJ/mol$$ **Equation 16**

This reaction, though highly favorable, may not occur in the presence of free silica or other oxides that are readily available for reduction by aluminum. The formation of magnesium based compounds by reaction with mullite is improbable as can be seen by the following reaction showing an Al/Mg ratio that is not in line with the alloy composition.

$$Al + 6.5Mg + 2Al_6Si_2O_{13} \rightarrow 6.5MgAl_2O_4 + 4Si \qquad \Delta G_{1273K} = -1078kJ/mol$$ **Equation 17**

Kyanite:

Kyanite ($Al2O_3.SiO_2$) was also tested as an aggregate material in several sample compositions. Similar to mullite, the silica in a kyanite structure is also susceptible to attack by molten aluminum.

$$Al + 0.75Al_2SiO_5 \rightarrow 1.25Al_2O_3 + 0.75Si \qquad \Delta G12 = -127kJ/mol$$ **Equation 18**

Reaction of kyanite with magnesium and aluminum leads to the formation of spinel by the reaction:

$$Al + 2.5Mg + 2Al_2SiO_5 \rightarrow 2.5MgAl_2O_4 + 2Si \qquad \Delta G_{1273K} = -512kJ/mol$$ **Equation 19**

Other Oxides:

Oxides such as TiO_2 are present in minor amounts. These are easily reduced by molten aluminum.

$$Al + 0.75TiO_2 \rightarrow 0.5Al_2O_3 + 0.75Ti \qquad \Delta G_{1273K} = -99kJ/mol$$ **Equation 20**

Some oxides have a positive free energy change and, as a result, their reduction by molten aluminum will be extremely limited. Based on statistical mechanics, the reactions in equations 20, 21, and 22 may still occur and if the end product metals (Ba, Ca, Mg) are soluble in molten Al and removed from the refractory surface, the reactions will not be reversible and the aluminum will pick up Ba, Ca and Mg. Such oxides, thermodynamically speaking, would make excellent refractory materials for aluminum contact applications. However, they are not commonly encountered because of cost factors. Typical examples are ZrO_2, CaO, and BaO.

$$Al + 1.5BaO \rightarrow 0.5Al_2O_3 + Ba \qquad \Delta G_{1273K} = 4kJ/mol$$ **Equation 21**

$$Al + 1.5CaO \rightarrow 0.5Al_2O_3 + Ca \qquad \Delta G_{1273K} = 115kJ/mol$$ **Equation 22**

$$Al + 1.5MgO \rightarrow 0.5Al_2O_3 + Mg \qquad \Delta G_{1273K} = 57kJ/mol$$ **Equation 23**

Aluminum Phosphate:

Two materials studied under this project were phosphate bonded. On contact with aluminum alloy, $AlPO_4$ is reduced to form corundum and P_2O_3 gas upon decomposition. Although the reaction is thermodynamically favorable, the actual penetration is reduced by the formation of P_2O_3 gas.

$$Al + 1.5AlPO_4 \rightarrow 1.25Al_2O_3 + 0.375(P_2O_3)_2 \qquad \Delta G_{1273K} = -343kJ/mol$$ **Equation 24**

As a localized occurrence in magnesium rich “hot-spots” in the alloy, the reaction may also lead to formation of spinel by the reaction.

$$Al + 2.5Mg + 4AlPO_4 \rightarrow 2.5MgAl_2O_4 + (P_2O_3)_2 \qquad \Delta G_{1273K} = -1090kJ/mol$$ **Equation 25**

Although this reaction may have a highly negative free energy value associated with it, it will still be limited by the fact that magnesium is present as a minor alloy component. The partial pressure of oxide gas will control the forward progress of these reactions. It is estimated, that in low permeability refractories, the oxide gas is trapped within the refractory and the reaction does not proceed as thermodynamically predicted.

The thermodynamic calculations presented are based on the interaction between one mole of aluminum alloy and various refractory components. Key materials from all tested refractory mixes have been included in the calculations. As a graphical summary, an Ellingham type diagram has been prepared (see Figure 97 below). This diagram allows us to quickly visualize, the reactions between one mole of aluminum and any refractory oxides present. Calculations have been made for a temperature range from 800°C to 1200°C, since these are values typically encountered in aluminum contact applications.

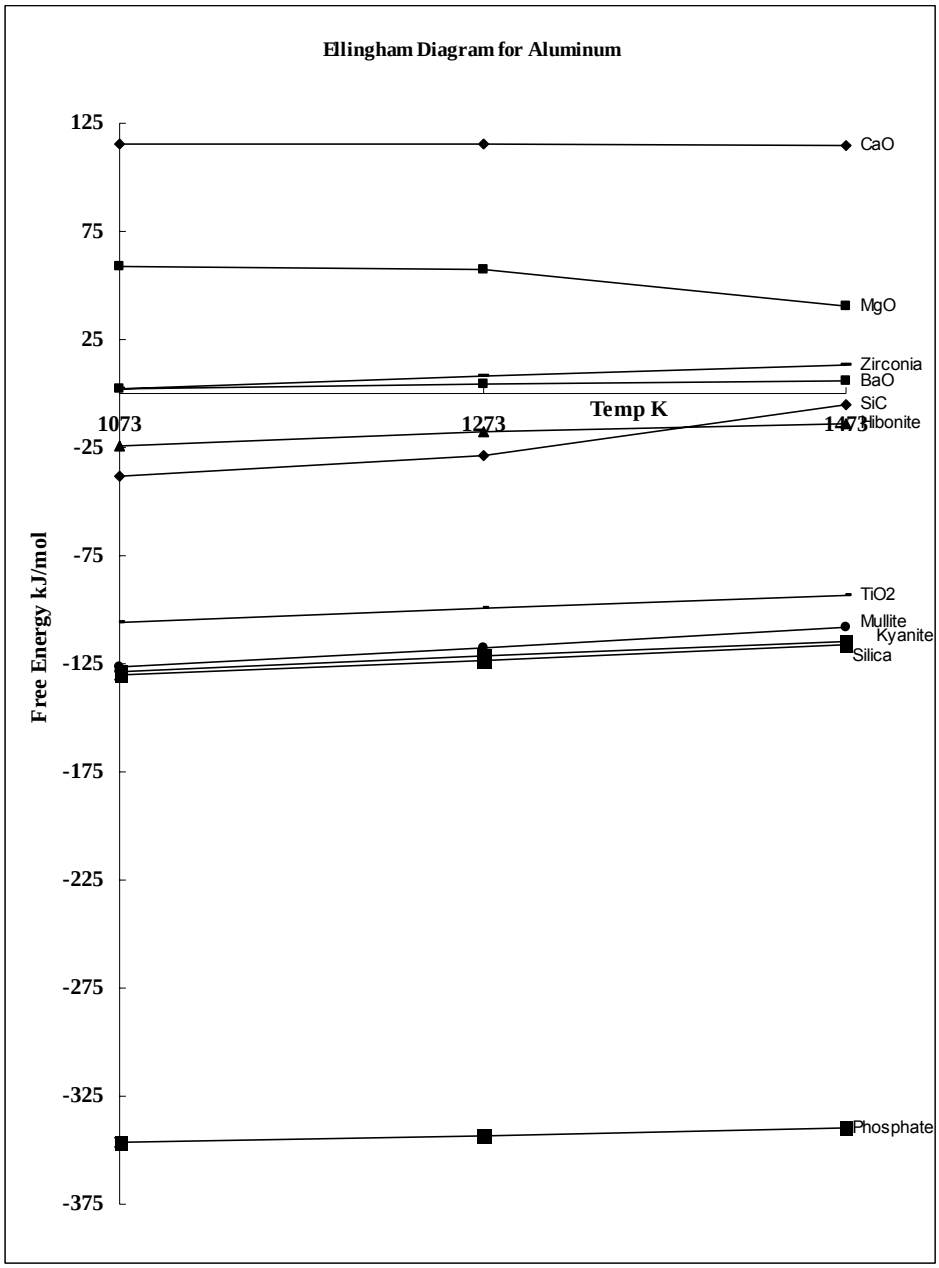

Figure 97: Ellingham Diagram for Aluminum and Common Refractory Materials

5.4.6 Identification of New Materials

New refractory materials were identified as failure and post mortem analysis results became available from characterization of current materials and corrosion testing. Development was focused on insulating castables based on kyanite and bonite materials. Efforts were also carried out to incorporate the corrosion resistance of TCON® materials with the insulating castable refractories. This system would either take the form of a layered or gradient structure as shown in Figure 21 in Section 4.4.

Based on the results of the refractory degradation mechanism analysis micronized kyanite was investigated to be used as a replacement for fumed silica. As seen in a postmortem analysis of spent aluminum furnace refractories, kyanite was found to be the only constituent that did not react under molten aluminum penetration. It was also shown that silica from the fumed silica reacted with calcia from the calcium aluminate cement and alumina from various sources (the bath, matrix phase and cement phase) to form anorthite leading to degradation of the refractory lining. Yet, although fumed silica has been shown to be detrimental in aluminum contact refractories, it is required for flow of the refractory castable during installation. Therefore, initial work by UMR and industrial partner Kyanite Mining Corporation (Dillwyn, VA) concentrated on identifying if micronized kyanite could be used to produce a castable refractory that still possessed sufficient flow during installation, but showed decreased corrosion rates. Unfortunately, a refractory with sufficient flow was not produced under the current project, although work has been continued by the industrial partners on developing such a refractory system.

Since the calcium aluminate cement phase was found to contribute to the refractory castable degradation through the creation of fine alumina particles formed by reduction of the cement particles, a more stable form of calcium aluminate, hibonite, CaO•6Al2O3 (CA6) was investigated as it had been shown to be resistant to reaction with molten aluminum and should make a better aggregate than the currently used bauxite, mullite, tabular alumina and fused alumina aggregates. Industrial partner Almatis Premium Alumina (Bauxite, AR) provided bonite, an industrially available CA6 aggregate, to researchers and producers for testing. Through testing it was determined that this aggregate was more resistant to corrosion by molten aluminum than due to low wettability, therefore work was carried out independently by Missouri Refractories Company, Inc. (MORCO) to incorporate this material into a refractory castable.

TCON®, developed and marketed by Fireline (Youngstown, OH), was also identified as another possible candidate material for aluminum applications. This material is an alumina-silicon carbide composite refractory containing a continuous network of interpenetrating microscopic scaled ceramic and metallic phases (approximately 53 wt. % SiC, 35 wt. % Al_2O_3, 12 wt. % Al/Si). The presence of metallic phases provides significant improvement in toughness and damage tolerance, while the ceramic phases lead to high hardness and improved performance at elevated temperatures. It was expected that this material would exhibit corrosion resistance to molten metal contact due to the low porosity and high alumina/low silica content and abrasion/wear resistance to damage caused by mechanical dross removal.

Two new refractory materials were identified for use in molten aluminum contact applications which were expected to exhibit improved corrosion and wear resistance, along with improved thermal management through reduced heat losses. The identification of these materials was based on understanding of the corrosion and wear mechanisms associated with currently used aluminum contact refractories through physical, chemical, and mechanical characterization and analysis performed by Oak Ridge National Laboratory (ORNL) and the University of Missouri, Rolla (UMR) along with their industrial partners.

TCON®, developed and marketed by Fireline (Youngstown, OH), was identified as one possible candidate material. This material is an alumina-silicon carbide composite refractory material containing a continuous microscopic network of interpenetrating microscopic scaled ceramic and metallic phases where the presence of metallic phases provides significant improvement in toughness and damage tolerance, while the ceramic phases lead to high hardness and improved performance at elevated temperatures. Additionally, silicon carbide particles added to the composites serve to increase wear resistance and thermal shock resistance. It was expected that this material would exhibit corrosion resistance to molten metal contact due to the low porosity and high alumina/low silica content and abrasion/wear resistance to damage caused by mechanical removal of dross. The other material developed was a bonite-based castable expected to provide corrosion resistance and thermal insulation in a composite lining system.

5.4.7 Refractory Component Testing

Materials exposed to the EIO trial were found to perform successfully for the extent of the 2000 hour trial. Upon inspection of the TCON® plates from the EIO trial, it was found that the solidified aluminum on the plates was easily removed from the refractory surface indicating non-wetting of the alloy to the refractory (as found previously through corrosion testing and sessile drop testing). There was also no sign of damage to the TCON® plates due to mechanical dross removal scraping. Additionally, there was no sign of aluminum penetration visually, by optical microscopy, or by SEM as shown in Figure 98 below.

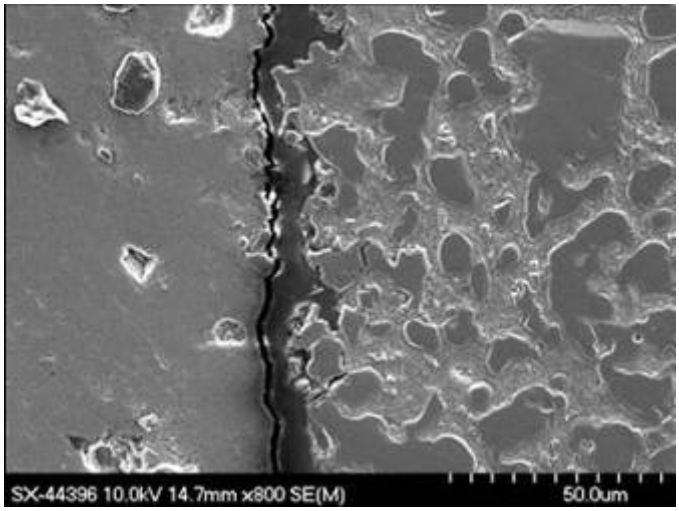

Figure 98: SEM Micrograph of TCON® Refractory after 2,000 hours of use showing no wetting or penetration
(note aluminum alloy on left of micrograph and TCON® on right)

Inspection of the bonite castable from the EIO trial (both behind the TCON® plates and below the metal line in the test vessel) also revealed positive performance of the experimental refractory system. Core drilled samples of the bonite castable showed no sign of metal penetration, nor alteration of the castable microstructure as shown in the SEM micrographs in Figure 99. There was no sign of a reaction zone on the refractory hot face and a consistent microstructure throughout the core sample.

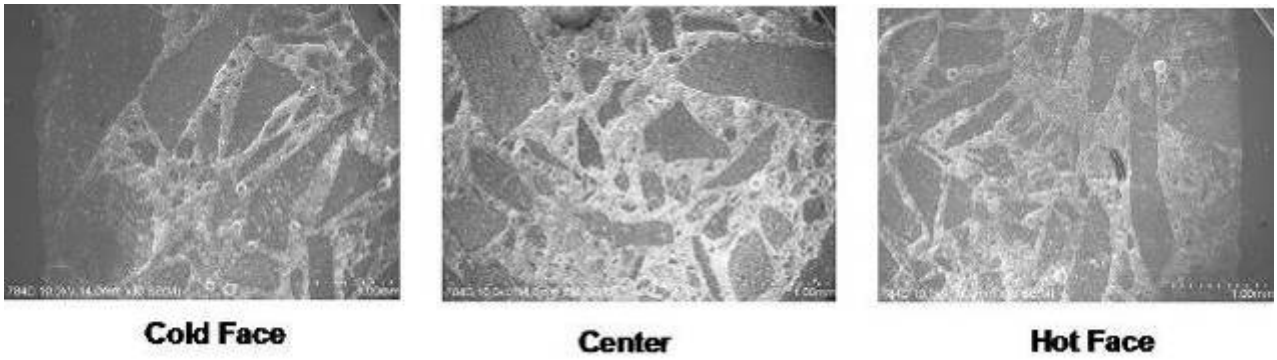

Figure 99: SEM Micrographs of the Castable Bonite Refractory after 2,000 hours of use

The Pennex trial was canceled due to problems with part complexity and installation. Parts for this application could not be produced or installed with current molds. As an alternative installation, parts were prepared for installation at Southwire Corporation in their Hawesville, KY aluminum rod and cable mill. TCON® wear plates backed by bonite castable were installed in the high wear area of their rotary degasser unit and parts are planned for a future installation in their launder system at the exit of the aluminum melter. These parts have been installed and will be monitored for performance until removal of the rotary degasser and launder system. TCON® materials were also considered for use in the Southwire copper production facility (Carrolton, GA) and in Aleris aluminum mills in Kentucky and Ohio as impact pads and for other aluminum contact applications.

Additionally, as in-kind cost share, independent trials were pursued by Fireline and MORCO on the TCON® and bonite materials, respectively. TCON® has been successfully trialed as hooks for use in an automated production cell for casting aluminum alloy diesel pistons and as melt impact pads used in 500 lb. aluminum alloy transfer ladles. Bonite castable has successfully been used in a drop out troughs for reverberatory aluminum melting furnaces.

ORNL, with the assistance of Fireline and MORCO, followed up with several domestic and foreign aluminum manufactures based on contact generated from the publication of the DOE/ITP E-bulletin highlight on the refractory side of the project and the associated articles published by ASM International (e-newsletter) and American Ceramic Society Bulletin. Negotiations have been handled by Fireline through their international distributor for the installation of TCON® in the aluminum processing facility of several foreign companies.

TCON® material was tried in two separate applications. The first was in an automated production cell for casting aluminum alloy diesel pistons where iron rings for embedding into pistons during casting are preconditioned in molten aluminum prior to casting. TCON® parts in the form of hooks were used as holders for the iron rings during the preconditioning process where they were subjected to corrosion by pure molten aluminum above 700^{o}C and mechanical wear due to rotation of the hooks in the bath [9]. The TCON® hooks (shown below in Figure 100) were found to last over three weeks longer than the previously used ceramic hooks which typically lasted one to three days. Additionally, the TCON® hooks were found to fail in a predictable and controlled manner, as compared to the current hooks which failed catastrophically and unpredictably. Modification of the original hook design resulted in further significant improvement in hook life and casting yields as defects from dross particles were eliminated [10]. Hook life was extended as much as ten weeks and dross accumulation at critical areas of the hook was eliminated.

Figure 100: Examples of the TCON® Hooks

The second application was in a 500 lb. transfer ladle for the transfer of molten aluminum alloy from the melting furnace to the holding furnace [11]. TCON® was used as a melt impact pad (located in the bottom of the ladle) to reduce erosion of the refractory in the ladle bottom as shown in Figure 101 below. Conventional refractory materials located in the bottom of the ladle were found to be eroded as the aluminum melt was poured into the ladle. This erosion led to the need to remove the ladle from service for repair or failure of the ladle if the erosion were allowed to become severe. Current maintenance practices require patching of the ladle every two to three weeks and replacement of ladles every 18-24 months adding cost and the need to have multiple ladles on hand. TCON® ECI (erosion, corrosion, impact) plates were installed in the bottoms of two ladles while they were being relined. After seventeen and twenty-four weeks of service, respectively, the pads in both ladles showed no observable corrosion or erosion. Further, during inspection the aluminum skin adhering to the TCON® surface was easily peeled away indicating a lack of wetting. Based on the performance in these two ladles, the customer has decided to add TCON® ECI plates to other ladles.

Figure 101: Reduce Erosion of the Refractory in the Ladle Bottom using TCON®

MORCO tested MORCOCAST CA6 against other commercial refractories in a drop out trough from a reverberatory aluminum melting furnace. This was a high abrasion, impact and thermal shock region for aluminum transfer. MORCOCAST CA6 outperformed materials conventionally used in this area as well as competing experimental castables. Effective lifetime of MORCOCAST CA6 is still unknown at the time of the writing of this document as the current trial installation is still in service past the previously expected lifetime of the installation. MORCOCAST CA6 has proven to be more resistant to aluminum metal and corundum growth than other commercial and experimental materials that it has been trialed against.

6.0 Accomplishments

Accomplishments under major project areas are presented below.

6.1 HDG coatings and materials issues

A new corrosion, wear, and dross-buildup resistant weld overlay, Alloy 2020, with greater than 5X lifetime improvements over current stainless steel has been developed and validated through the exposure of weld-overlay material samples for over 150-days in an industrial setting. Materials are functioning well with little evidence of corrosion. ORNL and WVU, through collaboration with industrial partners, have developed a welding process to apply the coating on steel substrate, and the joint patent application for this process has been filed to USPTO. The in-plant tests of real stabilizer rolls in three industrial GA/GI baths have shown the superior performance of this coating, as compared to current 316L stainless steel rolls.

Publications

1. Jing Xu; Xingbo Liu*; Mark A Bright; James G Hemrick; Ever J Barbero: "Reactive Wetting of an Iron-Base Superalloy MSA 2020 and 316L Stainless Steel by Molten Zinc-Aluminum Alloy", *Metallurgical & Materials Transaction A, 39A (June 2008) 1382-1391*
2. Jing Xu, Mark A Bright, Xingbo Liu*, Ever Barbero: "Liquid Metal Corrosion of 316L Stainless Steel, 410 Stainless Steel and 1015 Carbon Steel in a Molten Zinc Bath", *Metallurgical & Materials Transaction A 38A (2007) 2727-2736*
3. Xingbo Liu*, Ever Barbero, Jing Xu, Matthew Burris, Keh-Min Chang & Vinod Sikka: "Liquid Metal Corrosion of 316L, Fe3Al and FeCrSi in Molten Zn-Al Baths", *Metallurgical & Materials Transactions A, 36A (August 2005) p.2049-2058*
4. Ever Barbero, Carl Irwin, Xingbo Liu, Vinod Sikka, & Frank Goodwin*: "Development of the Next Generation of Bath Hardware Materials", *Iron and Steel Technology, 1 (October 2004), pp.31-37*
5. Xingbo Liu, Vinod K. Sikka, Mark Bright, Scott Sexton, Ever Barbero, James W. Hales: "DEVELOPMENT OF A NEW WELD OVERLAY FOR POT HARDWARE IN CONTINUOUS GALVANIZING LINES", presented at Galvtech'07 Conference, Osaka, Japan (November 2007)
6. Jing Xu, Xingbo Liu, Mark A Bright, James G Hemrick, Ever Barbero: "REACTIVE WETTING OF AN IRON-BASE SUPER Alloy MSA2020 AND 316L STAINLESS STEEL BY MOLTEN ZINC Alloy ", presented at Galvtech'07 Conference, Osaka, Japan (November 2007)
7. Liu, Xingbo, "Corrosion-Resistant Materials Extend Life and Efficiency of Molten Metal Processing." *ITP E-Bulletin*, April 2006
8. X. Liu, C. Irwin, E. Barbero, B. Kang: "Minimizing Dross Buildup on Rotating Galvanizing Bath Hardware", *ILZRO-GAP 2005*, (October 2005) Lexington, KY
9. X. Liu, E. Barbero, C. Irwin, V. Sikka, J. Hemrick, W. Headrick & F. Goodwin: "Development of Next Generation of Metallic and Refractory Materials for Molten Metals Handling", *AISTech 2005 Iron & Steel Technology Conference and Exposition*, Charlotte, NC
10. E. Barbero, X. Liu et al.: "Current Research on Zinc Pot Hardware and Molten Metal Containment" in *Galvanizers Association Annual Meeting 2004,* Charleston, SC.

11. X. Liu, E. Barbero, F. Goodwin: Progress on Improved Materials for Pot Hardware Project, in *Galvanized Autobody Partnership 2004*, Charleston, SC
12. X. Liu et al.: "Corrosion of Several Alloys in Industrial Hot-dipping Baths", in *Galvtech' 04*, Chicago IL, ISS, 2004
13. X. Liu, E. Barbero, F. Goodwin: Progress on Improved Materials for Pot Hardware Project, in *Galvanized Autobody Partnership 2004*, Chicago, IL
14. E. Barbero, X. Liu et al.: "Performance Evaluation of Current Hot-dip Pot Hardware Materials, in *Galvanizers Association Annual Meeting 2003*, Monterrey, Mexico
15. X. Liu, F. Goodwin: "Development of Improved Materials for Continuous Steel Hot-dipping Processes – Progress Report" in *Galvanized Autobody Partnership 2003*, Monterrey, Mexico.
16. X. Liu et al.: "Development of Improved Materials for Continuous Steel Hot-dipping Processes", in *Galvanized Autobody Partnership 2002*, Detroit, MI.

Dissertations/Theses

- "Dissolution and Diffusion Characteristics of 316L Stainless Steel in Molten Zinc Containing Variable Concentrations of Aluminum" by Mark A Bright
- "Kinetics Of Corrosion And Dross Build-Up In Molten Zn-Al Systems" by Jing Xu

Patents:

- "Overlay Cladding for Molten Metal Process" filed on May 1, 2007 by Mark Bright, Vinod K. Sidda, James W. Hales, Ravi Menon, Ever J. Barbero, Xingbo Liu, Jing Xu
- "High Temperature Electrochemical Characterization of Molten Metal Corrosion" filed on May 29, 2008 by Xingbo Liu, Jing Xu, Yinglu Jiang, and Frank Goodwin

Spin-off Program

- West Virginia University is developing a Corrosion Center using the industry contacts and the research results from this project.

6.2 Dross control and scraper design

(i) Established dross formation mechanism on the pot hardware in Galvalume line
(ii) Established better overlay materials (Stellite 6B and Tribaloy T-401 with > 3.5 X life improvement over Stellite 21) for the scraper to remove the dross build-up on the sink roll surface,
(iii) A more efficient new scraping procedure was also developed.

Publications

1. Kang, Bruce S., Chuanyu Feng and Kian Huat Tan, "Long-time Wearing Performance of Ceramic Inserts in Continuous Galvanizing Line", Society for Experimental Mechanics 2005 Annual Spring Conference, Portland, OR, 7-9 June 2005. (2005): 227-232.

2. Kang, Bruce and Ashok Varadarajan. "Evaluations of Wear-Resistant Scraper Alloys for Dross Removal in GL Galvanizing Bath." USA MS&T 06, Cincinnati, OH, 15-19 October 2006. (2006):

3. Kang, Bruce and Ashok Varadarajan. "Mechanism and Growth of Dross on the Submerged Pot Hardware in Galvalume (GL) Bath." MS&T 07, Detroit, MI, 16-20 September 2007. (2007):

4. Kang, Bruce, Ashok Varadarajan and Mark Bright. "Dross Formation Mechanisms On Stainless Steel Hardware In A Zinc-55%Aluminum Bath." Galvatech'07 Conference, Osaka, Japan, 18-22 November 2007. (2007): .

Dissertations/Theses

- "Dross Formation Mechanism and Development of Wear Resistant Scraper in 55Al-1.5Si-Zn Coating Bath " by Ashok Varadarajan, Ph.D (to be completed by December 31, 2008)

6.3 GEPDSS

The GEPDSS model will be provided on a CD as an executable file with its user's manual. The users will be able to install the model on most personal computers and be able to populate the model with data and observe results. The user's manual is detailed and is provided with the software. It takes the user step by step through the installation process. The web site that reflects the results of this project is:

http://www.iofwv.nrcce.wvu.edu/gepdss/index.html

Publications

1. Gopalakrishnan, B., Chavan, R., Benchmarking of Energy Consumption in Continuous Galvanizing Lines, *Proceedings of the Intelligent Systems in Design and Manufacturing VI Conference*, Society of Photo Optical Instrumentation Engineers (SPIE), Boston, MA, Vol.5999, pp. 59990T1-T8, 2005.

2. Gopalakrishnan, B. "New Software Tool Identifies Opportunities for Energy Savings in Galvanizing Lines." *ITP E-Bulletin*, July 2006.

Dissertations/Theses

- Raviraj R. Chavan, MS Thesis, "Analysis of energy consumption in continuous galvanizing lines," Dept. IMSE, CEMR, 2006.
- Subhasis Bhadra, MS Problem Report, "Analysis of Data Generated by the Galvanizing Energy Profiler Decision Support System", IMSE, CEMR, expected to be completed in December 2008.

Spin-Off Project

- Development and Enhancement of GEPDSS – Galvanizing Energy Profiler and Decision Support System funded by the International Lead Zinc Research Organization

6.4 Refractories

- Two new materials identified for molten metal contact applications, Fireline and MORCO bonite castable.
- Composite lining system designed incorporating two new materials.
- Industrial scale trial successfully completed (2000 hours) at Energy Industries of Ohio (EIO).
- Composite lining system industrially trialed successfully at Southwire Kentucky Rod and Cable mill in rotary degasser lining application.
- Developed materials independently trialed in various applications by industrial partners Fireline and MORCO.
- Project participants contacted by international companies for trials and installations of materials developed under this project.
- Research with Fireline has led to further DOE ITP funded work.

Publications

1. Karakus, M., W.L. Headrick and E.L. Feiner "Aluminum Melting Furnace Post-Mortem," Proceedings of the 41st Symposium on Refractories, 30-31 March 2005, St. Louis, MO. (2005): 136-156.
2. Hemrick, J.G., V. Sikka, and W. Headrick: “Multifunctional Refractory Materials for Molten Metal Contact Applications.” UNITECR’ 05 Meeting in Orlando Florida, November 2005. Ed. Jeffrey D. Smith. (2005): 222-226.
3. Hemrick, J.G. and E. Loveland. “Technique Development for Large Sample Thermal Conductivity Measurement.” UNITECR’ 05 Meeting in Orlando Florida, November 2005. Ed. Jeffrey D. Smith. (2005): 846-848
4. Karakus, Musa, William L. Headrick, and Eric L. Feiner. “Characterization of Post-Mortem Refractory Ceramics from Special Al-Metal Alloy and Super-Alloy Melting Furnaces.” TMS 2006 Annual Meeting & Exhibition, San Antonio, TX, 12-16 March 2006. (2006)
5. Karakus, Musa. ”Application of Cathodoluminescence (CL) Microscopy and Spectroscopy to Refractory Raw Minerals and Ceramics.” TMS 2006 Annual Meeting & Exhibition, San Antonio, TX, 12-16 March 2006. (2006)
6. Hemrick, James. “New Thermal Conductivity Technique”. American Petroleum Institute Meeting, Dallas, TX, 1-3 May 2006.
7. Shukla, D. “Testing of Advanced Refractory Materials for the Aluminum Industry”, Materials Science & Technology Conference, 17 October 2006. (2006):
8. Karakus, M.; “Characterization of Submerged and Metal Contact Refractory Materials from Aluminum Melting Furnaces”, Materials Science & Technology Conference, 17 October 2006. (2006): .
9. J.G. Hemrick, R.B. Dinwiddie, and E.R. Loveland. “Technique Development for Large Sample Thermal Conductivity Measurement of Refractory Ceramics”, Proceedings of the 43rd Symposium on Refractories, St. Louis, Missouri, 28-29 March 2007. (2007): 98-104.

10. Hemrick, J.G., J. Xu, K. Peters, X. Liu, and E. Barbero. “Wetting and Reaction Characteristics of Al_2O_3/SiC Composite Refractories By Molten Aluminum and Aluminum Alloy”, International Journal of Applied Ceramic Technologies 4 (2007): 514-523.

11. J.G. Hemrick, W.L. Headrick, and K.M. Peters. “Development and Application of Refractory Materials for Molten Aluminum Applications”, accepted (10//07) by the International Journal of Applied Ceramic Technology for publication.

12. Jing Xu, James G Hemrick, Mark Peters, Xingbo Liu*, Ever Barbero: “Wetting and Reaction Characteristics of Al2O3/SiC Composite Refractories by Molten Aluminum and Aluminum Alloy”, *International Journal of Applied Ceramics Technologies 4 (December 2007) [6] 514-523*

7.0 Summary and Conclusions

Summary and conclusions under major project areas are presented below.

7.1 HDG coatings and materials issues

7.1.1 Survey

A survey on hot-dipping hardware was distributed to all the industrial partners and companies worldwide through ILZRO. The results of this survey are summarized as below:

1. The molten metal temperature range in their baths is from 860 F (GI) to 1100 F (GL); the steel Sheet tension ranges from 2000 lbf to 11500 lbf; sheet gauge ranges from 0.02 in to 0.135 in; and line speeds are from 200 to 650 ft/min.
2. Reasons for Line Stoppage include: (4 lines) dross build up, (all) bearing wear, (all) preventative maintenance, and (2) product change between bath composition. Average time for one campaign is 14 to 30 days for GI/GA, and 4 days for GL, respectively.

7.1.2 Static and Dynamic Corrosion/Dross Buildup Tests

A series of alloys and coatings, including but not limited to, 316L, WC-Co coating, as-cast Alloy 2020, and weld overlay of Alloy 2020, were subjected to various static and dynamic corrosion/dross buildup tests in both laboratory scale and industrial pots, for as long as 150 days.

Alloy 2020 coating, an iron-based super alloy, on the 316L stainless steel substrate has been developed to reduce molten-metal corrosion and dross buildup on the stabilizer and sink rolls. Both single- and multi-layer welds have been developed. The following conclusions can be drawn:

1. This newly developed overlay has strong resistance to dross buildup; there is almost no buildup on the surface after a 15-day test. In comparison, 316L forms a continuous layer of dross after a 6-day test;
2. The line-scan and X-ray mapping micrographs show that there is a reaction/dissolution layer next to the overlay. Cobalt and iron are dissolved into the bath and aluminum from the bath diffuses into this layer;
3. Industrial tests in various galvanizing lines show that this overlay is a candidate for next generation coating on sink and stabilizer rolls in hot-dipping processes.

7.1.3 Sessile-Drop Wetting Tests

The reactive wetting behaviors of Alloy 2020-as cast, Overlay of Alloy 2020, and 316L stainless steel in contact with molten Zn-Al alloy were investigated by the sessile drop method. This investigation led to the following findings.

1. 316L not only suffered considerable wetting, but also reacted with the molten Zn-Al alloy at a higher rate than Overlay of Alloy 2020.
2. The contact angle of Overlay of Alloy 2020 wet by the molten Zn-Al alloy dropped to an acute angle when the temperature was increased to 500 C.

3. The surface reaction was found to initiate even though the liquid droplet and substrate were observed as non-wetting (contact angle larger than 90 deg).
4. The reaction mechanisms were identified in three stages. Initially, the Al diffused into the substrate to form an Fe-aluminide layer, which acted as the reaction front. Next, the reaction front penetrated the substrate through inward diffusion of Al. Finally, Zn-rich zones formed behind the reaction front as a result of Al depletion.
5. The alloying constituents (W, Mo, and Cr) in Alloy 2020 on the surface reduced its wettability by molten Zn-Al by covering the reactive sites on the solid-liquid interface.

In summary, the sessile-drop tests confirmed the excellent anti-corrosion properties of weld overlay of Alloy 2020, as compared to 316L stainless steel.

7.1.4 Coating Development and Component Tests

The techniques for weld overlay of Alloy 2020 coating on industrial-size stabilizer rolls were developed and a stabilizer roll donated by Nucor Steel –Crawfordsville was coated with this alloy. The coated roll processed 7,310,210 feet of sheet for the second cycle and 2,616,462 feet during the first cycle. The second trial being nearly 20 days is the longest time a trial roll has operated in service. This makes a total of 9,926,672 feet of in-line service totaling 26 days of in-line trial.

7.2 Dross control and scraper design

A series of tests were conducted to establish the actual dross formation mechanism over the submerged pot hardware by immersing and rotating 316L stainless steel samples in 55%Al-Zn bath. From the SEM/EDAX analysis on the cross section of the immersed samples, the dross formation mechanism was developed. As numerous researchers have accepted that the fundamental principle of adding silicon to the 55%Al-Zn bath was to control the sudden exothermic reaction between the aluminum in the bath and the iron.

From the scraper wear rate tests, better overlay materials (Stellite 6B and Tribaloy T-401 with >3.5 X life improvement) for the scraper to remove the dross build-up over the sink roll surface have been determined. A more efficient new scraping procedure was also developed, which can considerably reduce the frequency of the line stoppages and thus increasing the productivity with better quality of coatings as well as more energy savings, reduced repair and replacement costs.

Based on the results from this research, it may be possible to further understand the dross formation mechanisms of other alloys utilized in the actual coating lines. Development of new alloys, with good ductility and corrosion resistant, can lead to develop more efficient scraping process with better overlay coatings.

7.3 GEPDSS

The GEPDSS is a tool that paves the way for simulating the energy and economic impacts of improving the efficiency of specific aspects of the steel coated line, whether it be galvanizing, galvalume, or galvanneal. The industrial user will be able to analyze the effectiveness of investments on the galvanizing line from an energy and productivity improvement standpoint. Researchers who focus on improving the efficiency of specific aspects of the line will be able to

analyze the impact of their research on improving life of pot hardware in terms of energy and productivity.

7.4 Refractories

7.4.1 Survey

The conclusions drawn from the responses to the industrial survey were as follows:

1. Efforts should be concentrated on identifying alternative materials for use in the temperature range of 730-845^{o}C (1350-1550^{o}F) for aluminum production and 1150-1700^{o}C (2100-3100^{o}F) for super alloy production. (Later the focus was shifted to only the aluminum industry). Such efforts could lead to large energy savings since large amounts of energy are used in these two industries ($15.34M/year energy consumption costs).
2. Key refractory issues that needed to be addressed by the project were
    i. Thermal – cycling, shock (especially in Al melters)
    ii. Chemical – attack (Cl), absorption into melt (Cr, Na, C, Ca), erosion/corrosion
    iii. Mechanical – fracture due to impact, vibration, bending loads, and wear
    iv. Processing – refractory inclusions

7.4.2 Post-mortem Analysis

From materials analyses of the salvaged refractories, attack mechanisms and degradation paths were identified. Additionally, it was observed that the degradation of aluminum furnace linings is also largely due to mechanical damage of the refractory due to the furnace maintenance procedures

Problems associated with the degradation mechanisms identified included:

1. Low effectiveness of anti-wetting additives (CaF_2)
2. Poor refractory quality, mainly due to the poor quality of the refractory aggregate
3. Reaction of micro-silica with cement binder systems (silica with calcium aluminate)
4. Poor furnace maintenance practices leading to mechanically damaged refractory linings.

The proposed solutions for these problems would include

1. The identification and use of better anti-wetting additives or materials
2. Use of micronized kyanite in place of fumed silica
3. Use of higher purity aggregates (kyanite, CA2, CA6, or SiC)
4. Improved furnace maintenance procedures or identification of materials capable of better performance under current procedures.

Of these solutions; the use of kyanite in place of fumed silica, the use of higher purity aggregates, and the identification of materials better suited for current maintenance procedures were identified for further investigation under this project.

Microstructural, chemical, and mechanical characterization was used to evaluate materials for use in aluminum refractory applications. Sessile drop testing was used to determine the wetting

behavior of candidate refractory materials. Additionally, a thermal conductivity technique was developed and validated at ORNL for measurement of full sized brick and castable materials.

7.4.3 Materials Testing

The following conclusions were drawn from the development of the refractory corrosion model and the thermodynamic calculations performed:

1. The experimental data obtained matched information found in the literature.
2. Materials were ranked according to penetration depth with non-oxide materials and high alumina materials showing excellent resistance to penetration. There was no visible correlation found between open porosity and penetration depth.
3. An ideal refractory for aluminum contact applications would be one which is not wet by molten aluminum, if wet will not have a chemical reaction, and if reacted will form reaction products which will not cause mechanical damage to the refractory.
4. Thermodynamic calculations indicated that just by reducing wall losses, improvements in overall process thermal efficiency of up to 2% could be realized resulting in energy savings on the order of 1MBtu per year for a typical aluminum furnace.

7.4.4 Thermal Conductivity

Two new refractory materials were identified for use in molten aluminum contact applications which were expected to exhibit improved corrosion and wear resistance, along with improved thermal management through reduced heat losses. The identification of these materials was based on understanding of the corrosion and wear mechanisms associated with currently used aluminum contact refractories through physical, chemical, and mechanical characterization and analysis performed by Oak Ridge National Laboratory (ORNL) and the University of Missouri, Rolla (UMR) along with their industrial partners. TCON®, developed and marketed by Fireline (Youngstown, OH), was identified as one possible candidate material to provide improved corrosion and wear resistance. The other material developed was a bonite-based castable expected to provide corrosion resistance and thermal insulation in a composite lining system. The two identified refractory materials were validated through both an R&D industrial trial and independent commercial trials by the refractory manufacturers. The materials successfully performed for the extent of a 2000 hour “industrial scale” trial at Energy Industries of Ohio (EIO) with no detectable signs of aluminum penetration and no mechanical degradation due to surface cleaning of dross above the metal line. Additionally, the bonite castable material has been trialed against other commercial refractories in a drop out trough from a reverberatory aluminum melting furnace. Also, the TCON® material has been trialed in a hook application and as a pad to control erosion, corrosion, and impact in an aluminum ladle. Both trials confirmed superior performance of these newly identified TCON® and Bonite materials.

7.5 Energy, Cost, and Environmental Benefits

7.5.1 Benefits for Hot Dip Galvanizing Line Industry

Energy savings, cost savings, and carbon footprint reductions obtained due to improvement of pot hardware lifetime in galvanizing lines as determined using the GEPDSS software tool (discussed in Sections 4.3 and 5.3) are shown in the following tables. Increasing the life of the pot hardware from the current average of 0.67 week campaign period to a 4 week campaign

period will lead to significant increases in production since it is not necessary to shut down the line for frequent pot hardware replacement. The amount of energy used will be lesser for a given amount of production tonnage as the wastage of energy during extended shutdown periods is minimized. The total energy cost savings and the primary energy displaced per year for the varying number of facilities in various years has been calculated in a conservative manner. The reduction in emissions in terms of metric tons of CO2 per year has been determined from the primary energy displaced, assuming that 80% of the energy displaced is natural gas and 20% is electricity.

Table 18: Energy Benefits Resulting from the Project

Impact By Year	2005	2010	2015	2020	2025	2030
Total number of existing systems industry wide	0	6	16	36	59	78
% Market penetration	0	8%	21%	45%	71%	88%
Total primary energy displaced (10^{12} BTU/year)	0	0.0654	0.1744	0.3924	0.6431	0.8502

Table 19: Cost Benefits Resulting from the Project

Impact by Year	2005	2010	2015	2020	2025	2030
Total number of existing systems industry wide	0	6	16	36	59	78
Energy-cost savings ($\$10^9$/year)	0	0.4615	1.2307	2.769	4.5381	6.0000

Table 20: Environmental Benefits Resulting from the Project

Impact By Year	2005	2010	2015	2020	2025	2030
Total number of existing systems industry wide	0	6	16	36	59	78
Metric tons of CO_2 emissions reduction (10^5 tons/year)	0	11,561	30,829	69,365	113,682	150,292
Metric tons of carbon equivalent emissions reduction (10^5 tons/year)	0	3,153	8,408	18,918	31,004	40,989

7.5.2 Benefits for Aluminum Industry

Energy savings, cost savings, and environmental benefits for the aluminum industry presented below were calculated using the DOE GPRA software. For the analysis, a value of 397 trillion BTU/yr (0.770 billion cubic feet of natural gas) was assumed as the energy used by the aluminum industry utilizing current technology[1]. One hundred units were analyzed representing one hundred aluminum furnaces across the United States implementing the new technology developed under this project. A 5% improvement in energy efficiency resulting from improved thermal efficiency was assumed due to improved refractory materials being used in these one

[1] Based on values in Table 3 of "Refractories for Industrial Processing: Opportunities for Improved Energy Efficiency" (http://www.eere.energy.gov/industry/imf/pdfs/refractoriesreportfinal.pdf)

hundred furnaces leading to reduced refractory wastage due to corrosion/erosion. This resulted in a value of 377 TBTU (0.732 billion cubic feet of natural gas) for the energy used with implementation of improved technology or a net impact of 20 TBTU (0.038 billion cubic feet of natural gas). The project start date of 2003 was used with a 1.0% annual market growth, ultimate potential accessible market of 80% and a 30% likely market share.

Table 21: Energy Benefits Resulting from the Project

Impact By year	2005	2010	2015	2020	2025	2030
Total number of existing systems industry wide	0	3	21	71	96	99
% Market penetration	0	3	21	71	96	99
Total primary energy displaced (10^{12} BTU/year)	0	0.03	0.23	0.79	1.11	1.19

Table 22: Cost Benefits Resulting from the Project

Impact by Year	2005	2010	2015	2020	2025	2030
Total number of existing systems industry wide	0	3	21	71	96	99
Energy-cost savings ($\$10^9$/year)	0	0.226	2.373	8.355	11.739	12.576

Table 23: Environmental Benefits Resulting from the Project

Impact By Year	2005	2010	2015	2020	2025	2030
Total number of existing systems industry wide	0	3	21	71	96	99
Metric tons of CO_2 emissions reduction (10^5 tons/year)	0	7,246	53,811	71,349	91,636	153,927
Metric tons of carbon equivalent emissions reduction (10^5 tons/year)	0	1976	14,675	19,458	24,992	41,980

7.5.3 Consolidated Benefits for Hot Dip Galvanizing and Aluminum Industries

Projected benefits of the project for the hot-dip galvanizing and aluminum industries are shown in Table 24. The results of the project could further benefit other industry sectors that are subject to liquid metal corrosion of refractory and metal components, such as metal casting and superalloy production.

Table 24: Consolidated Benefits Resulting from the Project

Impact By year	2005	2010	2015	2020	2025	2030
Total primary energy displaced (10^{12} BTU/year)	0	0.0954	0.4044	1.1824	1.7531	2.0402
Energy-cost savings ($\$10^9$/year)	0	0.6875	3.6037	8.355	16.2771	18.576
Metric tons of CO_2 emissions reduction (10^5 tons/year)	0	18,807	84,640	140,714	205,318	304,219
Metric tons of carbon equivalent emissions reduction (10^5 tons/year)	0	5,129	23,083	38,376	55,996	82,969

8.0 Recommendations

8.1 HDG coatings and materials issues

During this project, it has been confirmed that Alloy 2020 weld overlay is a good candidate for next generation roll coating in continuous hot-dip galvanizing process. The future work should focus on optimizing coating compositions and welding parameters to achieve crack-free anti-corrosion/dross building up coatings. In the meantime, more effort should be invested on commercialization of this technology.

8.2 Dross control and scraper design

Based on our test results, we recommend that Stellite 6B and Tribaloy T-401 can be used as the new scrapper alloys in hot-dip continuous galvalume line to remove dross build-up, maintain the roll surface smooth and thus increase the interval of down time and minimize the energy losses. Overall performance is expected to provide >3.5 X life improvement.

8.3 GEPDSS

The GEPDSS model development research will be extended using funding from the International Lead Zinc Research Organization (ILZRO). This effort will pave the way towards commercialization. In addition, training of the GEPDSS at various galvanizing line locations is being planned subject to resources, in order to expand commercialization potential.

The research and development work that will enhance GEPDSS should focus on enabling the tool to allow line personnel to evaluate the energy and productivity impacts of producing varying steel grades such as dual phase and interstitial free steels.

The GEPDSS should also be enhanced to allow for the energy and productivity impact evaluation of producing particular grades utilizing varying heat treat cycles.

The emissivity of the various steel grades should also be incorporated in terms of enabling accurate heat balance calculations.

The follow up research should be focused on enabling GEPDSS to be sensitive to product parameters such as sheet steel material properties, gage thickness, and line speed in the furnace and through the pot.

8.4 Refractories

Commercialization should be pursued by the industrial partners associated with the development of the two new refractory materials identified under this project for use in molten aluminum applications. These materials have been shown to successfully perform in a superior manner to currently used materials leading to both energy and economic savings. Yet, development of materials is still needed for other molten metal applications such as copper, super alloys, and many metal casting alloys. There is also still a need to develop other innovative refractory compositions utilizing novel aggregates, binder systems, methods of phase formation, and refractory application systems. Work is also needed to determine and document the implementation rates and the resulting energy savings due to the use of the newly developed refractories in actual industrial aluminum applications.

9.0 References and Bibliography

1. K.J. Brondyke, "Effect of Molten Aluminum on Alumina-Silica Refractories", *Journal of the American Ceramic Society*, 36[5] 171-174 (1953).
2. W. Fahrenholtz, K. Ewsuk, R. Loehman, and P. Lu: Journal of the American Ceramic Society, 1998, vol. 81(10), pp. 2533-2541
3. Refractories, 4th Edition, F.H. Norton, McGraw Hill, 1968.
4. Introduction to Ceramics, 2nd Edition, W.D. Kingery, H.K. Bowen, and D.R. Uhlmann, John Wiley & Sons, 1976.
5. J.G. Hemrick, W.L. Headrick, and K.M. Peters, "Development and Application of Refractory Materials for Molten Aluminum Applications", accepted (10//07) by the International Journal of Applied Ceramic Technology for publication.
6. Clark, L. M., III, and Taylor, R. E., "Radiation Loss in the Flash Method for Thermal Diffusivity," *J. Appl. Phys., 46*, Vol. **714**, (1975).
7. Jing Xu, James G Hemrick, Mark Peters, Xingbo Liu, Ever Barbero: "Wetting and Reaction Characteristics of Al2O3/SiC Composite Refractories by Molten Aluminum and Aluminum Alloy", International Journal of Applied Ceramics Technologies 4 (December 2007) [6] 514-523
8. J.G. Hemrick, C.W. Kistler, A.A Wereszczak, M.K. Ferber, "Thermal Conductivity of Alumina Measured with Three Techniques", Journal of Testing and Evaluation, Vol. 31, No. 4 (2003).
9. "TCON Case History #1 – TCON TC1 Hook, Part # 953," Fireline TCON, Inc., (2006) (Klaus-Markus Peters, (330) 743-1164).
10. "TCON Case History #2 – TCON TC1 Hook, Part # 970," Fireline TCON, Inc., (2006) (Klaus-Markus Peters, (330) 743-1164).
11. "TCON Case History #3 – TCON TC2 ECI Plate, Part # 1007," Fireline TCON, Inc. (2006) (Klaus-Markus Peters, (330) 743-1164).
12. Gopalakrishnan, B., Chavan, R., Benchmarking of Energy Consumption in Continuous Galvanizing Lines, *Proceedings of the Intelligent Systems in Design and Manufacturing VI Conference*, Society of Photo Optical Instrumentation Engineers (SPIE), Boston, MA, Vol.5999, pp. 59990T1-T8, 2005.
13. Chavan, R., Analysis of Energy Consumption in Continuous Galvanizing Lines, Masters Thesis, West Virginia University, 2006.
14. A. Standage and M. Gani: *Journal of the American Ceramic Society*, 1967, vol. 50(2), pp. 101-105.
15. Marumo, and Pask: *Journal of Materials Science*, 1977, vol. 12(2), pp. 223-233.
16. E. Saiz and A. Tomsia: *Journal of the American Ceramic Society*, 1998, vol. 81(9), pp. 2381-2393.
17. W. Fahrenholtz, K. Ewsuk, R. Loehman, and P. Lu: *Journal of the American Ceramic Society*, 1998, vol. 81(10), pp. 2533-2541.
18. *Steel Industry Technology Roadmap*, U.S. DOE Industrial Technologies Program, page 46, December 2001.

19. DOE/ORO-2076 Report: "Opportunities for Advanced Ceramics to Meet the Needs of the Industries of the Future", D.W. Freitag and D.W. Richerson, U.S. DOE Office of Industrial Technologies, December 1998.

20. R.Y. Chen and D. J. Willis, "The Behavior of Silicon in the Solidification of Zn-55Al-1.6Si Coating on Steel", Metallurgical and Materials Transactions A, Vo. 36A, pp. 117-128, (2005).

21. N.-Y. Tang, "Silicon in Galvanizing," 2004 Galvatech Conference Proceedings, Chicago, IL, pp. 683-690, (2004)

22. Jing Xu, Mark A Bright, Xingbo Liu, Ever Barbero: "Liquid Metal Corrosion of 316L Stainless Steel, 410 Stainless Steel and 1015 Carbon Steel in a Molten Zinc Bath", *Metallurgical & Materials Transaction A 38A (2007) 2727-2736*

23. Xingbo Liu, Ever Barbero, Jing Xu, Matthew Burris, Keh-Min Chang & Vinod Sikka: "Liquid Metal Corrosion of 316L, Fe3Al and FeCrSi in Molten Zn-Al Baths", *Metallurgical & Materials Transactions A, 36A (August 2005) p.2049-2058*

24. Xingbo Liu, Vinod K. Sikka, Mark Bright, Scott Sexton, Ever Barbero, James W. Hales: "DEVELOPMENT OF A NEW WELD OVERLAY FOR POT HARDWARE IN CONTINUOUS GALVANIZING LINES", presented at Galvtech'07 Conference, Osaka, Japan (November 2007)

25. Jing Xu; Xingbo Liu; Mark A Bright; James G Hemrick; Ever J Barbero: "Reactive Wetting of an Iron-Base Superalloy MSA 2020 and 316L Stainless Steel by Molten Zinc-Aluminum Alloy", *Metallurgical & Materials Transaction A, 39A (June 2008) 1382-1391*

26. Jing Xu, Xingbo Liu, Mark A Bright, James G Hemrick, Ever Barbero: "REACTIVE WETTING OF AN IRON-BASE SUPER Alloy MSA2020 AND 316L STAINLESS STEEL BY MOLTEN ZINC Alloy ", presented at Galvtech'07 Conference, Osaka, Japan (November 2007)

27. *Aluminum Industry Technology Roadmap*, U.S. DOE Industrial Technologies Program, February 2003, pages 11, 20, and 24.

28. "ORNL Develops Improved Materials for Containing Molten Metal." *Oak Ridge National Laboratory Science and Technology Highlights*, Fall 2007, page 6.